https://doi.org/10.5194/egusphere-2026-5195
Preprint. Discussion started: 8 September 2026
© Author(s) 2026. CC BY 4.0 License.

A Theory of the Linkage between Volcanoes, Climate Cooling, Malnutrition and Epidemics: Case Study of Justinianic Plague

Vaughan T. J. Phillips[1], Sanne M. H. de Jong[2], Robert Garvey[3], Martin K. Skoglund[5,6], Torbjörn Ahlström[4], Fredrik Charpentier Ljungqvist[5,6], Mikael Pontarp[7,8], Joacim Rocklöv[3], Matthew Toohey[9], Jun-Ichi Yano[10], Helene Castenbrandt[11], Carl-Johan Fraenkel[12], Adam Linder[12], Henrik Sjödin[3] and Jesper Sjolte[1]

[1]Department of Earth and Environmental Sciences, Lund University, SE-223 62 Lund Sweden
[2]Radboud Institute for Culture and History, Radboud University, 6525 HT Nijmegen, Netherlands
[3]Department Department of Epidemiology and Global Health, Umeå University, SE-901 87 Umeå, Sweden
[4]Department of Archaeology and Ancient History, Lund University, SE-221 00 Lund, Sweden
[5]Department of History, Stockholm University, SE-106 91 Stockholm, Sweden
[6]Bolin Centre for Climate Research, Stockholm University, SE-106 91 Stockholm, Sweden
[7]Department of Biology, Lund University, SE-221 00 Lund, Sweden
[8]RISE Research Institutes of Sweden, Division Food, Unit Sustainable Food Systems, Lund, Sweden
[9]GEOMAR Helmholtz Centre for Ocean Research Kiel, Wischhofstraße 1–3, 24148 Kiel, Germany
[10]Centre Nationale de Recherche Scientifique (CNRS)/Meteo-France, Toulouse, France
[11]Department of Economic History, Lund University, 221 00 Lund, Sweden
[12]Division of Infection Medicine, Department of Clinical Sciences, Lund Faculty of Medicine, Lund University BMC (Biomedical Centre), SE-221 84 Lund, Sweden

Correspondence to: Vaughan Phillips (Vaughan.phillips@mgeo.lu.se)

https://doi.org/10.5194/egusphere-2026-5195
Preprint. Discussion started: 8 September 2026
© Author(s) 2026. CC BY 4.0 License.

Abstract. Major volcanic eruptions have long been proposed to have triggered and amplified historical plague pandemics through climatic shocks and harvest failures, but the mechanisms linking volcanic forcing, nutrition and disease remain poorly quantified. We develop a theoretical model of a single region with zero spatial dimensions ("0-D") that couples volcanic forcing, climate, agricultural productivity, food storage, malnutrition and plague epidemiology. The epidemiological component includes reservoir hosts, vectors, human-to-human transmission, disease-driven migration and waning immunity, with transmission and mortality rates dependent on nutritional status.

We first evaluate the model against agricultural and archaeological evidence from England following the 1345 CE eruption, shortly before the Second Plague Epidemic. The simulations reproduce the observed sudden drop in crop output and prolonged deterioration in nutritional conditions, as well as the observed relationship between plague mortality and an isotopic proxy for malnutrition derived from human skeletons. We then apply the model to the Justinianic Plague following the 536 and 540 CE eruptions. Representing three population groups with different vulnerability to harvest failure and malnutrition, the model predicts eventual plague mortality of about 39%, consistent with historical estimates. Sensitivity experiments show that removing the effect of volcanic forcing on malnutrition substantially reduces predicted plague mortality, whereas excluding disease-driven migration increases it. Doubling eruption intensity produces only a modest increase in total mortality, revealing nonlinear interactions among climate, nutrition and epidemic dynamics.

A reduced phase-space analysis further shows that epidemic feedbacks change from net positive to net negative as susceptible individuals are depleted, with the system transitioning from an initially unstable state towards a quasi-equilibrium attractor. Together, the simulations suggest that volcanic eruptions could have substantially amplified historical plague epidemics through their effects on failure of harvests and food production, malnutrition and human behaviour. The results provide a mechanistic framework linking volcanic climate forcing to epidemic severity and highlight nutrition as a potentially important mediator of climate–disease interactions.

https://doi.org/10.5194/egusphere-2026-5195
Preprint. Discussion started: 8 September 2026
© Author(s) 2026. CC BY 4.0 License.

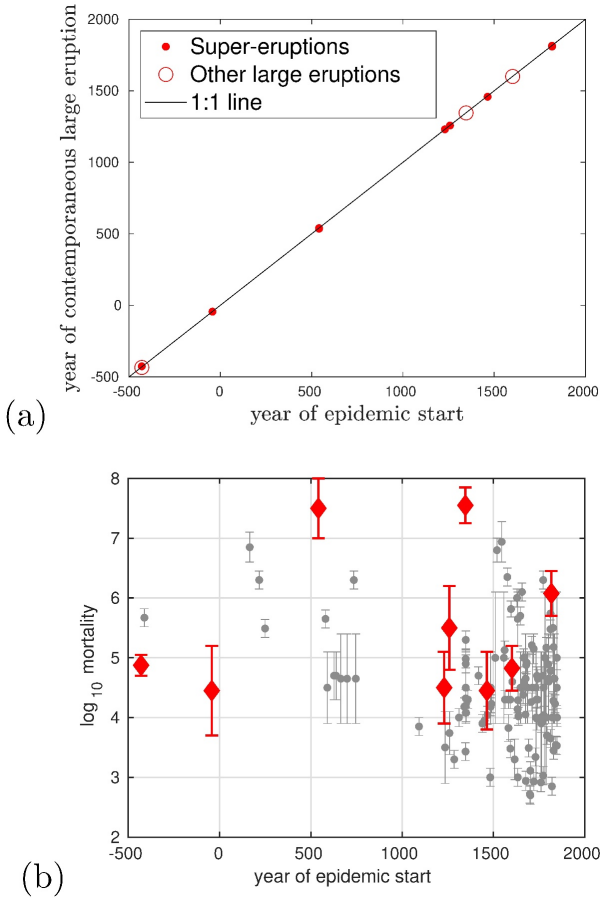

Figure 1: (a) Dates of 'super-eruptions' and other large eruptions (Sigl *et al.* 2015; Toohey *et al.* 2017), compared with the onset of major contemporaneous epidemics (1)–(9) (see text). A 1:1 line is shown for reference. The 1345 eruption is estimated to have approached the super-eruption threshold, with a radiative forcing approximately 1.9 times that of the 1991 Pinatubo eruption (Sections 2.1 and 3). Super-eruptions are defined here as eruptions producing at least twice the radiative forcing of the 1991 Pinatubo event. (b) Estimated mortality of all known epidemics before 1850 (small grey points), compiled from Wikipedia's List of epidemics/pandemics and the EpiMedDat webpages, including the same selected epidemics (1)–(9), (large red diamonds), shown in (a).

1 Introduction

1.1 Historical Background

Major volcanic eruptions and solar irradiance variability are widely considered to have produced episodes of abrupt climatic cooling in pre-industrial times, affecting crop yields through combinations of reduced temperatures, altered precipitation, shortened growing seasons and short-term weather extremes. Large eruptions can induce rapid anomalies of global mean

https://doi.org/10.5194/egusphere-2026-5195
Preprint. Discussion started: 8 September 2026
© Author(s) 2026. CC BY 4.0 License.

near-surface temperature (e.g. a peak global cooling of 0.3 to 0.4 °C for Pinatubo in 1991) within one to two years of the event due to injection of sulphate aerosol into the stratosphere, where it is transported globally (Stenchikov *et al*. 1998; Robock 2000; Thompson *et al*. 2009). The magnitude of the resulting cooling depends on the amount and altitude of sulphur injection, aerosol microphysical evolution and atmospheric circulation, producing substantial variability among eruptions (Burke *et al*. 2023). The volcanic aerosol in the stratosphere reflects extra solar radiation back to space, altering the net radiation entering the climate system (a radiative 'forcing' of climate change). Successive large eruptions only a few years apart (e.g. 536/540 CE) can produce an especially large impact from their forcings combining additively. For context, the difference in global mean surface temperature between the peak of an ice age and an interglacial is typically around 5 °C, with even greater regional and seasonal climate impacts.

A "*super-eruption*" is defined in the present study as an eruption producing at least twice the radiative forcing of the 1991 Pinatubo event. Our practical definition differs from that used by Self (2006) for deep geological time. Such events occur approximately every few centuries. Eruptions meeting this criterion have been identified at 426 BCE (with a smaller event in 434 BCE), 44 BCE, 536/540 CE, 1230, 1257, 1458, and 1809/1815 (Sigl *et al.* 2015), (Toohey and Sigl 2017, their Figure 6, assuming a time-integrated SAOD for Pinatubo of about 0.2 yr). A few other large eruptions, notably 1345 and 1600, are slightly below this threshold in the new dataset (Toohey and Sigl 2017).

Figure 1a shows how widespread, well-documented major epidemics are temporally proximate to these large eruptions (Stothers 1999; McMichael 2012; Fell *et al.* 2020), including: (1) the Plague of Athens (from 430 BCE, with recurrent waves in the 420s), attributed by Thucydides to war, in Greece and N Africa; (2) a pandemic, possibly plague, around 43 BCE in Europe and the Middle East; (3) the Justinianic Plague (541–549 CE) in Europe, W Asia and N Africa; (4) epidemics in Russia (1230-1232 CE), likely plague, and France (1235 CE) ('EpiMedDat' website); (5) epidemics in Europe and the Near East around 1258–1259; (6) the Black Death (1346–1353); (7) major plague outbreaks in 1464–1466 in Britain and continental Europe (Creighton 1891; Biraben 1975–1976; Shrewsbury 1970); (8) plague outbreak in western and northern Europe (1601-1603), (and a mystery unquantified epidemic in China/Korea in 1601), ('EpiMedDat' website); and (9) First Cholera (Asia/M East, 1817-1824) Pandemic and typhus (Europe, 1816-1819) epidemics. These events were commonly reported in near-contemporary historical sources as occurring during periods of climatic deterioration. Plague epidemics (3) and (6) were followed by recurrent waves over about two and five centuries, respectively, and were geographically transcontinental; they are therefore conventionally described as pandemics (e.g., Spyrou *et al.* 2022). Plague epidemic (7) occurred during an established phase of the Second Plague Pandemic, which the 1458 eruption may have amplified. oreover, almost all of these major epidemics ((2)–(9)) occurred less than about 6 years after the corresponding major eruption, consistent with the 2–3-year persistence of volcanic sulfate aerosols in the lower stratosphere and with the subsequent climate response extending over several years because of the thermal inertia of the ocean (Stenchikov et al., 2009), as well as with the slower responses of the ecological (e.g. the trophic cascade for spillover) and coupled agricultural, social and

https://doi.org/10.5194/egusphere-2026-5195
Preprint. Discussion started: 8 September 2026
© Author(s) 2026. CC BY 4.0 License.

malnutrition systems. An exception is (1), which apparently preceded the corresponding eruption but may have been amplified by it; the dating of the eruption in 426 BCE is uncertain by a few years, as is the chronology of the later phases of the Athenian epidemic. For example, coupled ocean–atmosphere simulations of Tambora (1815) show a global mean sea-surface-temperature anomaly of approximately −0.4 ºC still present in 1822, seven years after the eruption, and a peak cooling of −1.2 ºC lasting until two years afterwards (Stenchikov *et al*. 2009, their Figure 2a).

Generally, almost all of the excess heat stored in the climate system resides in the ocean, whose large heat capacity gives the climate system its thermal inertia. The timescale of the temperature response depends on the duration of the forcing and the depth over which the ocean exchanges heat with the atmosphere. For a persistent forcing such as an instantaneous doubling of atmospheric CO2, the climate system approaches equilibrium over decades or longer, with heat being exchanged progressively deeper into the ocean (Hansen *et al*. 2005). By contrast, a short-lived volcanic forcing is not maintained long enough for the full equilibrium response to develop, and the surface-temperature response is transient, though ocean thermal inertia can make it persist for several years after the volcanic forcing has mostly disappeared (Stenchikov *et al*. 2009).

Although epidemics generally have always occurred throughout history irrespective of eruptions, the selected epidemics (1)-(9) (Fig. 1a) are disproportionately represented among the higher-mortality events in the historical epidemic record (Fig. 1b). Some of them (red points in Fig. 1b) also seem to precede a train of other epidemics (grey points), consistent with a potential role for triggering subsequent waves.

Several mechanisms have been proposed to explain the temporal association between climatic variability and epidemic disease (reviewed by de Jong 2026). Climate perturbations of ecosystems, affecting reservoir species, has been shown to contribute to zoonotic spillover processes (Schmidt *et al*. 2015; Fell *et al.* 2020). For example, warm springs and wet summers in central Asia are seen to correlate with plague prevalence in great gerbils in the wild (Stenseth *et al.* 2006). Such climatic conditions persisted there for decades after the vast Samalas eruption in 1257, roughly coinciding with the genetic origin in central Asia of the strain of the bacterium causing the Black Death (Cui *et al.* 2013), (reviewed by Fell *et al.* 2020). There, the earliest skeletons attributed to plague by ancient DNA-analysis are from the 1330s (Spyrou *et al.* 2022). Spillover of plague from rodents in central Asia is well understood (Samia *et al.* 2011).

Another leading hypothesis is that abrupt climate shocks directly promoted agricultural failure, thereby increasing malnutrition and population susceptibility to infectious disease, amplifying the epidemic once the pathogen has crossed from the reservoir to humans (Stothers 1999, 2000; Baten 2001; Oppenheimer 2003, 2011; Lee *et al*. 2017; Guillet *et al*. 2017; Zonneveld *et al*. 2024; Ljungqvist *et al*. 2024). Disturbed conditions of temperature and precipitation needed for growth of crops may cause crop failures. For instance, a food shortage in 1258 in England and famine-related disease followed the super-eruption in 1257 (Campbell 2017), with epidemics and famine across Europe and the Near East (Stothers 2000; Guillet

https://doi.org/10.5194/egusphere-2026-5195
Preprint. Discussion started: 8 September 2026
© Author(s) 2026. CC BY 4.0 License.

et al. 2017). Also, famine and epidemic disease frequently coincided in late Roman and early Byzantine society (Stathakopoulos 2004; Ljungqvist *et al.* 2024). Lastly, other mechanisms proposed include climate-driven changes in human behaviour, such as migration, settlement crowding, and altered trade networks, facilitating pathogen transmission (e.g. Fell *et al*. 2020; Ljungqvist *et al.* 2024). Also, a combination of the above hypotheses is that climate shocks first cause disease (e.g. by zoonotic spillover) and that this then impairs the labour needed for agriculture, worsening nutrition further (Stothers 1999).

Specifically, plague is caused by the bacterium *Yersinia pestis*, which is transmitted initially by fleas associated with mammalian reservoir hosts and, in its pneumonic form, can also spread directly between humans by respiratory droplets. The dominant transmission pathway during historical plague pandemics remains debated. While the classical view emphasizes transmission by rodent-associated fleas, recently it has been argued that human ectoparasites, including body lice and human fleas, are needed to explain the rapid spread of medieval epidemics (e.g., Dean *et al.* 2018). Supporting this hypothesis, *Yersinia pestis* has been detected in body lice on plague patients (Blanc and Baltazard 1942), and infected lice are seen to transmit the bacterium to rabbits (e.g., Drancourt *et al.* 2006; Ayyadurai *et al*. 2010).

The role of famine in such epidemics is indirect. When crops fail, rats can be forced into proximity with humans when there is little food in the fields. Similarly, humans can migrate in response to famine, and in so doing spread the disease. Alternatively, the climate shock causing famine may cause reservoir species to seek new food or water sources, bringing new combinations of species together and allowing the pathogen to cross from species to species. Malnutrition weakens the human immune system (e.g., Scrimshaw *et al.* 1968; Katona and Katona-Apte 2008), especially in any vulnerable section of the population, undermining the fitness needed for migration and agricultural labour, creating a positive feedback.

A salient instance of a preindustrial climate shock is from two volcanic super-eruptions in the early Middle Ages in 536 and 540 CE. Ice-core, dendrochronological and geochemical evidence, constraining global modeling, all indicate they augmented stratospheric aerosol loading and caused climate cooling especially in the Northern Hemisphere (NH), (Sigl *et al*. 2015; Stoffel *et al*. 2015; Büntgen *et al.* 2016, 2022; Toohey *et al*. 2016; Dull *et al.* 2019; van Dijk *et al*. 2023). These and other subsequent eruptions initiated the 'Late Antique Little Ice Age', for which multiple palaeoclimate proxies, including global wood anatomical evidence, indicate exceptional NH summer cooling (Büntgen *et al*. 2016, 2017, 2022; van Dijk *et al*. 2022). The atmospheric anomaly from the 536 CE event was recorded by contemporary Mediterranean sources as an unusual dimming or "dust veil" (Arjava 2005). The 540 eruption was attributed to the volcanic caldera Ilopongo in modern-day El Salvador (Dull *et al*. 2019).

The Eastern Roman Empire was near its height under the rule of Emperor Justinian (r. 527–565), (Fig. 2a). Followingwritten historical evidence, the Justinianic plague appears to have entered the eastern Mediterranean through Egypt around 541 CE

https://doi.org/10.5194/egusphere-2026-5195
Preprint. Discussion started: 8 September 2026
© Author(s) 2026. CC BY 4.0 License.

(Stathakopoulos 2004; Huebner and Macdonald 2023; Preiser-Kapeller *et al.* 2025), reaching Constantinople in the spring of 542 (Procopius, 1914-1928, *The Wars* 2.22.9; Huebner and MacDonald 2023). There are multiple contemporary accounts of the plague from authors within the empire, notably Procopius (ca. 490–565) and John of Ephesus (ca. 507–588), (Procopius, 1914-1928, *The Wars* 2.3.1; Pseudo-Dionysius of Tel-Mahre, 1996, *Chronicle* III.74–98). Often cited is Procopius's report that, at the height of the epidemic in Constantinople, more than ten thousand people per day perished (Procopius, 1914-1928, *The Wars* 2.22), together with John Malalas' account of unburied bodies (*Chronographia* 18.95; Jeffreys *et al.* 1986, pp. 286–287 therein). John of Ephesus, whose account survived through The Chronicle of Zuqnin in Syriac, describes that in Constantinople "*those* [corpses] *were gathered from the city in heaps, were cast down in ships* [on this side of the sea shore] *and were thrown* [on the other side] *like litter on the face of the earth, but there was no-one* [to gather them]" (*The Chronicle of Zuqnin*, transl. Harrak 2017). At that time, John of Ephesus in the Middle East reported "*famine, plague, confusion, desolation and mourning*" (Payne Smith 1860).

The Justinianic Plague continued as the 'First Plague Pandemic' throughout the 6th and 7th centuries, with outbreaks on 8–12-year cycles (Perry and Featherston 1997). It spanned the 'known' world of Europe, N Africa and central and southern Asia. The fact that it spread throughout Europe is suggested by chroniclers in several regions throughout Europe. Drawing on contemporary Syriac, Arabic, Greek, Latin and Old Irish sources, Sarris (2022) concludes that the First Plague Pandemic was ubiquitous, severely affecting both urban and rural populations. Ancient-DNA analyses of 6th-to-8th century human remains have demonstrated that during the First Plague Pandemic several related bacterial lineages of *Yersinia pestis* causing it were in circulation across western Europe (Fig. 2b), (Harbeck *et al.* 2013; Wagner *et al.* 2014; Feldman *et al.* 2016; Keller *et al.* 2019). Geographically, these finds are confined within the former borders of the dwindling Roman empire, with finds from Britain (Edix Hill), France (Lunel-Viel and Saint-Doulchard), Germany (Unterthürheim and other Bavarian sites) and Spain (Valencia), (Keller *et al.* 2019). Another recent find has been reported from Jaresh in Syria (Adapa *et al.* 2025). The geographical distribution of DNA finds of *Yersinia pestis* (Fig. 2b) remains incomplete. In particular, genomic evidence for the First Plague Pandemic has not yet been recovered from Scandinavia.

The better documented Black Death of 1346–1353 CE, the first major wave of the Second Plague Pandemic (c. 1346–mid-nineteenth century), was also caused by *Yersinia pestis*, the pathogen responsible for the First Plague Pandemic (c. 541–767 CE). The Black Death in Europe was preceded by a food shortage and severe weather in Italy and Spain during 1345–47, with famine mitigated by Mediterranean grain trade (Bauch and Buntgen 2025), while food shortages affecting England in 1349 (Sec. 4). Ancient-DNA analysis has confirmed *Y. pestis* in Black Death victims (Bos *et al.* 2011). Mortality during the Black Death is better documented than during the First Plague Pandemic, particularly in some European urban and rural communities. Historical estimates have placed mortality at about 30–50% of populations affected by the Black Death in Eurasia (reviewed by Perry and Fetherston 1997), while Belich (2022) argues for mortality approaching 50% in Western

https://doi.org/10.5194/egusphere-2026-5195
Preprint. Discussion started: 8 September 2026
© Author(s) 2026. CC BY 4.0 License.

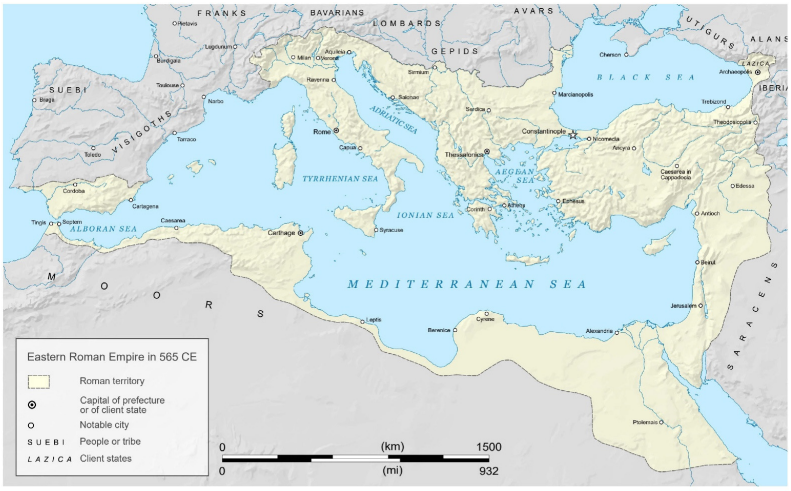

(a)

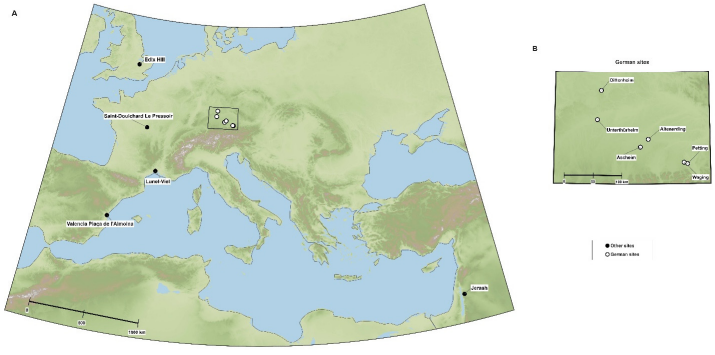

(b)

Figure 2: (a) The Eastern Roman (Byzantine) Empire at its greatest territorial extent in 565 CE, at the end of the reign of Emperor Justinian I. The First Pandemic, which began in 541 CE, recurred in multiple epidemic waves for more than two centuries. Adapted from Wikipedia Commons. Also shown is (b) locations of finds of *Yersinia Pestis* in skeletons from the First Pandemic in the 6th century, informed by Keller et al. (2019).

Europe. For example, Broadberry *et al.* (2015) estimate that England's population declined by almost half during the Black Death, while similarly severe mortality has been documented in some rural communities in France (e.g., Dean *et al.* 2018), (Appendix A). There is controversy about the extent of mortality from the Black Death in some regions of central Europe (e.g., Izdebski *et al.* 2022; Guzowski 2022), although such demographic inferences from pollen studies were criticised by

https://doi.org/10.5194/egusphere-2026-5195
Preprint. Discussion started: 8 September 2026
© Author(s) 2026. CC BY 4.0 License.

Curtis (2022) and Hamerow *et al.* (2025). Nevertheless, the Black Death therefore provides an important historical benchmark for assessing the potential demographic impact of *Y. pestis* during the First Plague Pandemic

Genetic evidence indicates that the *Yersinia pestis* strains responsible for the two pandemics shared key virulence-associated genes, despite belonging to different phylogenetic lineages (Wagner *et al.* 2014; Demeure *et al.* 2019). Consequently, estimates that the First Plague Pandemic, beginning with the Justinianic Plague, killed approximately 20-25%, 40-50% and 50-60% of the population of the 'known world', including the Eastern Roman Empire, over the first epidemic wave (first few years), by 600 CE and 700 CE respectively (Russell 1965, 1968; Perry and Fetherston 1997; Harper 2017) are biologically plausible, if the high mortality documented for the Black Death reflects the intrinsic capacity of *Y. pestis* to cause large-scale mortality in susceptible populations. Conversely, it could be argued that such high estimates only apply to densely populated regions.

Although the magnitude of mortality and the extent of societal disruption remain debated (e.g. Mordechai *et al.* 2019; Newfield 2022; Stathakopoulos *et al*. 2025), and some scholars caution against overly deterministic interpretations of environmental change as a driver of societal transformation (Izdebski 2019), substantial demographic and economic disruption across parts of the Eastern Roman Empire and western Europe in the middle 6th century after 536/540 CE is indicated by historical, legal and archaeological evidence. Contemporary legislation addressed abandoned land, labour shortages and inheritance, while coinage debasement has been interpreted as reflecting economic stress and declining tax revenues in the Eastern Roman Empire which could be related to issues connected to plague outbreak (Novellae 80; Novellae 122; Miller, Sarris 2018, pp. 551-552; Meier 2016; Sarris 2022). Independent palaeoclimate and archaeological evidence from the Byzantine southern Levant likewise indicates environmental and economic disruption during this period, including links between climate anomalies, precipitation changes and numismatic trends, with drought in Europe and flooding in the Levant after 536 CE (Fuks *et al.* 2017).

Contemporary accounts from Britain, Gaul and Italy describe mortality, settlement abandonment and disruption of agriculture (Little 2007; Maddicott 2007; Harper 2023). Gregory of Tours (1974, trans. by Thorpe) records that the first plague outbreak reached Gaul during the 540s, followed by outbreaks, including in rural Auvergne in 571. Epidemic disease may have affected Britain and Ireland during the mid-sixth century: Gildas describes widespread devastation, famine, and apparent depopulation alongside the collapse of social and political order in post-Roman Britain, while the Irish and Welsh annals record major pestilences in the decades following 540, often associated by modern historians with the Justinianic Plague (Winterbottom 1978; Mac Airt and Mac Niocaill 1983; Stokes 1895–1897; Williams 1860; Little 2007). Sediment cores show a sudden decline around 550 CE of metal-working industry in N England after both eruptions (Loveluck *et al.* 2025), consistent with arrival of plague and demographic collapse.

https://doi.org/10.5194/egusphere-2026-5195
Preprint. Discussion started: 8 September 2026
© Author(s) 2026. CC BY 4.0 License.

Maritime trade is widely considered an important mechanism for the long-distance dissemination of plague during the sixth century. Contemporary accounts describe plague first reaching Mediterranean port cities while Procopius reported its arrival at Pelusium, at the eastern mouth of the Nile, before spreading to Alexandria and Constantinople (McCormick 2007), (see also Bauch and Buntgen 2025). The Byzantine Mediterranean was also connected to commercial networks extending through the Red Sea and Arabia towards the Indian Ocean, providing potential routes for the movement of people, goods and pathogens between eastern Africa and the Mediterranean. Maritime and overland networks may likewise have facilitated the spread of plague beyond the Mediterranean, including to western Europe, (Maddicott 2007; Seaman 2023; Comeau *et al.* 2023). Gregory of Tours reported on plague spreading at Marseille from ships arriving there (McCormick 2021). The extensive urban, commercial and communication networks of the former Roman Empire, which was generally more densely populated, contrasted with the more rural and dispersed settlement patterns of other parts of Early Medieval Europe. Cities were denser and more inter-connected than outside the former Roman Empire. Sarris (2022) argues that these differences may have contributed to reduced plague spread in some European regions. Variation in connectivity, settlement and population distribution may therefore help explain the heterogeneous geographical impact of the First Plague Pandemic (McCormick 2001; Sarris 2022).

Consistent with the leading hypothesis noted above of the volcanic climate shock undermining harvests is, for example, the report from Cassiodorus in the Ostrogoth central administration in a letter to provincial governors in Italy (before it joined the Eastern Roman empire) in 537/538 CE:

> *"We have had a winter without storms, a spring without mildness, and a summer without heat. Whence can we look for harvest … if rain … is denied to it? …frost and unseasonable drought, must be adverse to all things that grow. Therefore let all store up the produce of the previous year"* (Cass. Variae 12.25.2., transl. Barnish 1992, pp. 179-180).

Climate-model studies have debated the duration and spatial extent of the post-536 cooling. Simulations indicate substantial regional cooling is predicted to persist for two decades after the eruptions, with cooling and drying pronounced in the first two growing seasons after each over Norway (van Dijk *et al*. 2022, 2023). Recent palaeoclimate and agricultural harvest studies with models (Toohey *et al*. 2016; van Dijk *et al*. 2023; Arthur *et al.* 2024) predicted that the 536/540 CE eruptions caused crop failures for northwestern and western, but less clearly in southern, Scandinavia, with local average cooling anomalies of up to 3.5 °C during the growing season. This agreed with pollen records and archaeological evidence of farm abandonment.

Stathakopoulos (2007) argues that flight was a common reaction to epidemic crisis in pre-modern societies. Flight from towns afflicted by the plague in the Eastern Roman Empire is illustrated by historical and legal evidence, for example by a

https://doi.org/10.5194/egusphere-2026-5195
Preprint. Discussion started: 8 September 2026
© Author(s) 2026. CC BY 4.0 License.

report from Evagrius (Ecclesiastical History 4.29, trans. Whitby 2000; Stathakopoulos 2007, pp. 112). Novel 128.7 from Justinian's Novellae ('laws') allocates the tax-duties of deserted land, presumably from victims of the plague, or people who had migrated (Novellae 128.7.; Miller and Sarris 2018, page 848 therein). Drawing on contemporary Syriac, Arabic, Greek, Latin and Old Irish sources, Sarris (2022) concludes that the First Plague Pandemic severely affected both urban and rural populations. Paul the Deacon (1974, translated by Foulke) in the early Middle Ages described flight from settlements and abandonment of agricultural land due to plague in some regions of Italy, as had John of Ephesus while travelling in the Eastern Roman Empire (Little, 2007). Paul wrote about an outbreak in Liguria in 565 CE: "*The dwellings were left deserted by their inhabitants… The flocks remained alone in the pastures with no shepherd at hand. You might see villas or fortified places lately filled with crowds of men, and on the next day, all had departed … Sons fled, leaving the corpses of their parents unburied; parents forgetful of their duty abandoned their children in raging fever*." Widespread flight in response to the plague was reported during the Second Plague Pandemic too (Martin 1996).

1.2 Aim of Paper, Hypotheses and Motivation

Focus is given in the present paper to the Justinianic Plague in the 6th century. The aim is to test the hypothesis that volcanic cooling shocks then disrupted agricultural production, causing malnutrition that amplified plague transmission. A related hypothesis is that disease-driven migration further influenced epidemic dynamics. We do not question the well-established role of climate-sensitive spill-over from wildlife reservoirs in initiating plague epidemics, nor the importance of long-range transport of infected reservoir species in seeding local outbreaks. To examine the mechanisms of volcanic-induced malnutrition and disease-driven migration amplifying epidemic spread, we develop a simple mathematical model linking volcanic climate forcing, failure of harvest/food production, malnutrition and plague transmission. Following the perspective of van Dijk *et al.* (2023) and Arthur *et al*. (2024), the model represents the average response of a specified region or population sector, while contrasting scenarios capture differences in resilience among subpopulations. Here 'resilience' refers to food insecurity rather than physiological health.

The rationale of the paper is that understanding of properties of epidemics may be advanced with a theory sufficiently simple to allow analytical development of the equations. The problem of why the epidemic explodes or decays is tackled. Equally, the simplicity of the model allows the role of mechanisms such as population vulnerability, disease-driven migration, volcanic malnutrition and volcanic intensity to be elucidated. The aim is not realism *per se*, which is why a 3D global model was not employed. Such complexity would obscure the causation of target processes, introducing compensating responses from other processes.

The paper is structured as follows. The following sections describe the epidemiological model and its climate-dependent forcing, with theoretical analysis of quasi-equilibria and feedbacks. Subsequent sections evaluate the model against observations, present control simulations for the 536/540 CE eruptions and related Justinianic Plague (the 'standard case'),

https://doi.org/10.5194/egusphere-2026-5195
Preprint. Discussion started: 8 September 2026
© Author(s) 2026. CC BY 4.0 License.

and examine the resulting climate, food supply, malnutrition and epidemic dynamics, together with sensitivity experiments. The paper concludes with a discussion of the limitations, uncertainties and conclusions.

2. Model Description

2.1 Overview

The model represents a region as a spatially averaged population whose state evolves in time following a volcanic climate shock. It consists of three interacting components for climate forcing, food and malnutrition, and epidemiological dynamics:

- The *climate component* converts volcanic aerosol forcing into a time-dependent temperature anomaly of the globe.
- The *food–malnutrition component* uses this climate forcing to determine changes in agricultural productivity and food storage, from which a malnutrition index and malnutrition-related mortality are calculated, in the given region.
- The resulting time-dependent malnutrition then enters the *epidemiological component*, where it modifies host susceptibility, plague mortality and transmission. The epidemiological component describes infection in humans, vectors and reservoir hosts, with population changes and migration altering the number of susceptible humans.

Thus, the core of the model is the epidemiological component while the other two components merely serve to drive it by providing a time-dependent boundary condition. The causal structure can be summarised as:

volcanic forcing → climate anomaly → food production and storage → malnutrition → plague transmission and mortality,

Population change and migration provide additional feedbacks on epidemic dynamics. The model can be applied to populations with different levels of food security and resilience, allowing the effects of the same climate shock to be compared across regions or population groups.

The detailed mathematical formulation of each component is given in the following sections. The standard parameter set represents the 536 and 540 CE eruptions and the subsequent climatic, nutritional and epidemiological perturbations.

2.2 Time-dependent Boundary Conditions for the Standard Case

2.2.1 Climate Component

From Geoffroy *et al.* (2013), the global mean surface temperature is constrained by a 0-D energy balance model (EBM) with two ocean layers, for the surface and deep ocean: (a) the fast-responding upper layer for the ocean surface boundary layer and atmosphere-coupled near-surface waters (subscript ‘s’), and (b) rest of the oceanic mixed layer (subscript ‘d’):

https://doi.org/10.5194/egusphere-2026-5195
Preprint. Discussion started: 8 September 2026
© Author(s) 2026. CC BY 4.0 License.

$$c_s \frac{dT_s'}{dt} = F(t) - Y\,T_s' - \gamma_{s,d}(T_s' - T_d') \,, \quad (1)$$

$$c_d \frac{dT_d'}{dt} = \gamma_{s,d}(T_s' - T_d') \quad . \quad (2)$$

This has an analytical solution (Geoffroy *et al*. 2013) with two fast and slow response modes. Their relaxation time-scales are $\tau_f = 0.36$ and $\tau_s = 7.1$ years respectively for an effective climate feedback parameter, $Y = 1.7$ and $\gamma_{s,d} = 3.8$ W m^{-2} K^{-1}, with climate column heat capacities for both layers of $c_s = 2.4$ and $c_d = 7.2$ W yr m^{-2} K^{-1} from the Hadley Centre model (Toohey and Marovati 2026). These values of c_s and c_d would correspond to oceanic layers of 18 or 55 m in average depth respectively, in a single oceanic layer EBM.

The radiative forcing associated with a single eruption ($t = 0$) has the form (Toohey *et al*. 2025):

$$F(t) = F_0 \left(1 - e^{-\frac{t}{\tau_{a,r}}}\right) e^{-\max(t - t_{lag}, 0)/\tau_{a,d}} < 0 \quad . \quad (3)$$

On time-scale, $\tau_{a,r}$, it reaches a plateau ($F(t) \approx F_0 < 0$). Onset of wash-out and settling of stratospheric aerosol is delayed by about a year. Only at $t > t_{lag}$ is there a decay towards zero on a time-scale, $\tau_{a,d}$. When numerically integrating Eqs (1)-(3), MKS (metres, kg, seconds) units are used.

Finally, the analytical solution (not shown) to Eqs (1)–(2) (Geoffroy *et al.* 2013), together with Eq (3), shows that the peak cooling is proportional to F_0/Y, multiplied by a factor that depends on time-scales of volcanic forcing and climate response. Hence, the wide range of volcanic forcing amplitudes for the last several millennia, some exceeding the 1991 Pinatubo eruption by several times, must have produced proportionally larger peak global coolings. Consequently, when considering sufficiently long periods, volcanic eruptions capable of producing peak global coolings exceeding 1 °C would be expected to occur occasionally (e.g. 540 CE).

Values for parameters in the forcing in Eq (3) are given and justified in Appendix B.

2.2.2 Food-Malnutrition Component

We introduce a simple regional model linking volcanic cooling, food storage and malnutrition. The dimensionless malnutrition index $\mathcal{M} \in [0,1]$ represents the aggregate effects from impairment of host immunity, where $\mathcal{M} = 0$ denotes adequate nutrition and $\mathcal{M} = 1$ extreme starvation (Table 1).

https://doi.org/10.5194/egusphere-2026-5195
Preprint. Discussion started: 8 September 2026
© Author(s) 2026. CC BY 4.0 License.

Table 1: Interpretation of the dimensionless malnutrition index $\mathcal{M}$. Values of $\mathcal{M}$ correspond to increasing levels of nutritional stress, ranging from adequate nutrition ($\mathcal{M} \approx 0$) to severe famine conditions ($\mathcal{M} \approx 1$). The associated physiological effects are indicative rather than quantitative and provide the basis for the nonlinear dependence of mortality and disease susceptibility on malnutrition in the model.

$\mathcal{M}$ range	Interpretation	Likely physiological effects
0-0.25	Adequate nutrition to mild chronic stress	Little excess mortality; normal immune function; modest micronutrient deficiencies in some individuals.
0.25-0.5	Moderate nutritional stress	Weight loss, reduced physical capacity, impaired wound healing, increased susceptibility to bacterial infections, especially in children and the elderly.
0.5-0.75	Severe malnutrition	Significant wasting, weakened innate and adaptive immunity, increased risk of secondary and opportunistic infections, reduced ability to recover from epidemic disease.
0.75-0.9	Very severe malnutrition / famine	Marked cachexia, major immune suppression, increased mortality from otherwise survivable infections, collapse of physiological reserves.
0.9-1	Near-starvation conditions	High mortality risk from starvation itself and opportunistic infections; severe weakness and inability to maintain normal activity.

Physiologically, $\mathcal{M}$ reflects combined impairment of three aspects of immunity (e.g., Scrimshaw *et al.* 1968; Katona and Katona-Apte 2008): (i) innate defences (epithelial barriers, phagocyte activity, cytokine response), (ii) adaptive immunity (T-cell and B-cell mediated responses and immune memory formation), and (iii) micronutrient-dependent immune function (notably zinc, vitamin A, iron, and selenium availability). Since different pathogens are controlled by distinct immune mechanisms, impairment of these immune components can alter susceptibility to different classes of infection. Innate defences are affected within days to weeks, adaptive immunity over weeks to months, and micronutrient-dependent recovery may require several months. Consequently, recovery of immune competence after prolonged deficiency occurs on a timescale, $\tau_{\mathrm{recover}} \sim 0.5$ years.

https://doi.org/10.5194/egusphere-2026-5195
Preprint. Discussion started: 8 September 2026
© Author(s) 2026. CC BY 4.0 License.

Note that $\mathcal{M}$ here is an aggregate indicator of persistent nutritional and physiological vulnerability affecting susceptibility to infectious disease. It represents persistent physiological impairment rather than instantaneous food availability. Although restoration of adequate food intake can reverse acute nutritional and immune dysfunction relatively rapidly, prolonged nutritional stress can have longer-lasting consequences for physiological resilience and susceptibility to infectious disease. The model therefore allows recovery of the malnutrition state to lag behind recovery of food storage.

The index $\mathcal{M}$ is mapped to an unbounded latent variable $m \in (-\infty, \infty)$ via:

$$\mathcal{M} = \frac{1}{1+e^{-m}}, \tag{4}$$

At equilibrium, $m = m_{eq}$ corresponds to a baseline nutritional state $\mathcal{M} = \mathcal{M}_{eq}$. Before 536 CE, $\mathcal{M}_{eq} = 0.25$ and $m_{eq} \approx -1.1$ are assumed.

A dimensionless food-storage variable f_s is introduced, with $f_s = 1$ representing baseline food reserves, such that $f_s < 1$ represents a deficit and $f_s > 1$ a surplus. The coupled system is given by

$$\frac{dm}{dt} = C_m(1 - f_s) - \frac{m - m_{eq}}{\tau_{\text{recover}}}\ , \tag{5}$$

$$\frac{df_s}{dt} = A_f\,(1 - \lambda_m \mathcal{M})\,\min\left(e^{\kappa T_s'}, 1\right)\frac{f_s + f_w}{1 + f_s} - \frac{f_s}{\tau_{\text{storage}}}\ . \tag{6}$$

Eqs (5) and (6) are formulations that are entirely new. Yet their general approach is consistent with previous dynamical treatments of food security, with prediction of food availability responding to external shocks (Smerlak and Vaitla 2016) and of food-system sustainability under climate perturbations (Goold *et al*. 2020). In Eq (5), the first term on the right is the source of malnutrition from lack of stored food, while the second treats the relaxation of malnutrition towards the background value when food storage is normal ($f_s = 1$).

Specifically, the variable f_s is defined as a dimensionless index of aggregate food reserves within the modeled region, rather than as a per-capita food-availability measure. Specifically, ($f_s = S/S_0$), where (S) denotes the regional food stock and (S_0) its pre-disturbance reference value. Thus, ($f_s = 1$) corresponds to baseline aggregate reserves, while ($f_s < 1$) represents regional depletion. In Eq. (5), the term $(1 - f_s)$ therefore represents a reduced-form food-scarcity forcing on nutritional status. The coefficient (C_m) subsumes the processes linking regional reserve depletion to effective food access and nutritional stress; population is not explicitly modeled in this formulation. Consequently, Eq (5) should not be interpreted as a per-capita food-balance equation.

https://doi.org/10.5194/egusphere-2026-5195
Preprint. Discussion started: 8 September 2026
© Author(s) 2026. CC BY 4.0 License.

Eq (6) balances harvest/food production inputs against consumption and deterioration. Harvest and other food production depends on baseline agricultural productivity (A_f), labour impairment by malnutrition (λ_m), climate-sensitive yields ($e^{\kappa T_s'}$), seed availability ($f_s + f_w$), and saturation of food storage. Only cooling shocks ($T_s' < 0$) are treated by the model, hence the "min" function. Also, $A_f = 2/(\tau_{\text{storage}}(1 - \lambda_m \mathcal{M}_{eq})(1 + f_w))\ \text{yr}^{-1}$, for long-term relaxation of $f_s \to f_{s,eq} = 1$. The factor, $f_s + f_w$, represents the seeding of the current harvest using storage (e.g. grain from past harvests), in addition to a minimal external amount (f_w). The factor, $(1 - \lambda_m \mathcal{M})$, limits the harvest according to malnutrition undermining effectiveness of agricultural labour (e.g., by illness or depopulation).

Consistent with the interpretation in Table 1, direct malnutrition mortality is assumed to remain negligible for $\mathcal{M} < 0.25$, where nutritional stress primarily increases susceptibility to infectious disease rather than causing starvation deaths directly. Above this threshold, direct malnutrition mortality is assumed to increase nonlinearly with $\mathcal{M}$, using a fractional rate per unit time of deaths of the population:

$$\mu = \mu_{m,max} \max\left(\frac{\mathcal{M} - 0.25}{0.75}, 0\right)^2 .$$

In the model, nutritional stress modifies plague transmission and severity continuously through the malnutrition-dependent transmission coefficients (Sec. 2.3), whereas the additional mortality term $\mu(\mathcal{M})$ represents the onset of extreme nutritional deprivation and associated collapse of physiological resilience, especially to non-plague diseases.

In summary, values for parameters in the equations here are given and justified in Appendix B. Moreover, early medieval communities likely differed substantially in agricultural resilience, crop choice, storage capacity, and access to resources (van Dijk *et al.* 2023; Arthur *et al.* 2024). We represent this population heterogeneity using three stylized groups: a majority population with intermediate conditions, a vulnerable population with lower crop resilience, limited storage capacity and elevated background malnutrition, and an affluent population with greater resilience, improved storage capacity and lower background malnutrition (Sec. 1). For the simulations, these groups comprise 60%, 20%, and 20% of the population, respectively. These proportions are illustrative rather than empirical estimates. The parameters for all three population-resilience scenarios are given in Table 2.

https://doi.org/10.5194/egusphere-2026-5195
Preprint. Discussion started: 8 September 2026
© Author(s) 2026. CC BY 4.0 License.

Variable	Majority-population scenario (central 60%)	Vulnerable-population scenario (lowest 20%)	Affluent-population scenario (highest 20%)
κ (K^{-1})	0.75	0.5	1.0
τ_{storage} (years)	1.0	0.75	1.5
$\mathcal{M}_{eq}$	0.25	0.15	0.35

Table 2: Values of parameters differing between the three population-resilience scenarios. The variable, τ_{life}, is life expectancy for natural long-term recovery of populations and is used only to diagnose background deaths for the alternative case (Appendix E).

2.3 Epidemiological Component

The model consists of eight dynamic compartments: infected vectors associated with the human environment (lice, fleas, and bedding arthropods), susceptible humans, vector-mediated infected humans and those who develop secondary pneumonic plague, human-to-human infected humans, recovered immune humans, migrated susceptible humans, and infected reservoir hosts (rodents/other mammals). Their population densities are denoted by $I_v, U_h, I_{hv}, I_{hvp}, I_{hh}, R_h, M_h$,and I_r, respectively, with $I_h = I_{hv} + I_{hvp} + I_{hh}$. Time is measured in days and densities in km^2. Terms such as 'infected' and 'transmission' generally here refer to plague.

Transmission is formulated as a density-dependent encounter process, analogous to collision kernels (volumetric sweep-out rates of collector particles) in kinetic theories of particle populations (e.g. Yano and Phillips 2011), allowing epidemic growth rates to vary with local population density. Moreover, a unique feature is disease-driven migration of humans, informed by historical observations (Sec. 1). Bubonic plague involves highly visible symptoms, such as buboes and rapid mortality. Both the onset and decline of an outbreak would have been apparent to the population, prompting rapid behavioural responses. Outward migration would be triggered on short time-scales (e.g. weeks) once visible cases exceed a threshold, while return migration would commence once symptoms and mortality visibly decline. Such migration is treated as a natural mechanism to limit the intensity of the epidemic.

Reservoir infection changes according to

$$\frac{dI_r}{dt} = e_r(T_s'(t), t) - \frac{I_r}{\tau_r}\ , \tag{7}$$

where e_r represents external seeding (e.g., introduction from other reservoir species or transport-mediated dispersal), and τ_r describes the slow loss of infection in reservoir hosts.

https://doi.org/10.5194/egusphere-2026-5195
Preprint. Discussion started: 8 September 2026
© Author(s) 2026. CC BY 4.0 License.

Infected vectors change according to

$$\frac{dI_v}{dt} = g_v I_h\left(U_{v,0} - I_v\right) + g_{rv} I_r\left(U_{v,0} - I_v\right) - \frac{I_v}{\tau_v}, \quad (8)$$

where the first two terms represent acquisition of infection from humans and reservoir hosts, and the final term represents vector mortality. $U_{v,0}$ is the total population density of the vectors (uninfected initially).

The uninfected susceptible human population follows

$$\frac{dU_h}{dt} = -\Phi_{out} + \Phi_{in} + \frac{U_{h,0} - U_h}{\tau_{U,pop}} - d_h(1 + \tilde{\alpha}_v \mathcal{M})^p U_h I_v - h_h(1 + \tilde{\alpha}_h \mathcal{M})^p U_h (I_{hh} + I_{hvp}) + \frac{R_h}{\tau_{wane}} - \mu U_h \ . \quad (9)$$

The migration fluxes are

$$\Phi_{out} = \frac{U_h(1 - \mathcal{M})\max(I_h/I_{panic} - 1, 0)}{\tau_{out}},$$
$$\Phi_{in} = \frac{M_h(1 - \mathcal{M})\max(1 - I_h/I_{return}, 0)}{\tau_{in}}. \quad (10)$$

Outward migration occurs only after disease prevalence exceeds a perception threshold I_{panic}, representing behavioural response to epidemic risk. The linear dependence near this threshold provides a first-order approximation of a more general response function. Return migration occurs on the longer recovery timescale τ_{in} when $I_h < I_{return}$. The dependence of migration on malnutrition reflects the assumption that sufficient health is required for individuals to undertake migration.

Migration is included as a potential demographic response to plague but is not modelled as a mechanism of spatial disease transmission. Migrating people could in principle transport *Y. pestis* through infected individuals or vectors; however, because the model is zero-dimensional, it applies only to a specific region and does not represent transmission between spatially distinct populations. The treatment of migration serves solely to test the hypothesis that disease-driven population movement can reduce mortality within the local affected population.

The third term in Eq (9) is the population recovery after the demographic shock, with improving fertility and life-expectancy, restoring U_h to its initial level, $U_{h,0}$. The fourth and fifth terms are the plague-infection terms, each being the product of susceptible human and infected (vector or human) densities and a transmission coefficient increasing with $\mathcal{M}$ (e.g., $d_h(1 + \tilde{\alpha}_v \mathcal{M})^p$, where d_h, $\tilde{\alpha}_v$ and p are constants). The final term in Eq (9) is malnutrition-related non-plague mortality (μ).

https://doi.org/10.5194/egusphere-2026-5195
Preprint. Discussion started: 8 September 2026
© Author(s) 2026. CC BY 4.0 License.

The infected human population is separated into vector-borne and pneumonic transmission pathways:

$$\frac{dI_{hv}}{dt} = -\frac{I_{hv}}{\tau_{I,mort,v}} - \frac{I_{hv}}{\tau_{I,rec}} + d_h(1+\tilde{\alpha}_v\mathcal{M})^p U_h I_v - \frac{I_{hv}}{\tau_{I,p}}\ , \tag{11}$$

$$\frac{dI_{hvp}}{dt} = -\frac{I_{hvp}}{\tau_{I,mort,h}} + \frac{I_{hv}}{\tau_{I,p}}, \tag{12}$$

$$\frac{dI_{hh}}{dt} = -\frac{I_{hh}}{\tau_{I,mort,h}} + h_h(1+\tilde{\alpha}_h\mathcal{M})^p U_h(I_{hh}+I_{hvp}). \tag{13}$$

Only vector-mediated infections can recover ($\tau_{I,rec}$), whereas pneumonic infections are always fatal ($\tau_{I,mort,h} < \tau_{I,mort,v}(\mathcal{M})$). Vector-borne infections may progress to secondary pneumonic infections that are infectious to humans ($\tau_{I,p}$). Recovery and migration compartments change according to

$$\frac{dR_h}{dt} = \frac{I_{hv}}{\tau_{I,rec}} - \frac{R_h}{\tau_{wane}} - \mu R_h, \tag{14}$$

$$\frac{dM_h}{dt} = \Phi_{out} - \Phi_{in} - \mu M_h. \tag{15}$$

Terms in Eq (14) treat recovery of vector-mediated infected humans, waning of immunity for return to the susceptible compartment and malnutrition-related non-plague mortality respectively. Finally, plague and non-plague malnutrition-related deaths are tracked using the passive variables

$$\frac{dD_h}{dt} = \frac{I_{hv}}{\tau_{I,mort,v}} + \frac{I_{hh}}{\tau_{I,mort,h}} + \frac{I_{hvp}}{\tau_{I,mort,h}}, \tag{16}$$

$$\frac{dD_m}{dt} = \mu(U_h + R_h + M_h). \tag{17}$$

Together, Eqs (7)–(15) define the coupled epidemic model, with Eqs (16) and (17) providing cumulative mortality.

2.4 Non-dimensional Formulation of the Epidemiological Model

2.4.1 General Formulation

The epidemiological model (Sec. 2.3) is expressed with dimensionless quantities denoted by a tilde symbol:

$$\frac{d\tilde{I}_r}{d\tilde{t}} = \tilde{e}_r(\tilde{t}) - \tilde{f}_r\tilde{I}_r\ , \tag{18}$$

$$\frac{d\tilde{I}_v}{d\tilde{t}} = \tilde{g}_v\,\tilde{I}_h(1-\tilde{I}_v) + \tilde{g}_{rv}\,\tilde{I}_r(1-\tilde{I}_v) - \tilde{I}_v\ . \tag{19}$$

https://doi.org/10.5194/egusphere-2026-5195
Preprint. Discussion started: 8 September 2026
© Author(s) 2026. CC BY 4.0 License.

Here $\tilde{t} = t/\tau_v$, while $\widetilde{g_v} = g_v U_{h,0} \tau_v$ with $\tilde{I}_v = I_v/U_{v,0}$ and $\tilde{I}_r = I_r/U_{r,0}$ where $U_{v,0}$ and $U_{r,0}$ are the reference values of total number density of all vectors and reservoir host animals respectively (e.g. initial values of I_v and I_r). Also, $\widetilde{g_{rv}} = g_{rv} U_{r,0} \tau_v$, and $\widetilde{f_r} = \tau_v/\tau_r$ while the external seeding term is $\widetilde{e_r} = \tau_v e_r(\tilde{t})/U_{r,0}$. For now, we treat $\widetilde{e_r}$ as a prescribed function of time, but in general it may also depend on the intensity of the climate shock. Similarly, $\tilde{I}_h = I_h/U_{h,0}$.

$$\frac{d\tilde{U}_h}{d\tilde{t}} = -\tilde{\Phi}_{out} + \tilde{\Phi}_{in} + \frac{1-\tilde{U}_h}{\tilde{\tau}_{U,pop}} - \widetilde{d_h}\tilde{U}_h \tilde{I}_v - \widetilde{h_h}\tilde{U}_h \left(\tilde{I}_{hh} + \tilde{I}_{hvp}\right) + \widetilde{f_h}\tilde{R}_h - \tilde{\mu}\tilde{U}_h \,. \tag{20}$$

Here $\tilde{U}_h = U_h/U_{h,0}$ while $\tilde{I}_h = I_h/U_{h,0}$, $\tilde{I}_{hv} = I_{hv}/U_{h,0}$, $\tilde{I}_{hvp} = I_{hvp}/U_{h,0}$ and $\tilde{I}_{hh} = I_{hh}/U_{h,0}$. Also, $\tilde{\Phi}_{out} = \tilde{U}_h(1 - \mathcal{M})\max(\tilde{I}_h/\tilde{I}_{panic} - 1, 0)/\tilde{\tau}_{out}$ with $\tilde{\tau}_{out} = \tau_{out}/\tau_v$ and $\tilde{\Phi}_{in} = \tilde{M}_h(1 - \mathcal{M})\max\left(1 - \frac{\tilde{I}_h}{\tilde{I}_{return}}, 0\right)/\tilde{\tau}_{in}$ with $\tilde{\tau}_{in} = \tau_{in}/\tau_v$. The slow relaxation demographically to the initial population after the shock is on the time-scale $\tilde{\tau}_{U,pop} = \tau_{U,pop}/\tau_v = 9.1 \times 10^3$. Also, $\widetilde{d_h} = d_h \tau_v U_{v,0}\, \tilde{c}_v$ where $\tilde{c}_v = (1 + \tilde{\alpha}_v \mathcal{M})^2$ and $\widetilde{h_h} = h_h U_{h,0}\, \tau_v\, \tilde{c}_h$ where $\tilde{c}_h = (1 + \tilde{\alpha}_h \mathcal{M})^2$ and $\widetilde{f_h} = \tau_v/\tau_{wane}$ while $\tilde{R}_h = R_h/U_{h,0}$.

$$\frac{d\tilde{I}_{hv}}{d\tilde{t}} = -\widetilde{j_h}\tilde{I}_{hv} + \widetilde{d_h}\tilde{U}_h \tilde{I}_v - \widetilde{f_p}\tilde{I}_{hv} \,, \tag{21}$$

$$\frac{d\tilde{I}_{hvp}}{d\tilde{t}} = -\widetilde{k_h}\tilde{I}_{hvp} + \widetilde{f_p}\tilde{I}_{hv} \,, \tag{22}$$

$$\frac{d\tilde{I}_{hh}}{d\tilde{t}} = -\widetilde{k_h}\tilde{I}_{hh} + \widetilde{h_h}\tilde{U}_h(\tilde{I}_{hh} + \tilde{I}_{hvp}) \,. \tag{23}$$

Here $\widetilde{j_h} = \tau_v/\tau_{\mathrm{I,ave}}$ where $\frac{1}{\tau_{\mathrm{I,ave}}} = \frac{1}{\tau_{I,\mathrm{mort,v}}} + \frac{1}{\tau_{I,\mathrm{rec}}}$. Here $\tau_{I,\mathrm{mort,v}} = a_I + b_I(1 - \mathcal{M})$ to express how malnutrition hastens death, boosting the case fatality rate, as is medically expected. Also $\widetilde{k_h} = \tau_v/\tau_{I,\mathrm{mort,h}}$ and $\tilde{I_h} = \tilde{I_{hvp}} + \tilde{I_{hv}} + \tilde{I_{hh}}$ while $\widetilde{f_p} = \tau_v/\tau_{I,p}$.

The recovered people density is $\tilde{R}_h = R_h/U_{h,0}$ and follows:

$$\frac{d\tilde{R}_h}{d\tilde{t}} = \frac{\tau_v}{\tau_{I,\mathrm{rec}}}\tilde{I}_{hv} - \widetilde{f_h}\tilde{R}_h - \tilde{\mu}\tilde{R}_h \,, \tag{24}$$

$$\frac{d\tilde{M}_h}{d\tilde{t}} = \tilde{\Phi}_{in} - \tilde{\Phi}_{out} - \tilde{\mu}\tilde{M}_h \,. \tag{25}$$

The dimensionless number of people killed from plague is $\tilde{D}_h = D_h/U_{h,0}$ and similarly for non-plague malnutrition-related deaths, $\tilde{D}_m = D_m/U_{h,0}$:

https://doi.org/10.5194/egusphere-2026-5195
Preprint. Discussion started: 8 September 2026
© Author(s) 2026. CC BY 4.0 License.

$$\frac{d\tilde{D}_h}{d\tilde{t}} = \widetilde{k_h}\tilde{I}_{hh} + \frac{\tau_v}{\tau_{I,\mathrm{mort,v}}}\tilde{I}_{hv} + \widetilde{k_h}\tilde{I}_{hvp}\,, \tag{26}$$

$$\frac{d\tilde{D}_m}{d\tilde{t}} = \tilde{\mu}(\tilde{U}_h + \tilde{M}_h + \tilde{R}_h)\,. \tag{27}$$

In summary, the complete model consists of eight coupled dimensionless evolution equations for reservoir hosts, vectors, humans, infection, recovery and migration (Eqs (18)–(25)), forced by the malnutrition index from the food-malnutrition component (Eqs (5)–(6)), which in turn is forced by the climate component. A passive equation tracks cumulative plague and malnutrition-related non-plague mortality (Eqs (26), (27)). Time is non-dimensionalised using the vector infectious lifetime, τ_v, while prognostic population densities are scaled by their respective reference (e.g., initial) values.

2.4.2 Parameter values for the standard case of the Justinianic Plague

The parameter values adopted for the standard representation of the Justinianic Plague and the climate shock following the 536/540 CE eruptions are justified in Appendix C and listed in Appendix D, together with a summary of all model variables.

3. Theoretical Analysis of Quasi-Equilibria, their Stability and Feedbacks

3.1 Approximate Equilibria

The epidemiological model (Sec. 2.4.1) has no true steady-state equilibrium because of time-dependent reservoir seeding, nonlinear migration, and waning immunity. However, before epidemic amplification it admits a quasi-equilibrium in which infection persists only at low levels in the reservoir, while vectors and humans remain almost entirely uninfected.

Assuming negligible human infection ($\tilde{I}_h \ll 1$), negligible migration, and weak feedback from humans, the reservoir equilibrium is

$$\tilde{I}_{r,eq} \approx \frac{\tilde{e}_r}{\tilde{f}_r}, \tag{28}$$

with

$$\tilde{I}_{v,eq} \approx 0,\ \tilde{U}_{h,eq} \approx 1. \tag{29}$$

To simplify the analysis, Eqs (21)-(23) are combined by assuming a constant fraction $\tilde{\phi} = (\tilde{I}_{hh} + \tilde{I}_{hvp})/\tilde{I}_h$, giving

$$\frac{d\tilde{I}_h}{d\tilde{t}} = -\tilde{J}_h^*\tilde{I}_h + \tilde{h}_h\tilde{U}_h\tilde{\phi}\tilde{I}_h + \tilde{a}_h\tilde{U}_h\tilde{I}_v, \tag{30}$$

https://doi.org/10.5194/egusphere-2026-5195
Preprint. Discussion started: 8 September 2026
© Author(s) 2026. CC BY 4.0 License.

where $\tilde{j}_h^* = \tilde{\phi}\tilde{k}_h + (1-\tilde{\phi})\tilde{j}_h$.

Retaining weak reservoir spillover gives, to leading order, $\tilde{I}_{v,eq} \sim \tilde{g}_{rv}\tilde{I}_{r,eq}$ so

$$\tilde{I}_{h,eq} \approx \frac{\tilde{d}_h \tilde{g}_{rv}}{\tilde{j}_h^*}\tilde{I}_{r,eq}, \tag{31}$$

where $\tilde{I}_{h,eq} \ll \tilde{I}_{r,eq}$. Equation (31) shows that the endemic human infection is proportional to the endemic infection in the reservoir, with the proportionality determined by reservoir-to-vector transmission, vector-to-human transmission, and human recovery/removal. Consequently, human infection is sustained by continual reservoir spillover rather than by a self-sustaining human–vector equilibrium. For representative parameters ($\tilde{e}_r \sim 10^{-6}$ on average), this endemic equilibrium corresponds to $\tilde{I}_{r,eq} \sim 10^{-4}$, $\tilde{I}_{v,eq} \sim 10^{-5}$, and $\tilde{I}_{h,eq} \sim 2 \times 10^{-5}$.

Hence, the pre-epidemic baseline is governed by slow reservoir persistence, with vector and human infection remaining slaved to the reservoir until amplification drives the system into the epidemic regime. The model also admits the trivial disease-free equilibrium, $\tilde{I}_{r,eq} = \tilde{I}_{v,eq} = \tilde{I}_{h,eq} = 0$.

Finally, there is also a long-term stable endemic quasi-equilibrium that the system tends towards as noted below (Sec. 3.2).

3.2 Stability and Feedback Analysis

Explosion from disease-free state. Linearising Eq (30) about the disease-free state, with $\tilde{I}_h = \delta\tilde{I}_h$and $\tilde{I}_v = \delta\tilde{I}_v$, gives

$$\frac{d\,\delta\tilde{I}_h}{d\tilde{t}} \approx \tilde{\eta}_h\,\delta\tilde{I}_h,$$
$$\tilde{\eta}_h \approx \widetilde{U}_h(\tilde{\phi}\tilde{h}_h + \tilde{\phi}_v\tilde{d}_h) - \tilde{j}_h^*(\tilde{\phi}). \tag{32}$$

Here $\tilde{\eta}_h$ is the dimensionless growth rate of infected humans. The two terms in the expression for it represent positive feedbacks from human-to-human (depending on pneumonic infected humans) and vector-to-human transmission (depending on infected vector density), and a negative feedback from depletion of infected humans from death and recovery. The positive 'transmission' feedback must weaken as $\widetilde{U}_h$ and $\tilde{\phi}_v$ decrease with time, until the net feedback becomes negative.

https://doi.org/10.5194/egusphere-2026-5195
Preprint. Discussion started: 8 September 2026
© Author(s) 2026. CC BY 4.0 License.

Initially, infection is confined to the reservoir and vector populations, with only negligible human infection, so $\tilde{\phi}_v = \tilde{I}_v/\tilde{I}_h \gg 1$. During the initial stage of epidemic amplification, feedback from infected humans to vectors remains negligible, so Eq. (19) reduces to $d\tilde{I}_v/d\tilde{t} \approx \tilde{g}_{rv}\tilde{I}_r$, since $\tilde{I}_r$varies only on the much longer reservoir timescale. Thus $\tilde{I}_v \approx \tilde{I}_{v,0} + \tilde{g}_{rv}\tilde{I}_r\Delta\tilde{t}$, whereas Eq. (32) gives $\tilde{I}_h \propto e^{\tilde{\eta}_h\Delta\tilde{t}}$. Consequently, $\tilde{\phi}_v$decreases with time, reducing the vector contribution to the growth rate in Eq. (32). Then as humans become infected during the explosive growth of the epidemic, there is a transition to a quasi-equilibrium of Eq (19) with $\tilde{\phi}_v \to \tilde{g}_v$, with rapid vector equilibration ($\delta\tilde{I}_v \approx \tilde{g}_v\delta\tilde{I}_h$).

For growth from an initial disease-free state, assuming $\tilde{U}_h = 1$, $\mathcal{M} \approx 0.5$, $\tilde{\phi} \approx 0.5$ and $\tilde{\phi}_v \approx 1$, the standard parameter set gives $\tilde{\eta}_h \approx 1.3$. This corresponds to a threefold increase in infection over a dimensionless time $\Delta\tilde{t} \approx 1$ (about 4 days), which justifies the choice of timescale (4 days) for normalization of time. Since $\tilde{\eta}_h > 0$, the disease-free equilibrium is unstable: a positive feedback from direct human transmission ($\tilde{h}_h$) and vector-mediated transmission ($\tilde{d}_h\tilde{g}_v$) outweighs losses due to recovery, mortality and migration represented by $\tilde{j}_h^*$. In Eq (32), $\tilde{\phi}_v$ decreases with time during the explosion, because as $\tilde{I}_v$ increases almost linearly initially ($\frac{d\tilde{I}_v}{d\tilde{t}} \sim \widetilde{g_{rv}}\,\widetilde{I_r}$) as $\widetilde{I_r}$ is as slowly varying as the external seeding, while $\tilde{I}_h$ increases exponentially, reducing the ratio of infected vectors to humans, $\tilde{\phi}_v$. Consequently, the growth rate $\tilde{\eta}_h$in Eq. (32) decreases. Eventually $\tilde{\eta}_h$ becomes negative and the peak of prevalence is reached: a negative feedback then prevails. Note how malnutrition, which linearly boosts $\tilde{h}_h$and $\tilde{d}_h$, is promoting the explosive growth. Figure 3 summarizes the competing positive and negative feedback pathways during epidemic growth.

Generally for any initial susceptible population, instability occurs when

$$\tilde{\eta}_h > 0 \Longrightarrow \tilde{U}_h > \tilde{U}_{h,\mathrm{crit}} \approx \frac{\tilde{j}_h^*(\tilde{\phi})}{\tilde{\phi}\tilde{h}_h + \tilde{\phi}_v\tilde{d}_h}. \tag{33}$$

From Eq (33), $\tilde{\eta}_h = \left(\tilde{U}_h - \tilde{U}_{h,\mathrm{crit}}\right)/(\tilde{\phi}\tilde{h}_h + \tilde{\phi}_v\tilde{d}_h)$. For the standard parameter set, initially ($\tilde{\phi} = 0.5$, $\tilde{j}_h^* = 1.25, \tilde{j}_h = 0.9, \tilde{k}_h = 1.6, \tilde{h}_h = 1.1$, $\tilde{d}_h = 2, \tilde{\phi}_v \sim 1$), $\tilde{U}_{h,\mathrm{crit}} \sim 0.5$ and $\tilde{\eta}_h > 0$. However, later once human infections are underway, when $\tilde{\phi}_v \approx \tilde{g}_v = 0.32$, then $\tilde{U}_{h,\mathrm{crit}} \sim 1.05$ and $\tilde{\eta}_h < 0$, so the explosive growth is soon curtailed, creating the initial major peak of infections.

Thus, the fraction of the population infected in the initial peak depends on how soon the growth of $\tilde{I}_h$ catches up with that of $\tilde{I}_v$ as the initial peak is approached, and on how quickly $\tilde{\phi}_v \to \tilde{g}_v$. As susceptibles are depleted, $\tilde{U}_h$falls below $\tilde{U}_{h,\mathrm{crit}}$, so Eq (33) predicts $\tilde{\eta}_h < 0$ and epidemic decline (Fig. 3b). Although the linearisation is no longer formally valid once nonlinear effects dominate, the sign change in $\tilde{\eta}_h$ correctly identifies the transition from epidemic growth to decay. The system relaxes toward the slowly varying reservoir-driven endemic state.

https://doi.org/10.5194/egusphere-2026-5195
Preprint. Discussion started: 8 September 2026
© Author(s) 2026. CC BY 4.0 License.

665

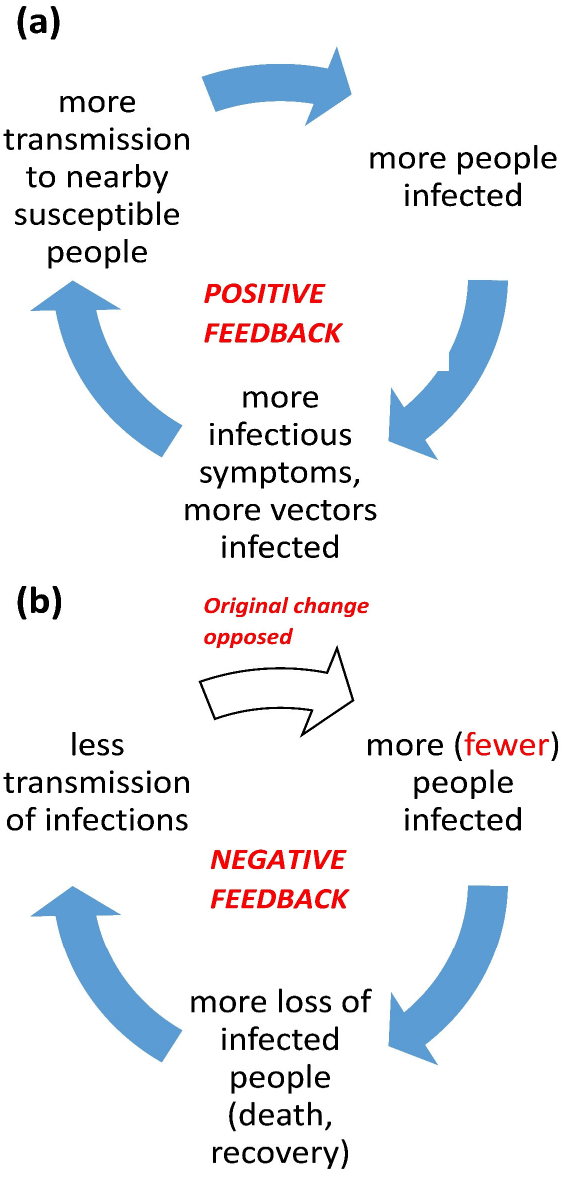

Figure 3: Schematic diagram of positive and negative feedbacks, for (a) explosive growth of an epidemic and (b) its limitation later.

https://doi.org/10.5194/egusphere-2026-5195
Preprint. Discussion started: 8 September 2026
© Author(s) 2026. CC BY 4.0 License.

Long-term behaviour. For the long-term phase-space behaviour, we consider an idealised 2D subsystem. Assuming rapid vector equilibration ($\tilde{g}_v\,\delta\tilde{I}_h \approx \delta\tilde{I}_v$) and neglecting recovery, migration and demographic terms in Eq (20), the evolution of perturbations about a trajectory $(\tilde{U}_h, \tilde{I}_h)$ is obtained by linearising Eqs (20) and (30). Defining $\tilde{\mathbf{X}} = (\delta\tilde{I}_h, \delta\tilde{U}_h)^T$ and $\tilde{K} = \tilde{\phi}\tilde{h}_h + \tilde{g}_v\tilde{d}_h$, the perturbation equations become

$$\frac{d\tilde{\mathbf{X}}}{d\tilde{t}} = \tilde{\mathbf{A}}\tilde{\mathbf{X}} = \tilde{\lambda}_h\tilde{\mathbf{X}},$$

$$\tilde{\mathbf{A}} = \begin{pmatrix} \tilde{K}\tilde{U}_h - \tilde{\jmath}_h^* & \tilde{K}\tilde{I}_h \\ -\tilde{K}\tilde{U}_h & -\tilde{K}\tilde{I}_h \end{pmatrix}. \tag{34}$$

The eigenvalues are

$$\tilde{\lambda}_h = \frac{\tilde{B} \pm \sqrt{\tilde{B}^2 - 4\tilde{K}\tilde{I}_h\tilde{\jmath}_h^*}}{2},$$

$$\tilde{B} = \tilde{K}\left(\tilde{U}_h - \tilde{U}_{h,\mathrm{crit}} - \tilde{I}_h\right). \tag{35}$$

Here, $\tilde{U}_{h,\mathrm{crit}} = \frac{\tilde{\jmath}_h^*}{\tilde{K}}$ is the critical threshold in the disease-free state. When $\tilde{I}_h \approx 0$, then the leading eigenvalue, $\tilde{\lambda}_h$, equals $\tilde{\eta}_h$. Perturbations evolve as $\tilde{\mathbf{X}} \propto e^{\tilde{\lambda}_h\tilde{t}}$ for the leading eigenvalue, so their amplitude is governed by

$$\mathrm{Re}\left(\tilde{\lambda}_h\right) \sim \frac{\tilde{B}}{2} \approx (\tilde{K}\tilde{U}_h - \tilde{\jmath}_h^* - \tilde{K}\tilde{I}_h)/2.$$

Positive values correspond to local instability and exponential amplification of perturbations, whereas negative values imply decay toward the local trajectory. The first term, $\tilde{K}\tilde{U}_h$, represents the positive transmission feedback from human and vector-mediated infection noted above (Fig. 3a). It is weakened by depletion of susceptible humans during the epidemic. The second term, $-\tilde{\jmath}_h^*$, (equivalently $-\tilde{K}\tilde{U}_{h,\mathrm{crit}}$) represents the negative feedback due to removal of infectious individuals through recovery and mortality, opposing transmission-driven growth (Fig. 3b). The third term, $-\tilde{K}\tilde{I}_h$, represents the nonlinear saturation associated with depletion of susceptible uninfected individuals. Since throughout the simulations $\tilde{I}_h \ll \tilde{U}_{h,\mathrm{crit}}$ (Sec. 5), susceptible depletion provides only a weak correction, and the dominant negative feedback is infectious removal through recovery and mortality. When $\tilde{B} = 0$, the eigenvalues are purely imaginary (provided $\tilde{K}\tilde{I}_h\tilde{\jmath}_h^* > 0$) with zero growth of the perturbation amplitude ($\mathrm{Re}\left(\tilde{\lambda}_h\right) = 0$). This defines the neutral boundary separating locally stable and unstable trajectories:

https://doi.org/10.5194/egusphere-2026-5195
Preprint. Discussion started: 8 September 2026
© Author(s) 2026. CC BY 4.0 License.

$$\boxed{\tilde{I}_h = \tilde{U}_h - \tilde{U}_{h,crit}}. \quad (36)$$

The endemic quasi-equilibrium, $\tilde{U}_{h,\mathrm{eq}} = \tilde{U}_{h,\mathrm{crit}} = \tilde{\jmath}_h^*/\tilde{K}$, lies within the stable region, as $\tilde{B} = -\tilde{I}_h\tilde{K} < 0$. Also, $\tilde{I}_{h,\mathrm{eq}}$ is controlled by the reservoir forcing as noted above. Near the neutral line ($\tilde{B}^2 < 4\tilde{K}\tilde{I}_h\tilde{\jmath}_h^*$), the root in Eq (35) is imaginary and the solution oscillates, spiralling around the quasi-equilibrium (an attractor). Explosive growth of the epidemic occurs where $\tilde{B} > 0$ (e.g. in the initial peak).

Figure 4 shows the phase plane, including the neutral line and the endemic equilibrium. Trajectories circulate anticlockwise while converging on the endemic equilibrium, which acts as a stable attractor. Immediately after epidemic onset the system lies in the unstable region, where the transmission positive feedback (Fig. 3a) drives rapid epidemic growth. As susceptible individuals are depleted, the trajectory crosses the neutral line into the stable region, quenching exponential growth and producing the epidemic peak before overshooting the endemic equilibrium. The subsequent motion consists of damped oscillations toward the attractor. If the reservoir equilibrium, $\tilde{I}_{r,eq}$, declines over longer timescales (e.g. due to weakening of seeding, $\tilde{e}_r$), the attractor moves along the line $\tilde{U}_h = \tilde{U}_{h,\mathrm{crit}}$ toward the disease-free state. The resulting succession of trajectories around the moving attractor gives rise to successive epidemic waves, whose amplitude is determined by the strength of the reservoir forcing.

An instantaneous effective reproduction number can be defined from Eq (30) as the ratio of infection sources to removal processes:

$$R_{\mathrm{eff}}(t) = \frac{\tilde{\phi}\tilde{h}_h\tilde{U}_h\tilde{I}_h + \tilde{d}_h\tilde{U}_h\tilde{I}_v}{\tilde{\jmath}_h^*\tilde{I}_h} = R_{\mathrm{eff},h} + R_{\mathrm{eff},v}, \quad (37)$$

where $R_{\mathrm{eff},h} = \tilde{\phi}\,\tilde{h}_h\tilde{U}_h/\tilde{\jmath}_h^*$, representing direct human-to-human transmission, and $R_{\mathrm{eff},v} = \tilde{d}_h\tilde{U}_h\tilde{I}_v/\tilde{\jmath}_h^*\tilde{I}_h$, representing vector-mediated transmission. Equivalently, the neutral condition $R_{\mathrm{eff}} = 1$ defines the instantaneous critical susceptible population once the epidemic is underway ($\tilde{g}_v \approx \tilde{I}_v/\tilde{I}_h$):

$$\tilde{U}_{h,\mathrm{crit}}(t) \approx \frac{\tilde{\jmath}_h^*}{\tilde{\phi}\tilde{h}_h + \tilde{d}_h\tilde{g}_v}. \quad (38)$$

Thus, $\tilde{U}_h > \tilde{U}_{h,\mathrm{crit}}$ corresponds to $R_{\mathrm{eff}} > 1$ and epidemic growth, whereas $\tilde{U}_h < \tilde{U}_{h,\mathrm{crit}}$ gives $R_{\mathrm{eff}} < 1$ and epidemic decline. The neutral line in the phase plane (Fig. 4, full black line) represents the instantaneous threshold $R_{\mathrm{eff}} = 1$, separating regions of epidemic amplification and decline.

https://doi.org/10.5194/egusphere-2026-5195
Preprint. Discussion started: 8 September 2026
© Author(s) 2026. CC BY 4.0 License.

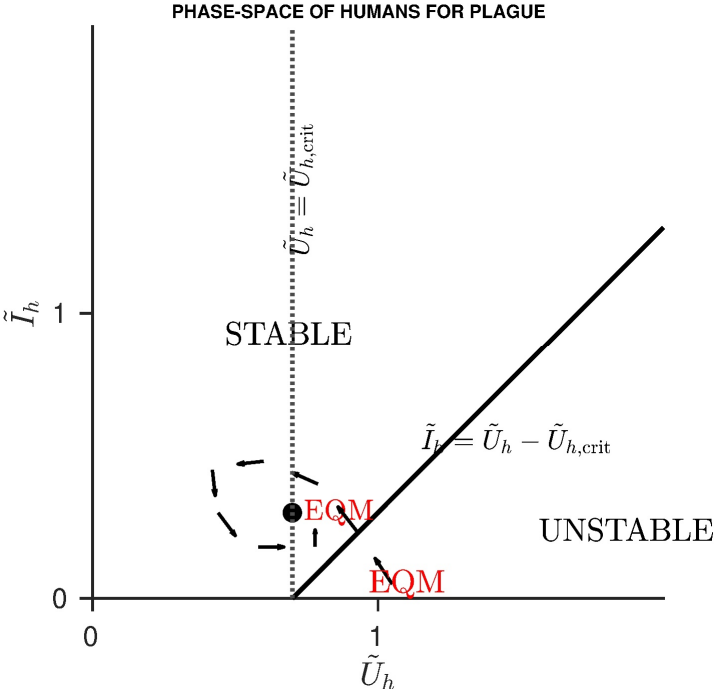

Figure 4: A schematic diagram of the phase-space of infected, $\tilde{I}_h$, and uninfected susceptible, $\tilde{U}_h$, humans. Equilibria can either lie on $\tilde{I}_h = 0$ line (disease free equilibrium, 'EQM') or at a point (black dot) on the $\tilde{U}_h = \tilde{U}_{h,crit}$ line (endemic disease equilibrium, 'EQM' also). The neutral line is (full black line) shown separating realms of stability and instability of perturbations to the trajectory during the epidemic.

In summary, in the formulation, population density enters multiplicatively through the contact terms, causing the effective growth rate (and equivalently the reproduction number) to scale almost linearly with susceptible population density. This produces a threshold population density above which coupled pneumonic–vector transmission becomes self-sustaining. Only sparsely inhabited regions with densities below about 5 people km^{-2} are predicted to remain below this threshold, whereas more densely populated agricultural or urban environments are predicted to support epidemic amplification.

4. Results for Validation of Model

Evaluation, against observations, of the climate-harvest-malnutrition (Campbell 2010; Broadbury *et al.* 2015) and malnutrition-disease (Godde *et al.* 2025) linkages in response to a climate shock are shown in Appendix E for an alternative case. This is the food crisis during the Black Death in England after the 1345 CE eruption, which was almost a super-eruption. Agreement of the predictions with observations is generally adequate.

https://doi.org/10.5194/egusphere-2026-5195
Preprint. Discussion started: 8 September 2026
© Author(s) 2026. CC BY 4.0 License.

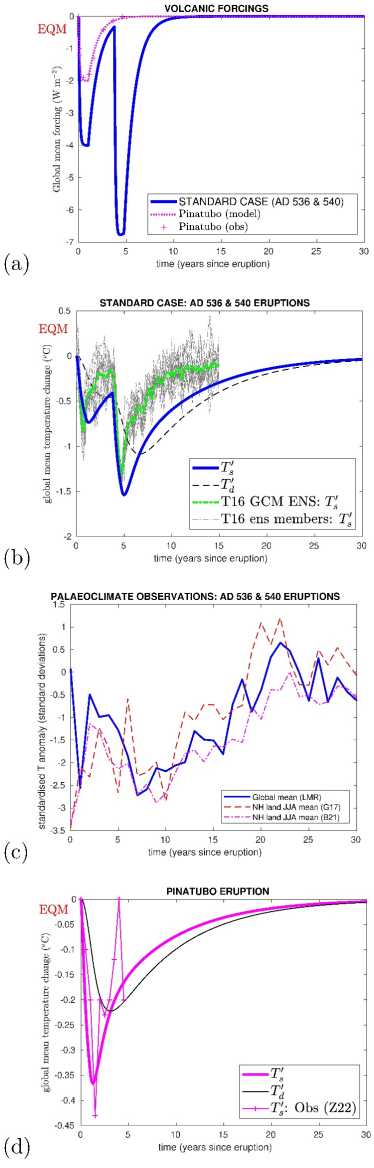

Figure 5: Evolution of volcanic forcing and climate response. (a) Global mean radiative forcing for the standard case (536 and 540 CE eruptions) and for the Pinatubo (1991) eruption. Satellite observations of Pinatubo forcing from GloSSAC are also shown. (b) Predicted surface and deep-ocean temperature anomalies for the standard case, compared with the ensemble simulations of Toohey *et al.* (2016). (c) Predicted NH summer land temperature response compared with reconstructions from Guillet *et al.* (2017; 'G17'), Last Millennium Reanalysis v2.1 (Tardif *et al.* 2019; 'LMR'), and Büntgen *et al.* (2021; 'B21'). (d) Predicted temperature response to the Pinatubo eruption compared with observations from the Hadley Centre/Climatic Research Unit Temperature dataset (version 5) by Morice *et al.* (2021), reproduced from Zanchettin *et al.* (2022; 'Z22').

https://doi.org/10.5194/egusphere-2026-5195
Preprint. Discussion started: 8 September 2026
© Author(s) 2026. CC BY 4.0 License.

5. Results for the Control Simulation of the Standard Case

5.1 Time-dependent Boundary Conditions

5.1.1 Climate Cooling

Figure 5a–b shows the numerical integration of Eqs. (1)–(3) for the standard 536/540 CE climate shock ('control simulation'). The model reproduces the observed global cooling following Pinatubo (−0.3 °C) and predicts peak global mean coolings of about −0.75 and −1.5 °C following the 536 and 540 CE eruptions, respectively, with each peak occurring about one year after the eruption. These values are consistent with the climate simulations of Toohey *et al.* (2016).

Applying the Northern Hemisphere amplification in Toohey *et al.* (2016) gives a peak NH mean cooling of about −2.3 °C. Accounting for the lower effective heat capacity of land relative to ocean gives an estimated peak NH land cooling of about −3 °C. This lies within the upper range of tree-ring-based temperature reconstructions (Büntgen *et al.* 2016, 2017, 2021; Sigl *et al.* 2015; Guillet *et al.* 2017).

The model gives a cooling recovery timescale of approximately 5 years, compared with about 2–2.5 years in the MPI climate simulations of Toohey *et al.* (2016) and about 8 ± 1 years in the tree-ring and temperature-proxy reconstructions of Guillet *et al.* (2017) and Tardif *et al.* (2019). The intermediate recovery timescale of the simple model therefore lies between the shorter simulated climate response and the longer proxy-based recovery.

Overall, the model reproduces the approximate magnitude and multi-year persistence of the post-536/540 cooling, providing the climate boundary condition for the subsequent food-storage and malnutrition simulations.

5.1.2 Crop Failure and Malnutrition Response

Proxy evidence from tree-ring reconstructions, archaeological activity records, and historical narratives indicates acute climatic and food stress following major volcanic eruptions (Stothers 1984; Rampino *et al.* 1988; Baillie 1991, 1994). We therefore distinguish an acute food-shortage phase from a subsequent recovery phase. Climate-model simulations and palaeoclimate evidence suggest that environmental perturbations following the 536–540 CE eruptions may have persisted for about two decades (van Dijk *et al.* 2022, 2023; Helama *et al.* 2018). Sea-ice feedbacks and oceanic heat exchange provide a possible mechanism for a prolonged cooling response, as simulated for Tambora eruption in 1815 (Stenchikov *et al*. 2009).

Figure 6a shows that the standard CE 536/540 eruption case (Sec. 5.1.1), using the parameters described in Sec. 2.2.2, is predicted to produce an acute food-shortage phase followed by about two decades of depressed food-storage conditions for the majority population (60%). Food storage declines over approximately 6 years to almost 10% of normal levels, while malnutrition reaches almost 0.75 after 7 years, about 3 years after the second eruption and 1 year after peak cooling. No direct malnutrition mortality is predicted for this population.

https://doi.org/10.5194/egusphere-2026-5195
Preprint. Discussion started: 8 September 2026
© Author(s) 2026. CC BY 4.0 License.

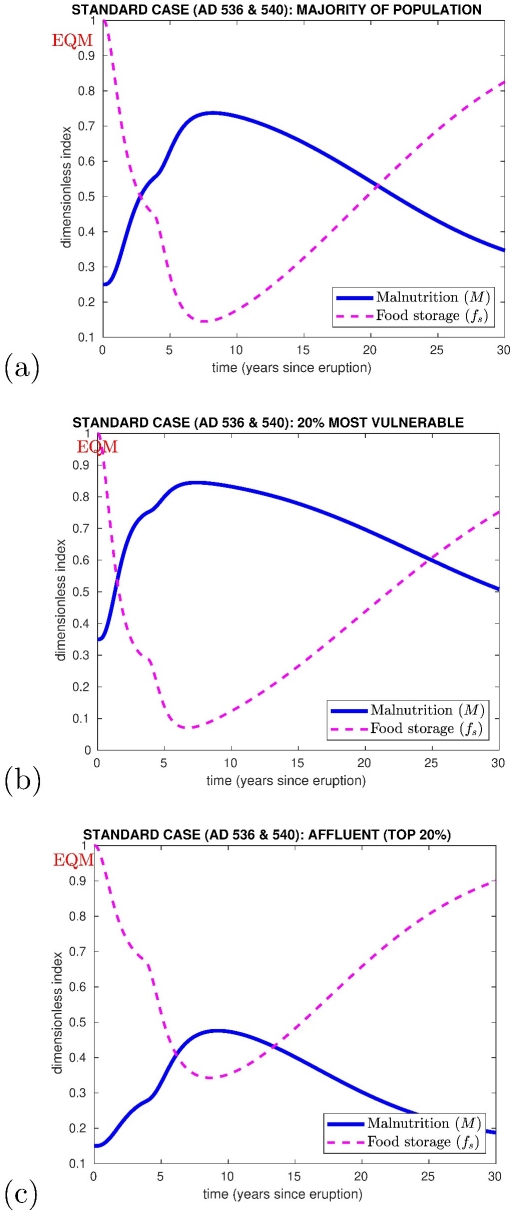

790 **Figure 6: Control simulations of malnutrition and food storage indices ($\mathcal{M}$ and f_s), for the standard case of the 536 and 540 CE eruptions. Time (years) plotted is since the first eruption (536 CE). Numerical integration of Eqs (4)-(6) is applied. Sectors of the population are shown for (a) the majority, (b) most vulnerable 20%, along with (c) the affluent (top 20%).**

https://doi.org/10.5194/egusphere-2026-5195
Preprint. Discussion started: 8 September 2026
© Author(s) 2026. CC BY 4.0 License.

For the vulnerable population, food storage falls to about 5% of normal levels by Year 5, while malnutrition remains severe from 538 to 551 CE. Indeed, the predicted global cooling exceeds the peak from Pinatubo (0.35 ºC) over approximately this same time period by up to a factor of 4 (Fig. 5b,d). If plague mortality were neglected, this collapse of food storage (to 5%) would produce appreciable mortality from malnutrition-related causes alone (Sec. 6). Most non-plague malnutrition-associated mortality is mediated through increased susceptibility to disease rather than direct starvation alone (Ljungqvist *et al*. 2024). Finally, recovery of the food storage is predicted to require external replenishment of seed resources.

In all three scenarios, it takes over a decade for recovery of $M$and f_s from the nutritional shock. Archaeological observations from fourteenth-century England suggest that the health consequences of nutritional deprivation can persist considerably longer than the immediate period of famine. DeWitte and Slavin (2013), for example, report evidence for chronic shortages of protein, calcium and vitamin B12 lasting at least one generation following the Great Famine and subsequent Great Bovine Pestilence. Thus, the model's assumption that nutritional vulnerability can persist beyond the immediate food shock is consistent with historical evidence (Sec. 7).

5.2 Epidemiological Simulation of Plague in Standard Case

The three population sectors identified in Sec. 5.1.2, namely the majority (60%), vulnerable (20%), and affluent (20%) sectors, were simulated separately using the simplified epidemiological model, with each sector retaining its own time-dependent malnutrition history (majority-, vulnerable-, and affluent-population scenarios). The overall population response may be inferred by weighting these scenarios according to their assumed population fractions.

For each scenario, Eqs (18)–(27) (Sec. 2.4.1) were solved numerically for the standard climate-forcing case, including the 536 (simulation start) and 540 CE eruptions. The corresponding malnutrition histories from the climate–harvest/food simulations (Sec. 5.1.2) were imposed as external boundary conditions, allowing transmission rates and migration responses to vary with nutritional state. Unless otherwise stated, $\tilde{I}_r$, $\tilde{I}_v$, $\tilde{I}_{hv}$, $\tilde{I}_{hvp}$, and $\tilde{I}_{hh}$were initialized at zero and $\tilde{U}_h = \tilde{U}_{h,0} = 1$.

To represent repeated introductions of plague from wildlife reservoirs, pulses in the reservoir-seeding parameter $\tilde{e}_r$ were applied every five years, beginning in 541 CE, corresponding to the earliest reports of plague in Europe (Sec. 1). Thus, climate forcing affects epidemic dynamics indirectly through its influence on malnutrition, which modifies both infection susceptibility and human mobility. In reality, the seeding events are driven by the volcanic climate shock, but in the present study they are prescribed without treating that dependency explicitly. Results for the control simulation in all scenarios are shown in Table 3 and described as follows.

https://doi.org/10.5194/egusphere-2026-5195
Preprint. Discussion started: 8 September 2026
© Author(s) 2026. CC BY 4.0 License.

Table 3: **Statistics for the three population-resilience scenarios of the control simulation for the standard case, starting in 536 CE. Values are percentages of the initial population. Over the entire simulation, peak prevalence denotes maximum simultaneous infection, and mortality denotes cumulative plague, malnutrition-related, and total mortality from both. Population-weighted values are given for the three scenarios combined.**

Population scenario	Population share (%)	Peak prevalence (%)	Plague mortality, year 1 (%)	Final plague mortality (%)	Malnutrition mortality (%)	Total mortality (%)	Population infected (%)	Migration (%)
Majority	60	1.9	15	38	19	**57**	41	46
Vulnerable	20	3.5	24	36	35	**71**	38	44
Affluent	20	0.7	14	27	3	**30**	29	14
Population-weighted	**100**	—	**17**	**36**	**19**	**55**	**38**	**39**

5.2.1 Majority-Population Scenario

Figure 7a shows the epidemic evolution for the standard case in the majority-population scenario. The first epidemic wave reaches a peak prevalence of $\tilde{I}_h \approx 0.019$ at $\tilde{t} = 482$ (5.3 years into simulation), about three months after the epidemic onset. By the end of the first and second years of the epidemic, cumulative plague-related deaths reach about 15% and 29% of the initial population, respectively. During the first seven years, four prevalence peaks occur, with the second, third and fourth peaks being successively weaker at prevalences of 0.3%, 0.09% and 0.03% respectively. Thereafter, epidemic waves become controlled directly by reservoir spillover events, weakening at peak prevalences of 10^{-6}% to 10^{-7} %. This behaviour is qualitatively consistent with Byzantine historical accounts of severe initial mortality (Sections 1 and 2.3.2).

By the end of the first year, 16% of the population has been infected, of whom almost three quarters are from human-to-human transmission. About 46% of the population has migrated away temporarily from the epidemic region, with return migration occurring over subsequent years.

https://doi.org/10.5194/egusphere-2026-5195
Preprint. Discussion started: 8 September 2026
© Author(s) 2026. CC BY 4.0 License.

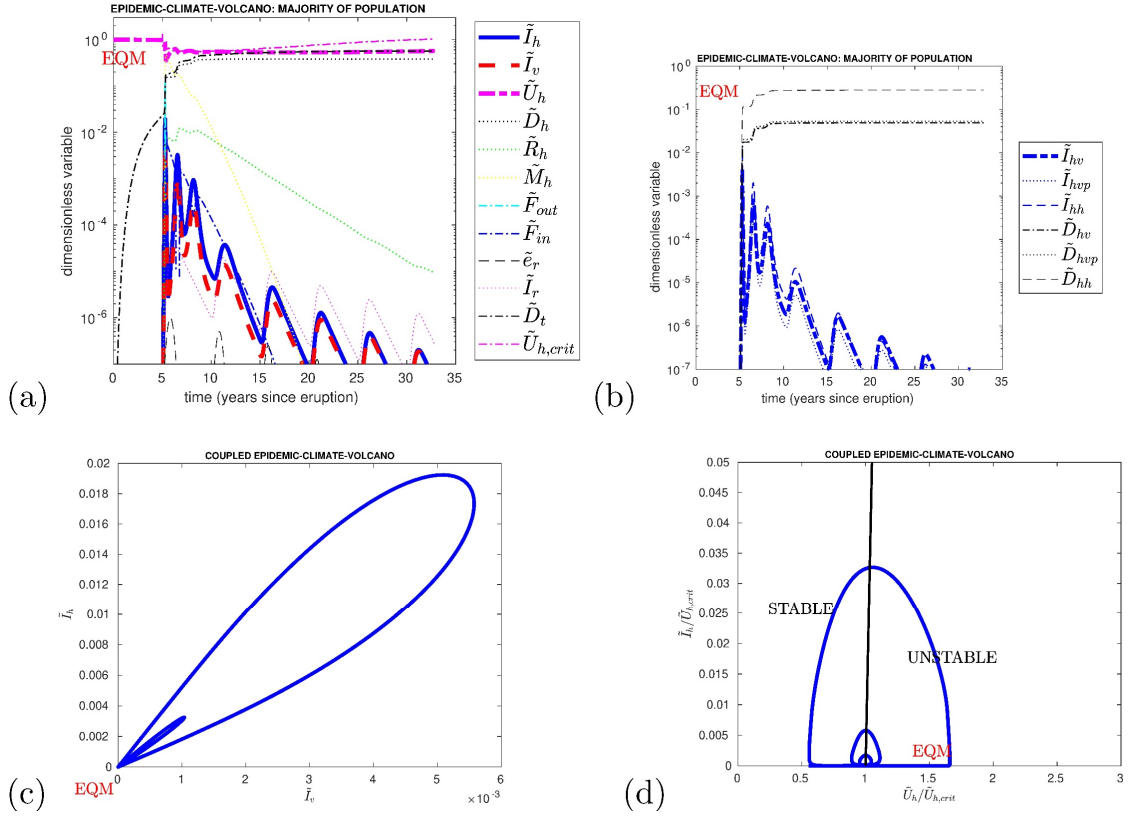

Figure 7: For the majority of the population following the eruption in 536 CE, the (a) evolution of plague over time of the system, Eqs (18)-(27). All prognostic variables are shown including those for infected vectors and humans and uninfected humans (thick lines). Cumulative deaths from the plague (faint black dotted line) and including also those from malnutrition (black dot-dashed line) are shown. The initial pre-epidemic equilibrium is marked ('EQM'). Shown in (b) are components of infectious prevalence and plague deaths arising from human-to-human (subscript 'hh') and vector-borne (subscripts 'hv' and 'hvp') transmission. Also, shown is the trajectory on the phase-spaces for (c) infected vectors and humans, and (d) infected humans and the ratio between uninfected susceptible humans and their critical threshold ($\tilde{U}_h/\tilde{U}_{h,crit}$). The neutral line (thick black line) separates the realms of stability and instability (Eq (35)).

The susceptible population rapidly declines to $\tilde{U}_h \approx 0.6$ during the first peak, largely due to this initial migration pulse and epidemic mortality, and subsequently remains near that value for the rest of the simulation. Because vectors equilibrate rapidly ($\tau_v = 4$ days), infected vectors closely track infected humans, producing the approximate proportionality between $\tilde{I}_v$ and $\tilde{I}_h$ (Fig. 7c). At later times, the system oscillates near the neutral line around transient quasi-attractors determined by successive reservoir-seeding events (Fig. 7d).

https://doi.org/10.5194/egusphere-2026-5195
Preprint. Discussion started: 8 September 2026
© Author(s) 2026. CC BY 4.0 License.

By the onset of the fourth epidemic wave (5.4 years after disease onset), cumulative plague mortality reaches approximately 38% of the initial population, with little extra mortality over the next two decades until the end of the simulation. Almost three quarters of plague deaths arise from pneumonic human-to-human transmission, while the remaining quarter are from vector-mediated transmission, of which almost half the deaths are purely bubonic and the rest being secondary pneumonic (Fig. 7b). The budget of total infections follows a similar ratio. Also, the total population (including births during the simulation) increases by approximately 14% over three decades.

In the first major peak, the initial explosive growth of prevalence occurs while $\widetilde{U}_h > \widetilde{U}_{h,\mathrm{crit}} \approx 0.6$, placing the system in the unstable regime described in Sec. 4 (Fig. 7d). The peak is created by $\widetilde{U}_h$ declining to equal $\widetilde{U}_{h,\mathrm{crit}}$. Just after the peak is reached, subsequent depletion of susceptible humans moves the system into the stable regime ($\widetilde{U}_h < \widetilde{U}_{h,\mathrm{crit}}$), causing progressively weaker prevalence. During the subsequent decades of plague, slight oscillations occur as $\widetilde{U}_h$ crosses the approximate stability boundary, though always remaining close to it.

5.2.2 Vulnerable-Population Scenario

Figure 8 shows that, compared with the majority-population scenario, the vulnerable population experiences a stronger initial epidemic response because of the higher malnutrition level. The first prevalence peak (3.5%) and first-year plague mortality (24%) are greater. Malnutrition mortality is also substantial, reaching about 33% by the end of the first year, accompanied by substantial migration (44% leaving and 16% returning in the first year).

However, the more severe nutritional shock rapidly depletes the susceptible population especially through both non-plague mortality and early plague-driven migration. The uninfected susceptible population falls to 50% at the first epidemic peak, after which $\widetilde{U}_h < \widetilde{U}_{h,\mathrm{crit}}(t)$, with an effective reproduction number (R_{eff}) below unity, (Fig. 8a). Consequently, after the initial outbreak, infection prevalence falls rapidly to low levels ($\sim 10^{-6}$ to 10^{-5}) for the rest of the first year.

By the end of the simulation, cumulative malnutrition mortality reaches approximately 35%, while plague mortality is limited to 36% of the initial population because the susceptible population has been substantially depleted. Slightly fewer become infected than in the majority-population scenario. Thus, although severe malnutrition initially amplifies plague transmission and mortality, it limits sustained epidemic spread by depleting susceptible individuals through non-plague mortality and migration. The total mortality from malnutrition and plague combined is increased to 71% from 57% for the majority scenario.

https://doi.org/10.5194/egusphere-2026-5195
Preprint. Discussion started: 8 September 2026
© Author(s) 2026. CC BY 4.0 License.

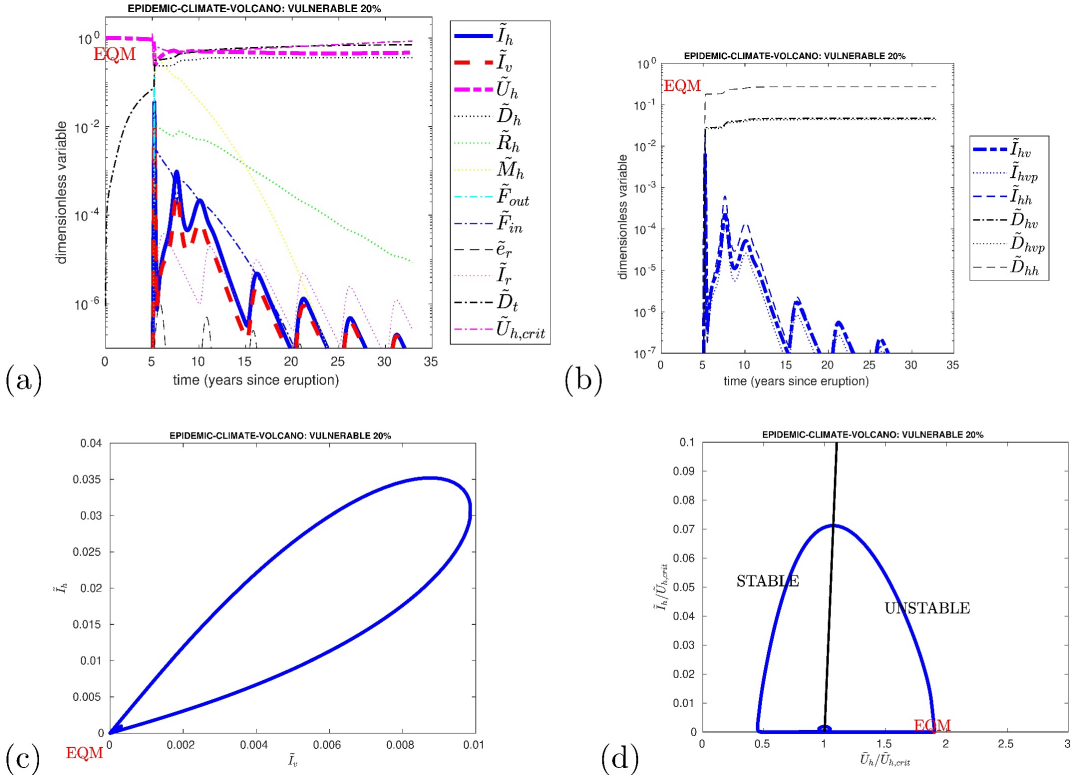

Figure 8: For the most vulnerable (20%) sector of the population, the plague as a function of time after 536 CE is shown, as well as the phase-spaces, plotted as in Fig. 7.

5.2.3 Affluent-Population Scenario

Figure 9 shows the simulation for the affluent 20% of the population (Fig. 6c). Compared with the majority-population scenario, improved nutritional status substantially reduces the severity of the epidemic. The first prevalence peak is delayed by half a year and reaches only 0.7%. Consequently, there is only weak migration (14%). With the much lower malnutrition index (40% versus 70% at the end of the first year of disease), first-year plague mortality (14%) is slightly lower than in the majority scenario, remaining lower thereafter.

By the end of the simulation, fewer (29%) of the population have been infected (two thirds of which are from human-to-human transmission). Very few malnutrition deaths (only 3%) occur, and eventual plague mortality is reduced to 27%.

https://doi.org/10.5194/egusphere-2026-5195
Preprint. Discussion started: 8 September 2026
© Author(s) 2026. CC BY 4.0 License.

5.2.4 Comparison of population scenarios and combined mortality

Weighting the three scenarios according to their assumed population fractions yields an overall plague mortality of approximately 36% after three decades, together with approximately 19% mortality from malnutrition-related non-plague causes (Table 3). The weighted plague mortality (36%) lies within the historical range of about 50% estimated for the First Plague Pandemic over two centuries and 20-30% for the first epidemic wave (Sec. 1).

Figure 10 shows that the contrasting scenarios demonstrate a nonlinear effect of malnutrition: greater nutritional stress amplifies the initial epidemic in the first year or so, but can subsequently suppress transmission by depleting the susceptible population through malnutrition mortality and migration in subsequent years. The vulnerable population experiences a stronger initial epidemic (prevalence up to almost 4% higher) than the control majority scenario because of greater malnutrition, but the subsequent depletion of susceptible individuals (by up to about 0.1 or 0.2 after the first year) through malnutrition mortality (long-term) and migration (short-term) suppresses later plague transmission. Plague mortality alone is slight reduced even (by 0.02).

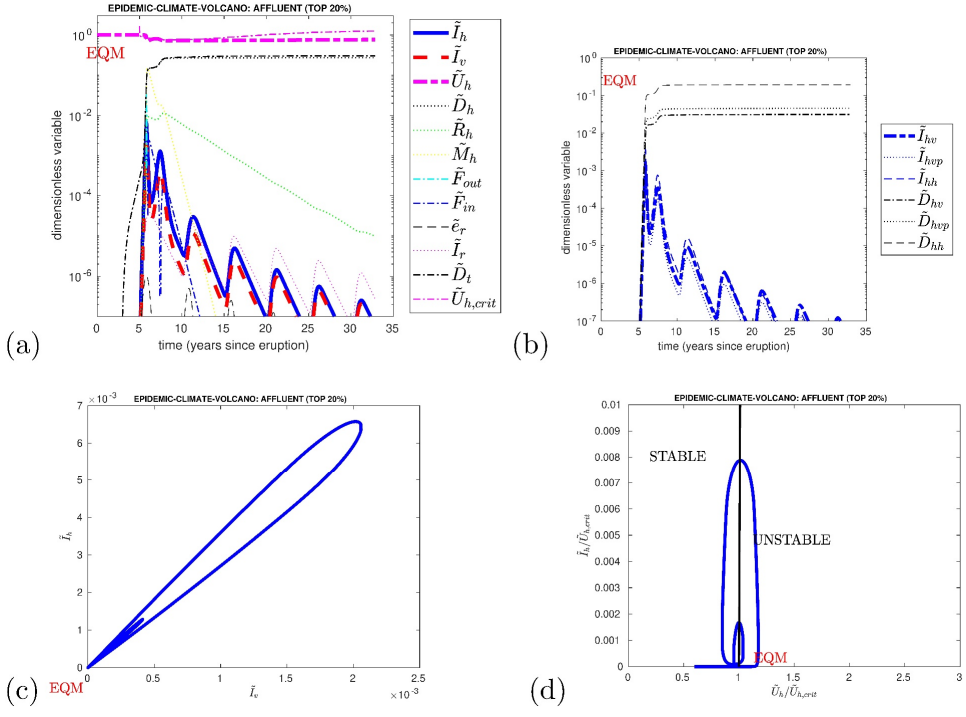

Figure 9: For the affluent (top 20%) sector of the population, the plague as a function of time after 536 CE and phase-spaces are shown plotted as in Fig. 7.

https://doi.org/10.5194/egusphere-2026-5195
Preprint. Discussion started: 8 September 2026
© Author(s) 2026. CC BY 4.0 License.

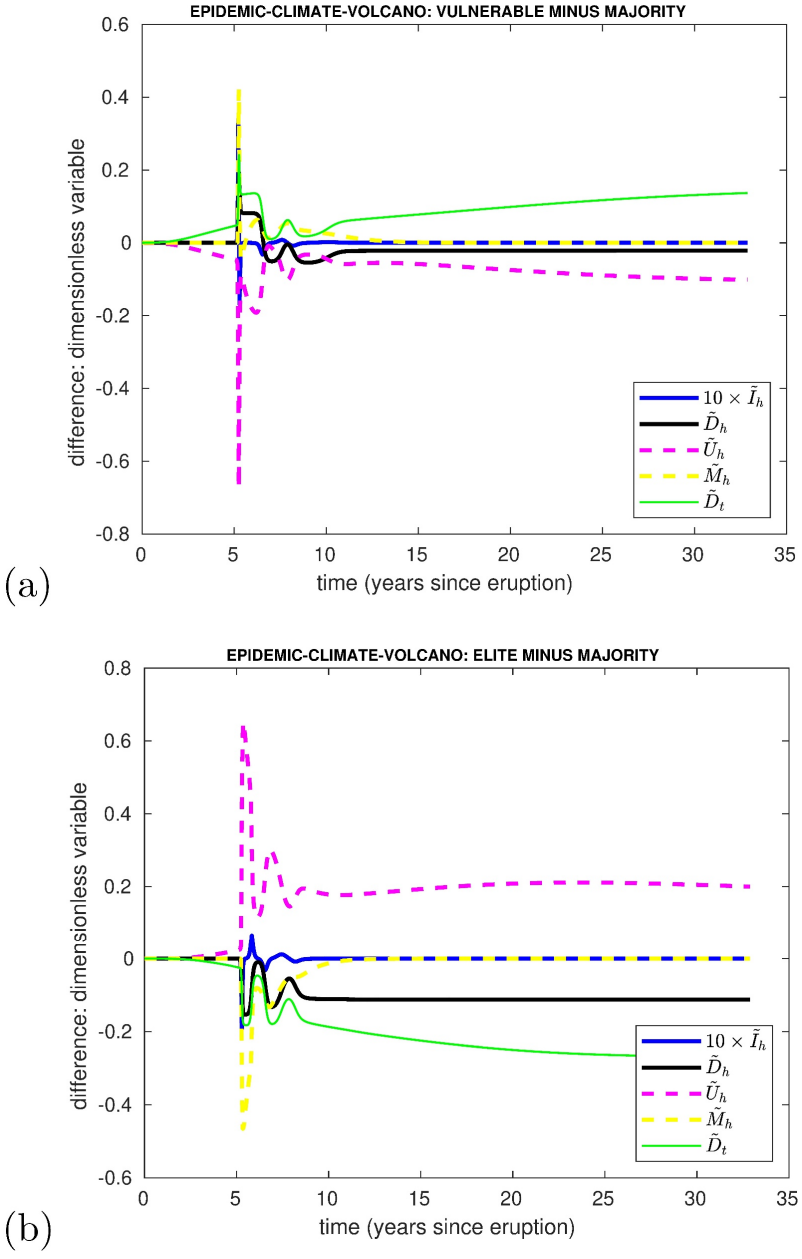

925 **Figure 10: Differences of (a) vulnerable and (b) affluent (20%) sectors of the population (Figures 8 and 9) relative to the majority (Fig. 7), for the prognostic variables of the plague epidemic.**

https://doi.org/10.5194/egusphere-2026-5195
Preprint. Discussion started: 8 September 2026
© Author(s) 2026. CC BY 4.0 License.

Table 4: Sensitivity of simulated epidemic outcomes to perturbations of the control simulation (Table 3). Values are percentages of the initial population; peak prevalence denotes maximum simultaneous infection, and mortality denotes cumulative plague, malnutrition, and combined mortality. Population-weighted results are shown for each perturbation.

Experiment	Population scenario	Peak prevalence (%)	Plague mortality (%)	Malnutrition mortality (%)	Combined mortality (%)	Migrated (%)
No volcanic malnutrition	Majority	0.008	3	0	**3**	0
	Vulnerable	0.5	21	2	**23**	0
	Affluent	0.002	0.5	0	**0.5**	0
	Population-weighted	—	**6**	**0.5**	**6**	**0**
No migration	Majority	6.4	61	13	**74**	**0**
	Vulnerable	9.1	66	21	**88**	**0**
	Affluent	1.0	30	3	**33**	**0**
	Population-weighted	—	**56**	**12**	**68**	**0**
No waning immunity	Majority	1.9	46	0	**46**	47
	Vulnerable	3.5	25	60	**85**	44
	Affluent	0.7	27	0	**27**	14
	Population-weighted	—	**38**	**12**	**50**	**40**
Doubled eruption forcing (intense-eruption run)	Majority	2.7	37	27	**65**	47
	Vulnerable	4.1	34	42	**76**	39
	Affluent	1.0	36	9	**45**	34
	Population-weighted		**36**	**27**	**63**	**43**
Enhanced forcing + seeding (intense-seed-eruption run)	Majority	2.7	38	27	**66**	47
	Vulnerable	4.1	35	42	**77**	39
	Affluent	1.0	36	9	**45**	34
	Population-weighted		**37**	**26**	**64**	**43**

https://doi.org/10.5194/egusphere-2026-5195
Preprint. Discussion started: 8 September 2026
© Author(s) 2026. CC BY 4.0 License.

6. Results from Sensitivity Tests

Table 4 summarises salient results from sensitivity tests modifying the control simulation (Sec. 5, Table 3).

6.1 Volcanic Eruption Impact on Plague via Malnutrition

To isolate the epidemiological effects of volcanic-induced malnutrition, the model was re-run with the malnutrition index held fixed at its equilibrium value throughout the simulation ($\mathcal{M} = \mathcal{M}_{eq} = 0.25$, 0.35 and 0.15 for the majority-, vulnerable- and affluent-population scenarios, respectively; Sec. 5.1). These 'no-volcanic malnutrition' runs were compared with the corresponding control simulations (Sec. 5.2), while external reservoir forcing was kept identical to isolate the effect of malnutrition from any climatic effect on reservoir spillover.

Figure 11 shows that removing volcanic malnutrition greatly weakens the initial epidemic. First-wave peak prevalence by one or two orders of magnitude relative to the control. Consequently, migration is negligible. After three decades, plague mortality is drastically reduced to 3%, 21% and 0.5%, with the least reduction for the vulnerable sector. The malnutrition-related mortality becomes almost zero.

Figure 12 shows the mechanism underlying these differences. Volcanic malnutrition strongly enhances transmission and migration during the first epidemic year, producing a much larger initial wave. Removing malnutrition therefore reduces early plague mortality. However, because fewer people subsequently die from malnutrition, a larger susceptible population remains, allowing continued transmission and partly reducing the difference between the two simulations at later times. This effect is particularly pronounced in the vulnerable and majority populations, where removing malnutrition mortality increases the susceptible population by more than 0.5.

Weighting the three scenarios by their assumed population fractions gives an overall plague mortality of approximately 6% without volcanic malnutrition, and the same for non-plague malnutrition mortality. Thus, in the control simulation, volcanic-induced malnutrition increases plague mortality by a factor of six. Total mortality is increased by an order of magnitude.

https://doi.org/10.5194/egusphere-2026-5195
Preprint. Discussion started: 8 September 2026
© Author(s) 2026. CC BY 4.0 License.

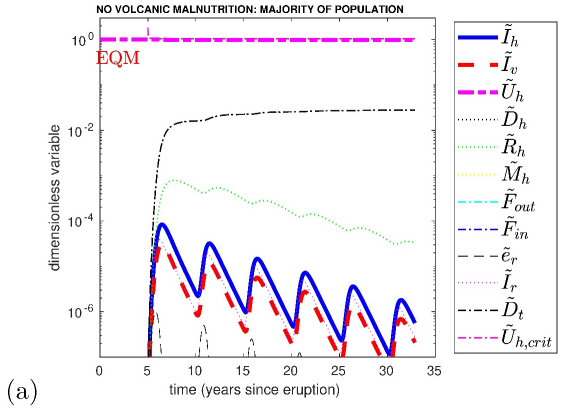

(a)

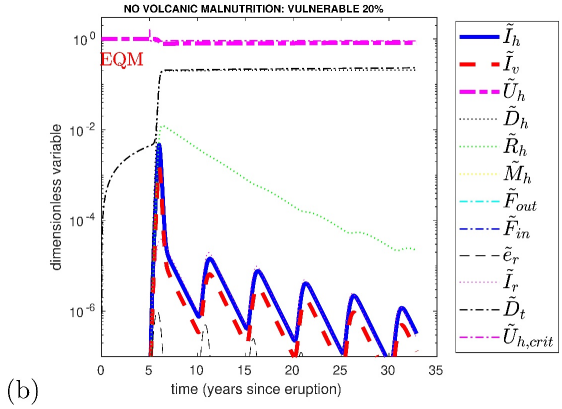

(b)

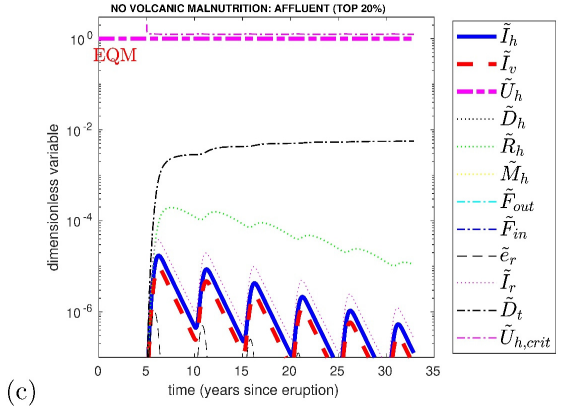

(c)

Figure 11: Prognostic variables for plague epidemic in the no-volcanic malnutrition run, plotted as in Fig. 7a, for the three sectors, for (a) the majority, (b) vulnerable 20% and (3) affluent 20% population scenarios.

https://doi.org/10.5194/egusphere-2026-5195
Preprint. Discussion started: 8 September 2026
© Author(s) 2026. CC BY 4.0 License.

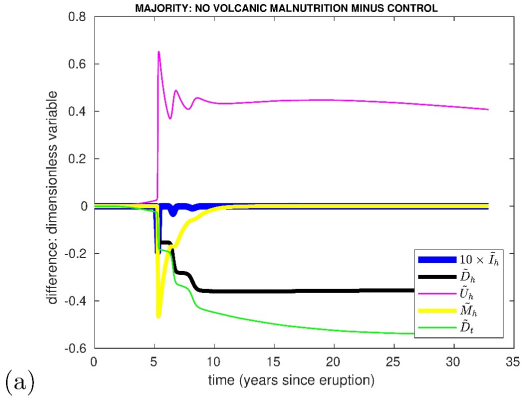

(a)

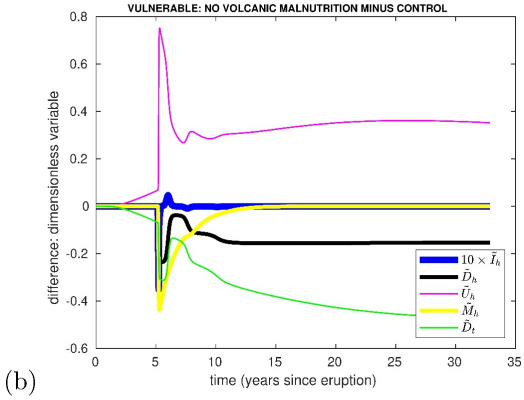

(b)

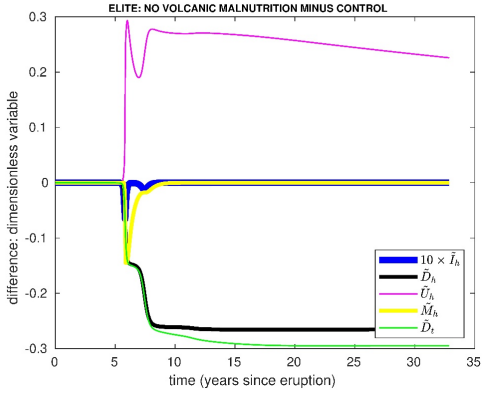

(c)

Figure 12: Effects from prohibiting the volcanic impact on malnutrition in the prediction of the plague, with the difference between the no-volcanic malnutrition run and the control, plotted for the three scenarios ((a)-(c)) as in Fig. 11.

https://doi.org/10.5194/egusphere-2026-5195
Preprint. Discussion started: 8 September 2026
© Author(s) 2026. CC BY 4.0 License.

6.2 Migration Impact on Plague

To assess the role of disease-driven human migration, the epidemic was re-simulated with migration prohibited while all other parameters were unchanged from the control runs (Sec. 5.2). Comparison of this 'no-migration' run with the control runs reveals the effects of migration.

Figure 13 shows that migration moderates the initial epidemic wave, allowing the epidemic to persist appreciably in the control run. In the majority-population scenario, excluding migration intensifies the first prevalence peak from 1.9% to 6.4% and delays it by almost two weeks, while first-year plague mortality rises from about 15% to 61%. Yet the resulting depletion of susceptible individuals subsequently suppresses transmission, with little further increase in plague mortality for the rest of the simulation (61%), compared to the eventual plague mortality of 38%.

The vulnerable population shows an even stronger response. Without migration, the first prevalence peak reaches about 9%, producing about 66% plague mortality during the initial outbreak. While continuing malnutrition mortality drives total mortality to 76% within three years and 88% by the end of the simulation. In all three scenarios there is a collapse of transmission after the first epidemic wave, reflecting the negative feedback associated with the susceptible population falling below the critical value. Prevalence remains less than about 10^{-4} % after the first wave.

Figure 14 shows the differences from the control simulations. Suppressing migration increases the susceptible population available for transmission during the initial outbreak, amplifying both prevalence and mortality. The effect is strongest in the vulnerable population, where the excess plague mortality persists throughout the simulation. The affluent population is comparatively insensitive because prevalence only slightly exceeds the migration threshold during the first wave.

Overall, the simulated disease-driven migration drastically reduces the intensity of the initial epidemic by temporarily removing susceptible individuals from transmission. Although migration can delay some infections and deaths, its net effect is to reduce cumulative plague mortality over three decades in the control. Weighting the three population scenarios gives approximately 56% plague mortality without migration, compared with 36% in the control simulations. The combined-scenario malnutrition non-plague mortality is reduced to 12%.

https://doi.org/10.5194/egusphere-2026-5195
Preprint. Discussion started: 8 September 2026
© Author(s) 2026. CC BY 4.0 License.

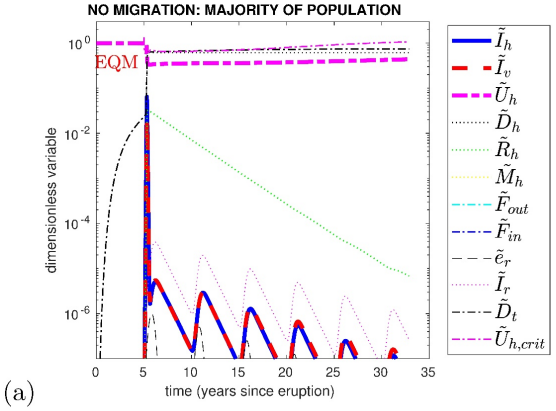

(a)

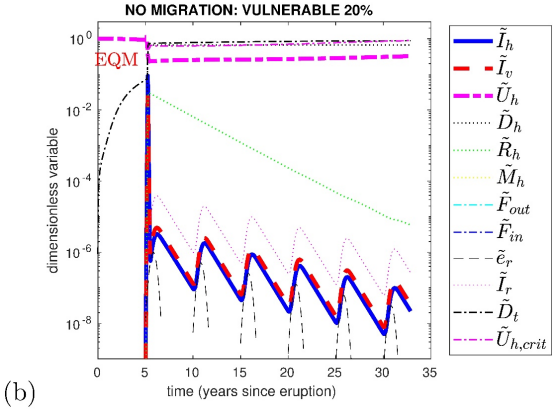

(b)

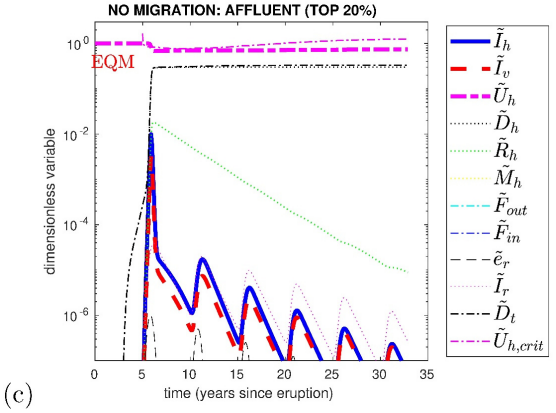

(c)

Figure 13: Epidemic evolution for no-migration run, plotted as in Fig. 11. Comparison with control run reveals effect from disease-driven migration.

https://doi.org/10.5194/egusphere-2026-5195
Preprint. Discussion started: 8 September 2026
© Author(s) 2026. CC BY 4.0 License.

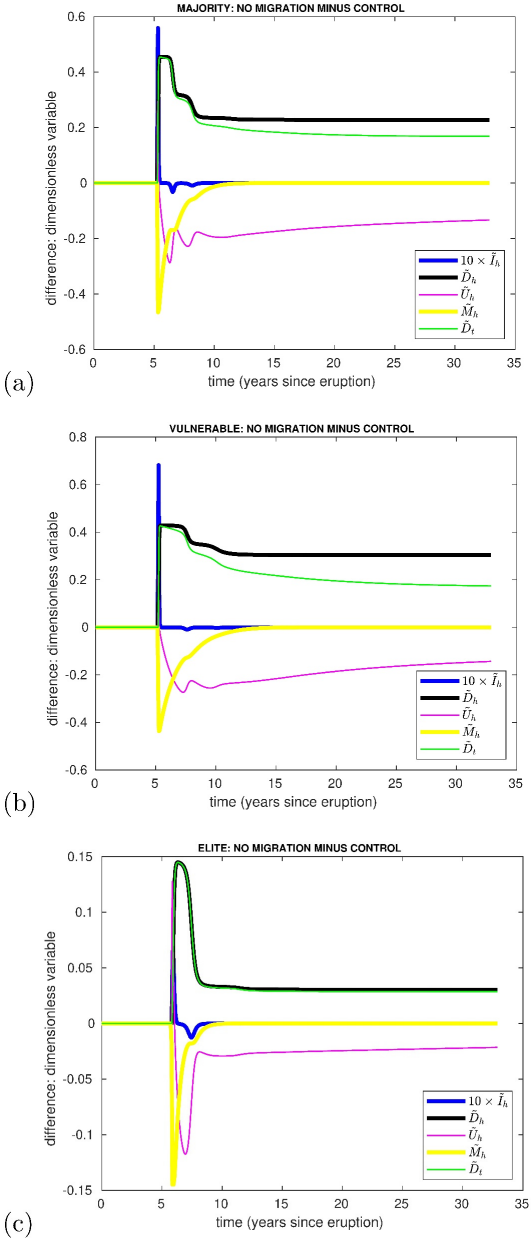

Figure 14: Difference between no-migration run and corresponding control runs for each scenario, plotted as in Fig. 12.

https://doi.org/10.5194/egusphere-2026-5195
Preprint. Discussion started: 8 September 2026
© Author(s) 2026. CC BY 4.0 License.

6.3 Impact from Waning Immunity on the Plague

Simulations were performed in which immunity following recovery from plague was assumed to be permanent, thereby eliminating waning immunity. Comparison of this 'no-waning-immunity' run with the control isolates the influence of waning immunity on epidemic dynamics. Overall, waning immunity has only a modest effect in all three population scenarios. For the majority-population scenario, the susceptible population is increased by about 4% of the initial population relative to the control after the first decade of disease, with the difference emerging gradually, since the initial reduction of the susceptible population reduces malnutrition-related mortality (by 0.11 eventually), later boosting the susceptible population. Consequently, plague mortality is similarly increased (by 0.07 eventually). The combined-scenario plague mortality is increased only slightly from 36% to 38%, while that for non-plague malnutrition mortality decreases from 19% to 12%.

6.4 Impact of Volcanic Eruption Intensity via Malnutrition

To assess the epidemiological sensitivity to volcanic forcing through malnutrition alone, the radiative forcing from both eruptions was doubled and the climate, harvest/food production and epidemiological simulations repeated for the majority-, vulnerable-, and affluent-population scenarios. Reservoir spillover forcing was kept identical to the control runs, so these 'intense-eruption' simulations isolate the malnutrition pathway and do not include any enhancement of spillover by stronger climatic forcing.

As expected, doubling the volcanic forcing approximately doubled peak global cooling (Fig. 15) and produced more severe and prolonged malnutrition (Fig. 16). In the majority population, peak malnutrition increased from 0.74 to 0.78, while in the vulnerable population it remained above 0.8 for approximately 15 years, reaching 0.86.

The epidemiological response was comparatively modest (Figs. 17 and 18). In the majority population, the first prevalence peak increased from 1.9% to 2.7% and occurred three weeks earlier, while migration was practically unchanged (47%). Despite the stronger initial epidemic, eventual plague mortality slightly decreased from approximately 38% to 37%, while malnutrition mortality increased from 19% to 27%. The vulnerable population showed a similar effect: stronger malnutrition increased the initial outbreak but slightly reduced eventual plague mortality to approximately 34% from 36% in the control, because the susceptible population was depleted by malnutrition mortality being boosted to 42% from 19%. The affluent population showed only modest changes in prevalence and plague mortality.

Across the three scenarios, the weighted eventual plague mortality is approximately 36%, practically unchanged from the control value, whereas malnutrition mortality rose from 19% to 27%. Thus, stronger volcanic forcing produces little change in cumulative plague mortality through the malnutrition pathway alone. Increased malnutrition mortality removes susceptible individuals, partly offsetting the stronger transmission caused by nutritional stress. In addition, the infection-fatality ratio is

https://doi.org/10.5194/egusphere-2026-5195
Preprint. Discussion started: 8 September 2026
© Author(s) 2026. CC BY 4.0 License.

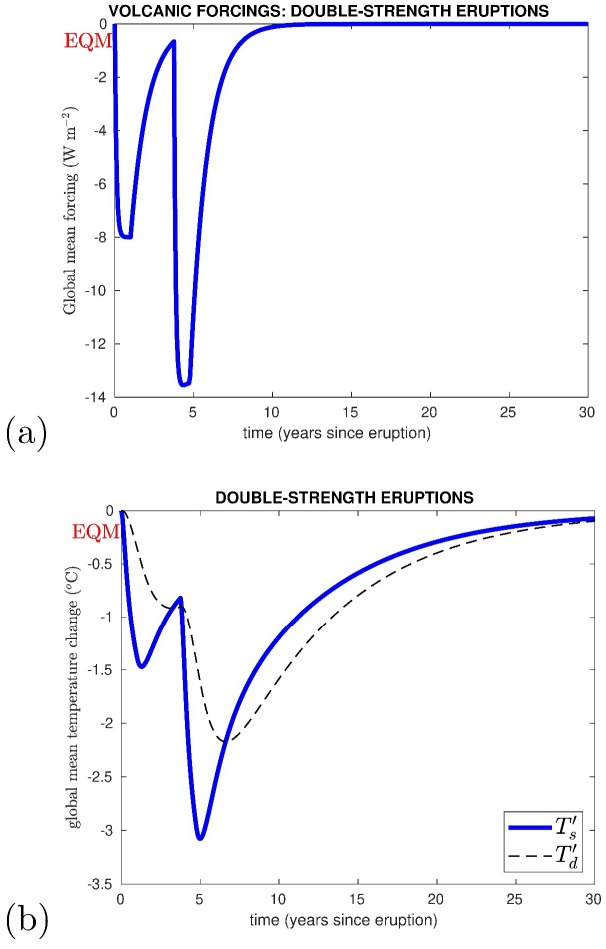

Figure 15: For the intense-eruption run (a) the radiative forcing; and (b) global mean near-surface temperature anomaly, plotted as in Fig. 5.

https://doi.org/10.5194/egusphere-2026-5195
Preprint. Discussion started: 8 September 2026
© Author(s) 2026. CC BY 4.0 License.

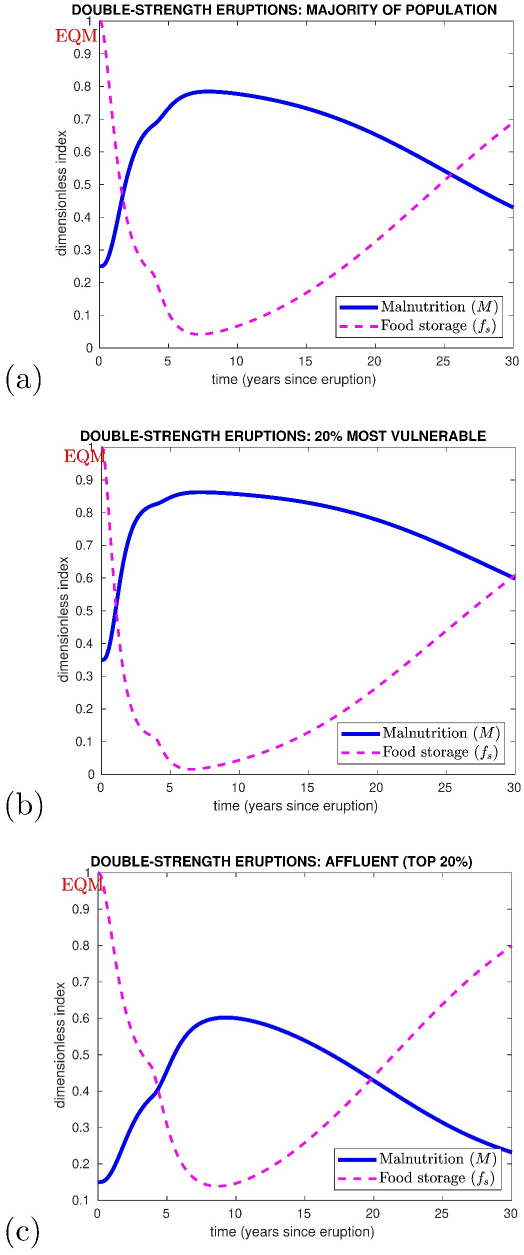

Figure 16: Intense-eruption simulations of malnutrition and food storage indices ($\mathcal{M}$ and f_s), along with the cumulative malnutrition-related deaths (D_m), plotted as in Figure 6.

https://doi.org/10.5194/egusphere-2026-5195
Preprint. Discussion started: 8 September 2026
© Author(s) 2026. CC BY 4.0 License.

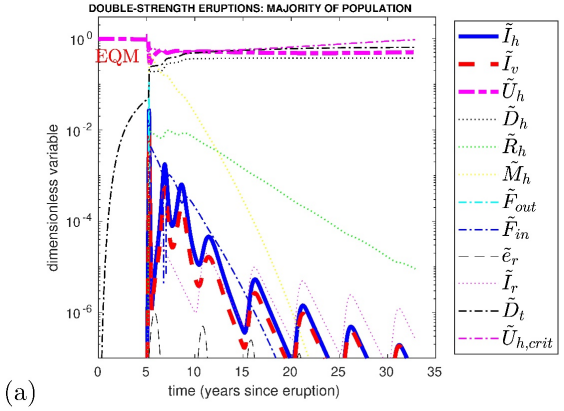

(a)

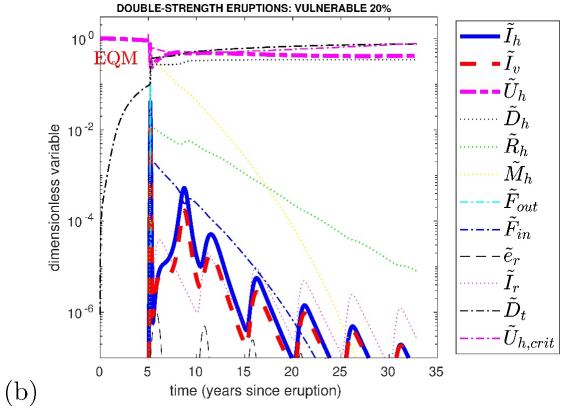

(b)

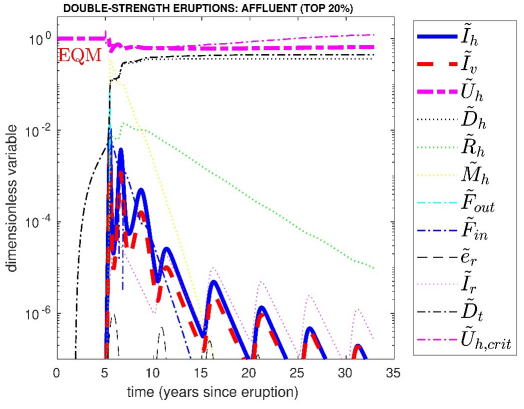

(c)

Figure 17: Intense-eruption simulations of the plague epidemic with doubled forcing in standard case, plotted as in Fig. 11.

https://doi.org/10.5194/egusphere-2026-5195
Preprint. Discussion started: 8 September 2026
© Author(s) 2026. CC BY 4.0 License.

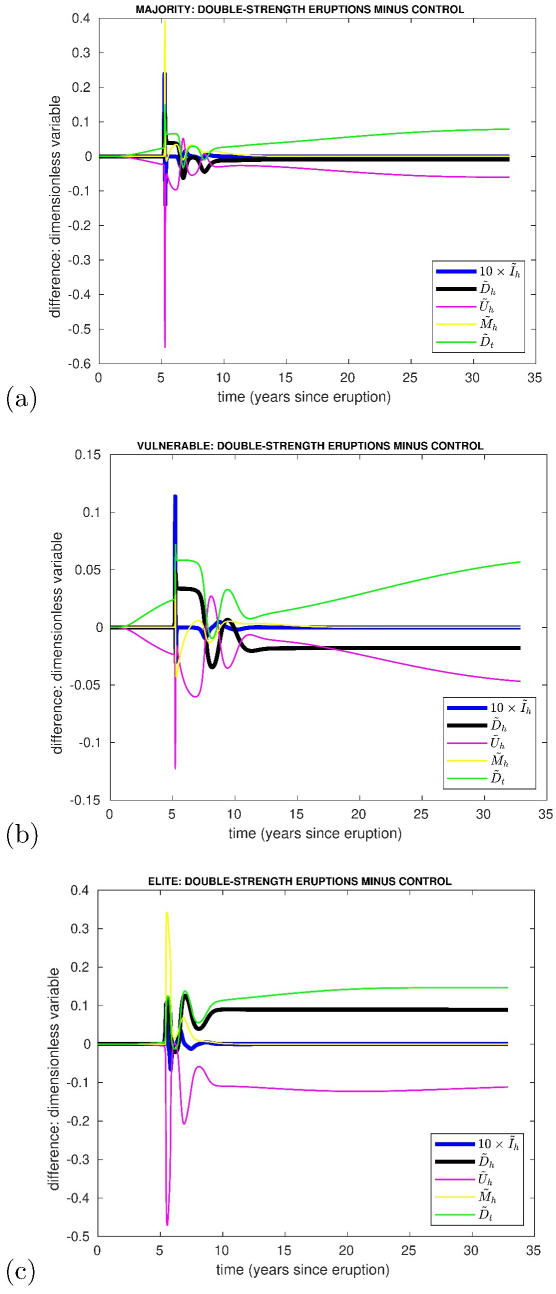

Figure 18: Differences between the intense-eruption and control runs in each scenario, plotted as in Fig. 12.

https://doi.org/10.5194/egusphere-2026-5195
Preprint. Discussion started: 8 September 2026
© Author(s) 2026. CC BY 4.0 License.

already close to saturation in the control simulation, so further increases in malnutrition have only a small effect on mortality among those infected (Appendix C). The result is a competition between increased disease severity and depletion of the susceptible population.

This conclusion applies only to the malnutrition pathway. Stronger eruptions could have a substantially larger epidemiological effect if they also increased reservoir spillover, which is held fixed in this sensitivity experiment.

6.5 Impact of Volcanic Eruption Intensity via Seeding and Malnutrition

Because the relationship between volcanic forcing and pathogen spillover is poorly constrained, the standard model prescribes the external seeding term rather than coupling it explicitly to climate forcing. Stronger climatic perturbations could nevertheless enhance spillover through ecological disruption, altered reservoir dynamics, or increased reservoir–human contact. As a sensitivity test, the peak seeding pulse was increased by a factor of 2.5, consistent with the stronger cooling perturbation considered in Sec. 6.4. This 'intense-seed-eruption' case therefore combines enhanced malnutrition with enhanced pathogen seeding. The increase is intended as a sensitivity perturbation rather than a calibrated prediction of spillover.

The resulting epidemic response (not shown) produces little change in combined-scenario cumulative plague mortality, which remains approximately 37%, as in the control and intense-eruption simulations. Scenario-specific plague and total mortality, as well as peak prevalence are similar to the intense-eruption simulation (Sec. 6.4).

Thus, within the model, allowing stronger volcanic forcing to enhance pathogen seeding produces little effect. The dominant effect of stronger forcing remains the additional malnutrition mortality and consequent depletion of the susceptible population.

7. Discussion

Several epidemiological processes are simplified in the model presented here. First, disease-driven migration is assumed to involve only susceptible individuals, whereas infected individuals may in reality have travelled during the incubation period before symptoms became apparent. Such movement could have contributed to the introduction of infection into new settlements, including through the transport of infected vectors, and thereby increased the geographical spread of plague. The importance of mobility and trade networks as mediators between climatic stress, food insecurity and epidemic emergence has recently been emphasized for historical pandemics (Bauch and Büntgen 2025). More generally, migration has long been a pervasive human response to environmental stress, conflict, political instability and economic hardship, although its scale and character have varied widely (Livi-Bacci 2012, 2021).

https://doi.org/10.5194/egusphere-2026-5195
Preprint. Discussion started: 8 September 2026
© Author(s) 2026. CC BY 4.0 License.

Our model instead treats migration as a local demographic response to perceived disease risk rather than explicitly representing spatial transmission. Because the model is zero-dimensional, representing a single location or the average properties of a region, it cannot resolve the spatial redistribution of infection resulting from population movement. The migration term is therefore intended as a phenomenological representation of behavioural responses to local epidemic conditions.

A related simplification concerns the destination of migrants. The model implicitly assumes that individuals responding to disease risk can migrate to another location where they can obtain as much food as they had before migrating. This assumption is clearly more plausible for some population groups than others. Affluent urban populations may have had greater resources and opportunities to relocate, whereas vulnerable rural populations—including children and the elderly—would have faced greater constraints. Nevertheless, restricting migration to the more affluent would introduce an additional and poorly constrained assumption about the social distribution of mobility during the sixth century. We therefore assume that migration is a demographic response available across population groups, while recognizing that its actual propensity and feasibility probably differed among them. This is consistent with the broader demographic perspective of Livi-Bacci (2012, 2021), which treats migration as a widespread component of population dynamics.

The assumption is also motivated by the relatively low instantaneous prevalence generated by the model. Even during the first wave, plague prevalence remains always less than a few per cent, while the prevalence would in reality have been spatially heterogeneous. Thus, a population confronted with increasing local mortality could potentially respond by moving to less affected settlements. Given the high infection-fatality rate of plague (Appendix C), disease avoidance provides a plausible behavioural motivation for such movement, although the material constraints on migration are not explicitly represented. Essentially, our objective is not to reconstruct the historical migration rates of different social groups, but to investigate the existence and magnitude of a migration-mediated demographic mechanism. The assumption of a common migration propensity therefore provides a parsimonious baseline that can be tested through the migration sensitivity experiment.

A further simplification is that reservoir spillover is prescribed through an external seeding term rather than resolved mechanistically through wildlife, vector and human ecological interactions. Ancient genomic evidence confirms repeated circulation of Yersinia pestis during the First Plague Pandemic (Feldman *et al.* 2016; Keller *et al.* 2019; Wagner *et al.* 2014), but does not constrain the precise ecological mechanisms governing individual spillover events. Representing the complete cascade from wildlife and vectors to a local reservoir and subsequently to humans would therefore require substantial additional ecological assumptions that are poorly constrained for the sixth century. To preserve the simplicity and generality of the theoretical model, this process is not explicitly resolved.

https://doi.org/10.5194/egusphere-2026-5195
Preprint. Discussion started: 8 September 2026
© Author(s) 2026. CC BY 4.0 License.

The dependence of transmission and mortality on malnutrition is also uncertain. Its magnitude is constrained here by comparison of observed plague outbreaks between two urban areas (Givry in 1348 and Florence in 1400) with inferred nutritional conditions and fitted transmission coefficients for the Black Death (Appendix C), (Dean *et al.* 2018). Yet this comparison necessarily assumes that differences between historical populations were substantially related to nutritional status. Other factors, including population density, social organisation and local transmission dynamics, may also have contributed. The resulting malnutrition dependence should therefore be regarded as an informed but uncertain component of the model. Likewise, absolute mortality estimates are uncertain because some plague parameters are calibrated from modern pneumonic plague and the Black Death, whereas the Justinianic pandemic involved an older *Yersinia pestis* lineage.

Arguably, another simplification of the model is that it neglects the incubation period during which infected victims are not infectious. But an additional sensitivity test (not shown in Sec. 6) including an explicit pneumonic incubation period delayed the first peak by approximately one month but changed its magnitude little, suggesting that this additional complexity does not alter the principal conclusions here.

Finally, the epidemiological model assumes a homogeneously mixed and fully interconnected population. This may be a reasonable approximation for cities such as Constantinople, or for rural communities in former Roman provinces of western Europe that were closely connected to major trade networks (e.g. Auvergne, France). However, other rural communities, particularly in heavily forested parts of central Europe, may have comprised relatively isolated settlements, potentially limiting the spread of plague and helping to explain the lack of apparent impact on land use in parts of central Europe (e.g., Izdebski *et al.* 2022), (Sec. 1). The geographical applicability of the present model is therefore uncertain.

Despite these limitations, the model captures the target processes of our hypotheses (Sec. 1.2), for feedbacks between volcanic forcing, food availability, malnutrition, epidemic transmission and human migration. This approach is consistent with broader efforts to understand historical disease outbreaks as outcomes of coupled environmental, ecological and societal processes (e.g., Zonneveld *et al.* 2024; Büntgen *et al.* 2026). The sensitivity experiments identify two important mechanisms. First, volcanic-induced malnutrition strongly amplifies the initial epidemic and increases cumulative plague mortality, demonstrating that nutritional stress can provide an indirect pathway by which climate shocks increase epidemic severity. Second, disease-driven migration acts as a negative feedback by temporarily removing susceptible individuals from transmission during the initial epidemic. Migration thus accelerates the transition from the unstable regime ($\widetilde{U}_h > \widetilde{U}_{h,\mathrm{crit}}$) to the stable regime ($\widetilde{U}_h < \widetilde{U}_{h,\mathrm{crit}}$), (Sec. 4; Fig. 3). Suppressing migration therefore is predicted to produce a substantially larger initial epidemic peak and higher cumulative mortality, particularly in the vulnerable population. These results suggest that models neglecting behavioural migration may overestimate the initial epidemic peak while misrepresenting subsequent epidemic persistence.

https://doi.org/10.5194/egusphere-2026-5195
Preprint. Discussion started: 8 September 2026
© Author(s) 2026. CC BY 4.0 License.

In the literature, behavioural responses to epidemics have hitherto been incorporated in only a few models, including agent-based studies of flight and self-isolation (Epstein *et al.* 2008; Zanette and Risau-Gusmán 2008) and compartmental models with prevalence-dependent transmission (Del Valle *et al.* 2005). Historical and modern observations likewise demonstrate that severe outbreaks rapidly alter human behaviour, including voluntary isolation during the Black Death (Scott and Duncan, 2001) and mass flight during the suspected plague outbreak in Surat, India, in 1994–1995 (Campbell and Hughes, 1995), while similar responses have been documented during recent plague outbreaks (Ripoll *et al*. 2022). Such responses should also be considered alongside evidence for institutional and societal adaptation during Late Antiquity (Haldon *et al.* 2022).

A further result is that the model predicts that between approximately two thirds and three quarters of infections and deaths respectively arise through human-to-human pneumonic transmission rather than the vector-mediated pathway. This prediction is uncertain and should not be interpreted as an estimate of the historical proportion of pneumonic plague. Modern plague is predominantly bubonic, while direct epidemiological observations from the Justinianic pandemic are unavailable. Nevertheless, contemporary descriptions by Procopius are compatible with both pathways. He reports that patients developed "*a bubonic swelling*" and that "*With many also a vomiting of blood ensued without visible cause and straightway brought death*" (Procopius, 1914-1928, *The Wars* 2.22, 15; 17; 31, transl. Dewing, pp. 457). He also notes that *"Death came in some cases immediately, in others after many days*" (Procopius, 1914-1928, *The Wars* 2.22, 15; 17; 31, transl. Dewing, pp. 457). These observations cannot establish the relative contributions of bubonic and pneumonic transmission, but they are consistent with substantial clinical heterogeneity and with the coexistence of both manifestations represented in the model.

A timescale of over a decade is predicted after AD 540 for recovery of $\mathcal{M}$ and f_s from the nutritional shock. Is this realistic? Although acute malnutrition can normally improve within several months when adequate nutrition is restored, this is different from recovery following a prolonged regional food-system shock, in which food availability itself remains constrained. Population-level nutritional consequences may therefore persist through heterogeneous recovery among individuals, residual physiological impairment, and effects on subsequent cohorts. DeWitte and Slavin (2013) report evidence that much of the English population before the Black Death suffered chronic shortages of protein, calcium and vitamin B12 for at least one generation, "*over a much longer period than the three years of bad harvests and grain famine typically attributed to the Great Famine* [1315–1317]" arising from inclement weather. The related Great Bovine Pestilence of 1319–1320 killed an estimated 62% of bovine animals in England and Wales, substantially reducing milk and other dairy products and contributing to prolonged nutritional deficiency. DeWitte and Slavin (2013) argue that the subsequent dairy shortage left a generation in poorer physiological condition and more susceptible to the Black Death. Thus, restoration of individual nutritional status need not coincide with rapid recovery of regional food availability. In the present model, $\mathcal{M}$ represents an aggregate population-level state of nutritional and physiological vulnerability that is dynamically coupled to

https://doi.org/10.5194/egusphere-2026-5195
Preprint. Discussion started: 8 September 2026
© Author(s) 2026. CC BY 4.0 License.

food storage, and can therefore remain elevated while f_s remains depleted. More generally, the knock-on effects of bad harvests can be long-lived through impacts on livestock, agricultural labour, the local economy and human health. Moreover, historical studies of medieval food crises indicate that the consequences of agricultural shocks were mediated by food storage, distribution, markets and differential access to food, implying that the response of food security to a climatic or harvest shock need not be instantaneous (Franklin-Lyons, 2022). This is consistent with the coupled agriculture–food-storage–malnutrition system in the present model having characteristic response/recovery timescales governed by the coupling.

In summary, our principal conclusion is therefore not a quantitative reconstruction of the Justinianic plague, but a mechanistic demonstration of how a volcanic climate shock could have amplified epidemic mortality through interacting nutritional and behavioural feedbacks. The framework provides a basis for testing these mechanisms despite the substantial uncertainty in the historical and epidemiological parameters.

8. Conclusions

A simplified theoretical model of a single region with zero spatial dimensions ('0-D') has been developed to represent the coupled volcano–climate–harvest/food–health system during a plague pandemic. The model combines a simple climate EBM for global volcanic cooling with a climate-sensitive food-malnutrition model that determines food storage and malnutrition, driving an epidemiological model including reservoir hosts, vectors, susceptible, infected and recovered humans, disease-driven migration, and waning immunity.

A reduced phase-space analysis (Sec. 4) provides a simple geometric interpretation of the epidemic dynamics. Epidemic growth occurs only while trajectories lie in the unstable region, whereas depletion of susceptible individuals drives the system across a neutral boundary ($\tilde{I}_h = \tilde{U}_h - \tilde{U}_{h,crit}$) into a stable regime, producing the epidemic peak and subsequent damped oscillations towards an endemic attractor. Although this reduced analysis is only approximate, it provides a useful framework for interpreting the positive and negative feedbacks governing epidemic evolution:

- The '*transmission positive feedback*': an increase of infected people transmits more infections to more susceptible people, either directly (pneumonic disease) or indirectly (vector-mediated disease), boosting the increase, with this feedback weakened by depletion of susceptible people (e.g. by the epidemic itself or by disease-driven migration);
- The '*infected-human depletion negative feedback*': an increase in infected people leads to their loss by death or recovery from the epidemic system, acting to reduce further transmission and counteracting the increase.

https://doi.org/10.5194/egusphere-2026-5195
Preprint. Discussion started: 8 September 2026
© Author(s) 2026. CC BY 4.0 License.

Both component feedbacks always co-exist and their sum is the net epidemic feedback. Thus, the depletion of uninfected susceptible humans is central to the transition from net positive to net negative feedback during each wave of the epidemic, as it weakens the transmission positive feedback. A measure of the net feedback of the epidemic is the excess of susceptible population density beyond its critical value, with a growth rate $\propto \tilde{U}_h - \tilde{U}_{h,\mathrm{crit}} - \tilde{I}_h \approx \tilde{U}_h - \tilde{U}_{h,\mathrm{crit}}$. Thus, an epidemic can only happen when the initial susceptible density is super-critical, which explains urban regions are observed to be more prone than remote rural regions to the plague in historical pandemics (Sec. 1). Disease-driven migration, by lowering $\tilde{U}_h$ is predicted to arrest the intensification of the epidemic by rendering the system subcritical.

Three population-resilience scenarios (Sec. 5.1.2) were simulated, representing the majority (60%), vulnerable (20%) and affluent (20%) sectors of society. The model was applied to the standard case of the 536 and 540 CE volcanic eruptions.

The principal conclusions are as follows:

- *Validation of the climate–harvest model and malnutrition-dependence of epidemiological model (Appendix E)*. For the alternative case of the 1345 CE eruption, the simulated reduction in agricultural output agrees satisfactorily with historical observations from England (Campbell 2010; Broadberry *et al.* 2015), predicting a sudden drop of about 60% in annual output during the first five years and a reduction of about 40% in decadal-mean output (1350s vs before 1345). The predicted malnutrition index likewise reproduces the timeline of observed broad deterioration in nutritional conditions. Slope of observed correlation, between an isotopic malnutrition proxy from skeletons in London and statistics of mortality (plague vs other) from Godde *et al*. (2025), is predicted.

- *Climate response*. For the standard case of the 536 and 540 CE eruptions, the model predicts a peak global cooling of approximately 1.5 ºC, with recovery over roughly the following decade. This response is broadly consistent with the global simulations of Toohey *et al.* (2016) and lies within the range of reconstructed mid-sixth-century cooling estimates (Helama *et al.* 2018; van Dijk *et al.* 2022), with a relaxation time intermediate between that model and available palaeoclimate reconstructions.

- *Standard epidemiological control simulation*. Combining the majority-, vulnerable- and affluent-population scenarios using population weightings of 60%, 20% and 20% yields eventual ‘combined-scenario’ plague mortality of approximately 36% of the initial population after three decades, together with a combined-scenario non-plague mortality of 19% attributable to malnutrition-related disease. These values are within the range reported for major plague outbreaks and severe historical famine-associated mortality, although historical estimates generally combine direct and indirect causes of death.

- *Role of volcanic malnutrition*. Suppressing all volcanic effects on malnutrition while retaining identical reservoir spillover reduces the combined-scenario plague mortality from 36% to 6%, while malnutrition mortality falls from

https://doi.org/10.5194/egusphere-2026-5195
Preprint. Discussion started: 8 September 2026
© Author(s) 2026. CC BY 4.0 License.

19% to zero. Thus, within the framework of the present model, volcanic malnutrition boosts eventual plague mortality by over a factor of six.

- *Role of disease-driven migration*. Suppressing migration increases combined-scenario plague mortality to 56%. This indicates that migration can act as a major negative demographic feedback by temporarily reducing the susceptible population available during the explosive phase of the epidemic. Migration also delays infections among those who leave until later in the epidemic.

- *Role of waning immunity*. Eliminating waning immunity has only a modest influence on epidemic evolution, perturbing only slightly (by 2%) the combined plague mortality, because epidemic waves change on timescales much shorter than the assumed duration of immunity (3 years).

- *Sensitivity to eruption intensity via malnutrition*. Doubling the volcanic forcing has little effect on the combined plague mortality. This is because non-plague mortality from malnutrition rises substantially (19% to 27%), depleting the susceptible population available for infection. Consequently, total mortality increases from 55% to 63%, while the cumulative fraction infected changes little because the infection fatality ratio is already close to its theoretical upper limit (Appendix C). This result applies only to the malnutrition pathway, since any climate-driven enhancement of reservoir spillover was excluded from the standard model.

- *Sensitivity to eruption intensity via both seeding and malnutrition.* When a supplementary sensitivity experiment allows the reservoir seeding pulse to increase linearly with peak volcanic cooling beyond a threshold, the resulting plague mortality (37%) and total mortality (64%) remain almost identical to those obtained without enhanced seeding. This seeding term represents possible climate-related changes in pathogen introduction, including altered reservoir ecology, increased contact between reservoir hosts and humans, or movement of infected reservoir hosts. The weak sensitivity, with respect to altering seeding, reflects the role of reservoir spillover as a trigger rather than a rate-limiting process: once sufficient spillover occurs to initiate an epidemic wave, subsequent epidemic dynamics are controlled primarily by transmission within the human–vector system and by depletion of susceptible individuals.

Regarding the findings on disease-driven migration, the model assumes that migrants can relocate to less-affected areas where food and other resources remain available. It does not explicitly model conditions in destination populations, including their carrying capacity, food availability, or subsequent plague transmission. Thus, the migration effect represents the potential local demographic benefit of disease-driven population movement rather than a complete model of migrant survival and transmission between regions. Regarding the combined-scenario malnutrition-related non-plague mortality of 19% in the control run, this magnitude is biologically plausible because bioarchaeological evidence from medieval London

https://doi.org/10.5194/egusphere-2026-5195
Preprint. Discussion started: 8 September 2026
© Author(s) 2026. CC BY 4.0 License.

around the time of the Black Death indicates that nutritional stress was associated with increased mortality risk during periods of famine (Godde *et al.* 2025).

Overall, the model suggests that the climatic impact of the 536 and 540 CE eruptions could have substantially amplified the Justinianic Plague through harvest failure, prolonged malnutrition and their effects on human susceptibility and behaviour. This interpretation is consistent with growing evidence that historical epidemics emerged from interactions among climate variability, ecological disruption, food systems and human mobility rather than from single causal drivers (McMichael 2012; Ljungqvist *et al.* 2024; Zonneveld *et al*. 2024). Naturally, the model predicts no epidemic when no pulse is given, with the system staying indefinitely in the unstable disease-free equilibrium. So the seeding (e.g. spillover from other reservoir species in the remote wild) pulse is the ultimate trigger for the epidemic.

More generally, the model shows that epidemic dynamics can be interpreted as a competition between positive feedback from disease transmission and negative feedback from loss of infected individuals. Depletion of susceptibles (e.g. from migration) weakens the positive feedback, allowing the negative feedback to prevail. The results further suggest that epidemiological models formulated in terms of population densities, and incorporating behavioural responses such as migration, provide a natural framework for understanding large-scale historical epidemics. Future work should focus on better constraining the ecological mechanisms linking climatic shocks, wildlife reservoirs and spillover into human populations. Our 0-D model provides a flexible framework that could in future work be elaborated to treat spatial transmission due to migration in an idealised way, say with a few adjacent subpopulations linked by a migration term.

https://doi.org/10.5194/egusphere-2026-5195
Preprint. Discussion started: 8 September 2026
© Author(s) 2026. CC BY 4.0 License.

Appendix A

Documentary Evidence for Plague and Mortality during the Black Death

This is a list of entries about known outbreaks of plague in Europe in the Black Death. All are from the database, "EpiMedDat", except for the final two entries.

Date	Location	Historical source / EpiMedDat record	What the source reports	Mortality information	Evidence type
1348	Bohemia	Francis of Prague	Travellers from Bologna saw cities and castles where few people remained alive, and in some places everyone was dead; many houses had no one able to care for the sick. Most of the students travelling with them died.	No denominator	Severe qualitative mortality
1349	Bohemia/Moravia	Administrative evidence	Brno was described as depopulated by plague, followed by tax exemptions to encourage settlement.	No percentage	Administrative evidence of depopulation
1350	Bohemia	Francis of Prague / other sources	Plague continued; people fleeing toward Rome died on the journey or after arrival.	No denominator	Qualitative mortality
1349	Austria	*Continuatio Novimontensis*	Plague reached Vienna and surrounding areas; "hardly one third" remained. Five large pits outside Vienna were filled with corpses.	Source implies ~67% mortality	Quantitative historical claim
1349	Austria	*Continuatio Claustroneoburgensis*	"Great and unheard-of mortality"; in one city 1,000 people were reportedly buried in one day, with rural burials in fields.	1,000 deaths/day; no denominator	Absolute mortality claim
1349	Austria / Bavaria	*Annales Matseenses*	A "most cruel plague" reportedly eliminated about one-third of the	~33% claimed	Quantitative historical claim

https://doi.org/10.5194/egusphere-2026-5195
Preprint. Discussion started: 8 September 2026
© Author(s) 2026. CC BY 4.0 License.

Date	Location	Historical source / EpiMedDat record	What the source reports	Mortality information	Evidence type
			people; very high daily death numbers are given for Vienna and Passau.		
1352	Pskov/Rus'	Novgorod First Chronicle	"Very great plague" in Pskov.	No denominator	Severe qualitative mortality
1352–53	Novgorod/Rus'	Novgorod First Chronicle	Great plague; "a countless number" died; sudden death was reported and the epidemic spread beyond Novgorod.	No denominator	Severe qualitative mortality
1349	Poland	Medieval Polish sources	Plague is recorded in Poland, with descriptions of serious mortality.	No robust regional denominator	Qualitative
1349	Baltic / Denmark	Danish annals	"Great mortality" recorded in Denmark.	No denominator	Qualitative
1349	Sweden	Swedish annals	Great mortality / "the big death" recorded.	No denominator	Qualitative
1348–49	Germany	Various German chronicles	Numerous reports of severe plague mortality and mass burial.	Variable	Qualitative/quantitative
1349	Strasbourg	Closener	Extraordinary mortality, mass burial, and a reported 16,000 deaths.	16,000 reported; denominator uncertain	Absolute mortality claim
1348	Givry, Burgundy	Dean *et al.* (2018)	Parish mortality reconstructed from unusually detailed records.	636 deaths / c.1,500 population ≈ 42%	Strong quantitative demographic evidence
1348–50	England	Manorial/parish demographic evidence (Campbell 2010; Broadbury *et al.* 2015)	Population and agricultural output collapsed dramatically.	~40–50% commonly reconstructed	Strong demographic evidence

1310

https://doi.org/10.5194/egusphere-2026-5195
Preprint. Discussion started: 8 September 2026
© Author(s) 2026. CC BY 4.0 License.

Appendix B

Specification of Parameter Values for Climate and Food-Malnutrition Components for Standard Case

Volcanic aerosol forcing:

Eq (3) represents the prescribed global radiative forcing from volcanic stratospheric aerosols following an eruption. To estimate the time-scales of the radiative forcing of volcanic stratospheric aerosols, we fitted Eq (3) to the volcanic radiative forcing inferred from GloSSAC (Global Space-based Stratospheric Aerosol Climatology) satellite observations of the Pinatubo eruption by Toohey *et al*. (2026), yielding $\tau_{a,r} =$ 0.1 yr and $\tau_{a,d} = t_{lag} = 1$ yr, consistent with results computed by Toohey *et al*. (2025), and their estimated 2-year stratospheric lifetime (Fig. 5a). We assign $F_0 = -2$ W m^{-2}. For Pinatubo, the time-integrated forcing from satellite data (3.7 W yr m^{-2}) was lower than that from ice-cores (Sigl *et al*. 2015), (6.5 W yr m^{-2}).

For both 536 and 540 CE, $\tau_{a,r}$ and t_{lag} are assumed the same as Pinatubo (0.1 and 1 yr). Inspection of the SO4 deposition of an ice-core in Greenland for both eruptions from Toohey *et al*. (2016, their Fig. 2) implies $\tau_{a,d} = 1.1$ yr (see also Larsen *et al*. 2008). This gives a residence time of about 2 years, as for Pinatubo, representing a compromise between competing expectations. Although stronger eruptions such as 536/540 CE may have injected aerosols higher into the stratosphere, prolonging their lifetime (Schoeberl *et al*. 2025; Toohey *et al.* 2025), very large eruptions may also produce larger particle sizes and enhanced collisional growth, accelerating sedimentation and limiting the climatic impact (Timmreck *et al.* 2010).

Historical reports of dim hazy skies from March 536 CE lasting about 18 months (Stothers 1999; Toohey *et al.* 2016) are consistent with the assumed values of the timescales. Cassiodorus in the same letter (Sec. 1) wrote: "*The Sun … lost his wonted light, and appears of a bluish colour. We marvel to see no shadows of our bodies at noon*" (Barnish 1992) and Procopius (1914-1928, The Wars 4.14.5) wrote "*The sun gave forth its light without brightness*".

Forcings for the 536 and 540 CE eruptions were estimated by adjusting F_0 to match the time-integrated forcing with ice-core derived values. Toohey and Sigl (2017) reported the observed average of stratospheric aerosol optical depth (SAOD) for each eruption from the eVolv2k dataset of ice cores from Greenland and Antarctica. Rescaling SAOD yields $\int_0^\infty F(t)dt = -7.9$ and -13.1 W yr m^{-2}, which yields $F_0 = -4.0$ and -6.6 W m^{-2} for both eruptions respectively.

Food-Malnutrition Component:

Eqs (5) and (6) represent the dynamics of malnutrition and food storage respectively. In Eq (6), we assume $f_w = 0.1$ to represent agricultural resilience from crop diversity, access to external seed sources, and spatial heterogeneity in climatic impacts, reflecting limited buffering to short-term harvest failures.

https://doi.org/10.5194/egusphere-2026-5195
Preprint. Discussion started: 8 September 2026
© Author(s) 2026. CC BY 4.0 License.

The parameter λ_m controls the feedback of malnutrition on agricultural labour productivity. We set $\lambda_m = 0.5$, allowing malnutrition to reduce agricultural productivity by up to approximately 50% under severe nutritional stress. This value is not intended as a direct empirical estimate of medieval labour productivity; rather, it is a model calibration. In combination with the other parameters, $\lambda_m = 0.5$ reproduces the approximately two-decade persistence of depressed agricultural conditions observed ($f_s < 0.65$) following the CE 536–540 volcanic shocks.

In Eq (5), the parameter κ represents the effective sensitivity of regional food availability to climatic cooling. It is not intended to describe the physiological response of an individual crop species to temperature alone, but rather the combined regional effects of shortened growing seasons, changes in precipitation and solar radiation, crop and fodder failures, livestock impacts, food storage and disruption of food supply. Values in the range $\kappa = 0.5$–$1\ \mathrm{K}^{-1}$ are adopted, so that a peak global-mean cooling of 1°C (peak NH land mean cooling of 2-3 °C) reduces effective food production with a factor $e^{\kappa T_s'} \approx 0.6$ to 0.37, corresponding to a 40–60% reduction. Modern weather impacts on European agriculture depend sensitively on the interaction between temperature, precipitation, crop species and location (Beillouin *et al*. 2020). While harvest data are only available for select periods and regions in the pre-industrial period, cooling at the multi-decadal scale has been shown to be associated with increased grain prices across Europe as well as China during the early modern period (Ljungqvist *et al.* 2022; Ren *et al*. 2025).

Regarding the 536–540 CE eruptions, Toohey *et al.* (2016) developed a temperature-dependent dimensionless Cultivation Suitability Index ($\mathrm{CSI_T}$), predicting anomalies below about -0.2 across the Baltic region for several years, indicative of substantially reduced agricultural suitability. Similarly, van Dijk *et al.* (2023), combining climate-model ensembles with pollen and archaeological evidence, found that their coldest simulations (regional cooling of 3 °C, corresponding to about 1.5 °C global cooling) best matched the palaeo-record in W Scandinavia. A Growing Degree Days model indicated widespread failure of wheat and oats and only marginal viability of rye and barley. As volcanic dimming of solar radiation was not included, these losses may be conservative. Their results are consistent with a 70% reduction in food output ($e^{\kappa T_s'} \approx 0.3$) for $T_s' \approx -1.5$ °C, implying $\kappa \approx 0.75\ \mathrm{K}^{-1}$. Arthur *et al.* (2024) combined archaeological radiocarbon dates with palaeoclimate simulations to examine the impact of the 536–540 CE eruptions on Scandinavia, finding particularly pronounced negative impacts in northwestern Scandinavia and some inland regions, but more heterogeneous impacts in southern Scandinavia. Taken together, these studies support the adopted range of κ.

The timescale $\tau_{\mathrm{storage}} \approx 0.75$ to 1.5 years represents effective turnover of food reserves under pre-industrial household storage and consumption constraints, depending on the vulnerability of the sector of population. The purpose of storage of grain was to allow preindustrial communities to store enough to survive one harvest failure and to provide enough seed

https://doi.org/10.5194/egusphere-2026-5195
Preprint. Discussion started: 8 September 2026
© Author(s) 2026. CC BY 4.0 License.

(ideally 20% of the harvest) for the next year. A default value of $\tau_{\text{storage}} \approx 1$ yr with $\kappa = 0.75$ K^{-1}, is set for a standard run for the majority of the population.

In Eq (5), C_m controls the rate at which food deficit increases malnutrition. We adopt $C_m = 5\ \text{yr}^{-1}$, corresponding to order-unity deterioration in nutritional status over a few months under sustained famine, while $\tau_{\text{recover}} \approx 0.5$ yr represents the slower physiological recovery following nutritional restoration. Together these values permit moderate climatic shocks to produce nonlinear food shortages with delayed recovery, yielding $m_{\text{peak}} \approx m_{\text{eq}} + C_m \tau_{\text{recover}}(1 - f_w)$, corresponding to $\mathcal{M}_{\text{peak}} \approx 0.7$. This is consistent with historical reports of severe malnutrition without complete population collapse.

Regarding the treatment of malnutrition-related non-plague mortality, we set the hypothetical maximum mortality rate, $\mu_{m,max}$ to 0.1 yr^{-1}. This value provides an approximate independent constraint on the mortality function: at $\mathcal{M} = 0.75$, corresponding to the onset of the very severe malnutrition/famine regime in Table 1, the resulting mortality rate is 0.044 yr^{-1} corresponding to about 36% cumulative mortality over a decade. Hence, $\mu_{m,max} \approx 0.1$ yr^{-1} is a plausible upper-bound parameter for sustained extreme nutritional deprivation, reflecting mortality arising from the combined effects of energy deficiency, impaired immune function, and secondary infections.

Appendix C

Specification of Parameter Values for Simplified Epidemiological Model for Standard Case

We apply the simplified epidemiological model (Eqs (18) to (27)), (Sec. 2.4.1), to an outbreak region (e.g. N or W Europe) for the standard case of the plague following the eruptions of 536 and 540 CE. Here the parameter values for the model are derived as follows.

C1. Reference population densities and scaling assumptions

A reference value of population density at the time of the Justinianic Plague is $U_{h,0} = 10$ people per km^2. During an epidemic there would be about 10 lice per person on average, implying order of 0.1 plague-infected vector per person (order of 1% of lice are infected), which is $U_{v,0} = 100$ per km^2. The lifetime of plague-infected lice is $\tau_v = 4$ days, as they die earlier from the plague than people. Similarly, the total density of the reservoir species (infected and uninfected) is $U_{r,0} = 100$ per km^2, with one reservoir individual for every vector.

C2. Vector–human transmission parameters

https://doi.org/10.5194/egusphere-2026-5195
Preprint. Discussion started: 8 September 2026
© Author(s) 2026. CC BY 4.0 License.

C2.1 Human/vector infection coefficient $\tilde{g}_v$

A plausible estimate for the dimensionless coefficient ($\tilde{g}_v$) can be obtained by comparison with the ectoparasite model of Dean et al. (2018). Their vector-infection term is proportional to $\left(\beta_{\text{low}} I_{\text{low}} + \beta_{\text{high}} I_{\text{high}}\right) = \bar{\beta}\bar{I}$ where $I_{\text{low}}, I_{\text{high}}$ and $\bar{I} = I_{\text{low}} + I_{\text{high}}$ (their terminology, rather than ours) denote numbers, rather than densities, of infected humans in the mild, high-bacteremia, and total classes, respectively. Their fitted transmission coefficients are typically $\beta_{\text{low}} \approx 0.04\ \text{d}^{-1}$ and $\beta_{\text{high}} \approx 0.3\ \text{d}^{-1}$. Assuming a quasi-steady epidemic state, the relative sizes of these classes can be estimated from their durations and the fraction of cases progressing to high bacteremia. Since the high-bacteremia stage lasts only ~ 2 days, compared with ~ 8 days for mild bacteremia, and approximately 60% of cases progress to the highly infectious stage, we expect $I_{\text{high}}/I_{\text{low}} \approx 0.6 \times 2/8 \approx 0.15$. The corresponding effective transmission coefficient is therefore $\bar{\beta} = \left(\beta_{\text{low}} I_{\text{low}} + \beta_{\text{high}} I_{\text{high}}\right)/\left(I_{\text{low}} + I_{\text{high}}\right) \approx (0.04 + 0.3 \times 0.15)/1.15 \approx 0.074\ \text{d}^{-1}$. Thus, we adopt the representative value ($\bar{\beta} \approx 0.08\ \text{d}^{-1}$) (in the terminology of Dean *et al*. 2018). Identifying $\bar{\beta} = g_v U_{v,0}$, the dimensionless coefficient is $\tilde{g}_v = \bar{\beta}\tau_v$. For the adopted infected-vector lifetime $\tau_v = 4$ days, this gives $\tilde{g}_v \approx 0.08 \times 4 \approx 0.32$.

C2.2 Vector-to-human transmission coefficient $\tilde{d}_h$

The dimensionless vector-to-human transmission coefficient was constrained using the human ectoparasite model of Dean *et al.* (2018). In their formulation, the rate of new bubonic plague infections is, in their terminology, $\beta_l S_h I_l / N_h$, where S_h is the number of susceptible humans, I_l is the number of infected human ectoparasites (body lice or human fleas), N_h is the total living human population, and $\beta_l \approx 0.05\ \text{d}^{-1}$ is the fitted transmission coefficient. Comparing this with the corresponding infection term in the present model, $d_h \tilde{c}_v U_h I_v$, and expressing both systems in terms of population densities yields $d_h \tilde{c}_v = \beta_l / U_{h,0}$, where $U_{h,0}$ is the initial human population density and $\tilde{c}_v = (1 + \alpha_v \mathcal{M})^2$ is the malnutrition enhancement factor. Using the definition of the dimensionless transmission coefficient, $\tilde{d}_h = d_h \tau_v U_{v,0} \tilde{c}_v$, the factor c_v cancels, giving

$$\tilde{d}_h = \beta_l \tau_v \frac{U_{v,0}}{U_{h,0}}.$$

Adopting an infected-vector lifetime of $\tau_v = 4$d and a lower-bound estimate of the ectoparasite burden of $U_{v,0}/U_{h,0} \approx 10$, corresponding to the low end of the range of 10–68 lice per person reported by Dean *et al*. (2018), yields $\tilde{d}_h \approx 0.05 \times 4 \times 10 = 2.0$.

C3. Human-to-human pneumonic transmission parameters

The dimensionless human-to-human transmission coefficient, $\tilde{h}_h$, was constrained using the analysis of pneumonic plague outbreaks by Gani and Leach (2004). They estimated a basic reproduction number of $R_{0,h} \approx 1.3$ prior to the introduction of control measures and found a mean infectious period of approximately 2.5 d. In the present model, the dimensionless

https://doi.org/10.5194/egusphere-2026-5195
Preprint. Discussion started: 8 September 2026
© Author(s) 2026. CC BY 4.0 License.

removal rate for pneumonic plague is $\tilde{k}_h = \tau_v/\tau_{I,\mathrm{mort},h}$, which for $\tau_v = 4$ d gives $\tilde{k}_h = 1.6$. Linearising Eq (23) about the disease-free state $(\tilde{U}_h \simeq 1,\ \tilde{I}_h \ll 1)$ yields $\frac{d\tilde{I}_{hh}}{d\tilde{t}} \approx (\tilde{h}_h - \tilde{k}_h)\tilde{I}_{hh}$, implying a basic reproduction number $R_{0,h} = \frac{\tilde{h}_h}{\tilde{k}_h}$ when only pneumonic cases are introduced ($\tilde{I}_{hvp} \approx 0$). Using $R_{0,h} = 1.12$ from pooling a subset of the older rural outbreaks from Gani and Leach (Ecuador, 1939; NW Madagascar, 1957; Zambia, 1993) therefore gives $\tilde{h}_h = R_{0,h}\tilde{k}_h \approx 1.12 \times 1.6 = 1.8$. (These calibration outbreaks from the 20th century are assumed to represent the reference nutritional state of $\mathcal{M} = 0.5$ for calibration.) Because the nutritional status of the historical outbreak populations is not known quantitatively, no further correction has been applied. The reproduction number for vector-borne transmission is $R_{0,v} = \frac{\tilde{g}_v\tilde{d}_h}{\tilde{j}_h} = 0.7$, so that the total reproduction number is $R_{0,v} + R_{0,h} = 1.8$, which is in the range of values fitted by the most accurate model (ectoparasite) by Dean *et al*. (2018) of 1.5 ± 0.3 for the various cities in the Black Death in the late Middle Ages.

Secondary pneumonic plague was represented by a characteristic progression timescale of $\tau_{I,p} = 5$ days following vector-borne infection. This value is consistent with descriptions of secondary pneumonic plague in the WHO *Plague Manual*, which indicate that pulmonary involvement typically develops after several days of acute illness (Dennis *et al.* 1999).

C4. Epidemic-scale constraints and peak prevalence

At the epidemic peak, from Eq (18), seeding is negligible and because vector equilibration in Eq (19) is rapid (timescale of 4 days), $\widetilde{g_v}\,\tilde{I}_h \approx \tilde{I}_v$. Here, the Justinianic Plague is estimated to have killed about 20-30% of the population over the first major epidemic wave (around 541-544 CE), (Russell 1965, 1968; Perry and Fetherston 1997), (Sec. 1). Conservatively taking 30% as a representative cumulative fraction infected during the first major outbreak (the actual fatality ratio would imply a higher fraction from 20-30% killed) and assuming that most transmission occurs during an active epidemic phase lasting a few months (100 days), while infected individuals remain infectious for approximately 7 days, the peak prevalence may be estimated as the product of the total fraction infected and the ratio of infectious period to epidemic duration: $\tilde{I}_h \approx 0.3 \times \frac{7}{150} \approx 0.014$.

C5. Reservoir dynamics and external seeding

Regarding the reservoir host, we assign $\tilde{f}_r = \tau_v/\tau_r = 0.011$, with $\tau_r = 1$ year. The reservoir-to-vector transmission term g_{rv} represents infection of vectors through contact with infected reservoir hosts (e.g. fleas transferring between rodent colonies and human-associated environments). This pathway is assumed to be weaker than direct human–vector amplification but sufficient to maintain a delayed environmental reservoir, with a representative dimensionless value $\tilde{g}_{rv} = 0.1$. For comparison, applying the rat–flea model of Dean *et al*. (2018) to the present non-dimensionalisation gives values of order $\tilde{g}_{rv} \sim 0.5$ to 1, based on flea release following rodent mortality. However, because the present model represents transmission through human-associated ectoparasites rather than a rat-flea enzootic cycle, and because reservoir infection

https://doi.org/10.5194/egusphere-2026-5195
Preprint. Discussion started: 8 September 2026
© Author(s) 2026. CC BY 4.0 License.

acts primarily as an external source of introduction rather than the dominant epidemic amplification mechanism, the lower value is adopted.

Before the epidemic ($I_h \approx 0; I_v \ll U_{v,0}$), sustained human transmission cannot occur without external introduction from infected reservoirs or other populations. Initial introduction is therefore represented by transient forcing through the seeding term $\tilde{e}_r(\tilde{t})$, corresponding to episodic spillover events associated with long-distance movement of infected hosts, vectors, or contaminated materials.

A pre-epidemic reservoir infection fraction of order $\tilde{I}_{r,eq} \sim 10^{-4}$ is adopted, consistent with previous plague modelling studies (e.g. Keeling and Gilligan, 2000). However, the effective seeding required to initiate a pandemic-scale outbreak need not correspond to this weak endemic background level. The Justinianic pandemic represents an unusually large geographical expansion of plague, and therefore the introduction term is interpreted as a rare amplification event rather than continuous low-level spillover.

Accordingly, the initial Gaussian seeding pulse is assigned a maximum amplitude of

$$\tilde{e}_r = 10^{-6},$$

with subsequent pulses occurring every five years and decreasing by a factor of two. This value represents the estimated background forcing ($\sim 10^{-6}$) and accounts for the possibility of multiple simultaneous introductions through trade networks, human migration, and animal/vector dispersal during the initial pandemic expansion. The recurrence interval of five years is chosen to represent the approximate spacing of early documented Justinianic plague recurrences, including the outbreak of 546–547 CE approximately five years after the initial pandemic onset.

C6. Disease-driven migration parameters

C6.1 Outward and return migration timescales

Regarding the evolution equation for uninfected humans, for disease-driven migration and its return we set $\tilde{\tau}_{out} = \frac{\tau_{out}}{\tau_v} = 5$ and $\tilde{\tau}_{in} = \frac{\tau_{in}}{\tau_v} = 25$, corresponding to timescales of 20 and 100 days respectively. The outward migration timescale is chosen to be comparable to the epidemic growth timescale, so that migration occurs while the epidemic is still expanding rather than after mortality has peaked (just over an order of magnitude of increase of $\tilde{I}_h$ in the build-up towards the epidemic peak requires about $\Delta\tilde{t} \sim 5$, as justified below). We set $\tilde{I}_{return} = \tilde{I}_{panic}/4$ because 100 days is an order-of-magnitude estimate for the timescale over which displaced populations might begin returning after local epidemic conditions improve. This reflects the economic pressure to resume cultivation and other subsistence activities once epidemic risk has declined. Return

https://doi.org/10.5194/egusphere-2026-5195
Preprint. Discussion started: 8 September 2026
© Author(s) 2026. CC BY 4.0 License.

is assumed to occur more gradually than outward migration because confidence that the epidemic has subsided would likely develop more slowly than the initial decision to flee. Historical accounts of the Justinianic Plague indicate that outbreaks in a given location typically subsided within a few months, after which economic and social activity gradually resumed. Thus, a return timescale of a few months is both socially and economically well-motivated.

C6.2 Panic threshold and behavioural response

We choose the panic threshold ($\tilde{I}_{\text{panic}} = 0.005$) to represent the stage at which the epidemic becomes sufficiently visible within a settlement to trigger collective behavioural responses, including temporary flight and self-isolation. Although individuals respond to locally observed illness and mortality rather than population-wide prevalence, settlement-scale prevalence provides a convenient macroscopic proxy for the probability that a typical resident encounters multiple symptomatic cases within their social neighbourhood. The threshold is not intended to represent a directly measurable epidemiological quantity, but rather a phenomenological parameter describing the recognisability of an unfolding epidemic. Behavioural responses to epidemics are understood to arise from local observation of visibly ill individuals, deaths among neighbours and relatives, and the cumulative perception that disease is spreading, rather than from knowledge of population-wide prevalence.

We therefore require only that $\tilde{I}_{\text{panic}} < \tilde{I}_h^{\text{peak}}$, so that migration begins once the epidemic is well established but before mortality reaches its maximum. The lower return threshold introduces behavioural hysteresis: populations flee once the epidemic becomes unmistakable, but return only after infection has declined to substantially lower levels. For settlements with populations of 10^2, $10^3$and 10^4, $\tilde{I}_{\text{panic}} = 0.005$ corresponds to approximately 1, 5 and 50 simultaneously symptomatic infectious individuals, respectively. Given the conspicuous clinical presentation of bubonic plague, its rapid progression, and the high probability of death within a few days, such numbers would be expected to produce multiple visible cases and successive deaths within residents' local social neighbourhoods. This provides a plausible trigger for fear-driven migration.

Contemporary accounts of the Justinianic Plague are consistent with the existence of a behavioural transition from normal activity to widespread flight. Procopius and John of Ephesus describe the rapid breakdown of normal civic life, widespread fear and the abandonment of affected settlements once plague became established, although they do not quantify the prevalence at which these responses began. The chosen value of $\tilde{I}_{\text{panic}}$should therefore be regarded as an order-of-magnitude behavioural parameter that represents the transition from isolated cases to a clearly recognizable epidemic.

C7. Demographic recovery and immunity parameters

$\tau_{U,pop}$ corresponds to a century, so $\tilde{\tau}_{U,pop} = 9.1 \times 10^3$. This corresponds to observations of slow rates of change of pre-industrial populations. We take the waning immunity timescale as $\tau_{\text{wane}} = 3$ years, representing an effective population-level

https://doi.org/10.5194/egusphere-2026-5195
Preprint. Discussion started: 8 September 2026
© Author(s) 2026. CC BY 4.0 License.

immunity memory that includes partial biological immunity, behavioural adaptation, and cohort turnover. While on the upper end of biologically plausible durations for plague immunity, this choice captures the slower decay of post-infection protection relevant for repeated epidemic waves: $\tilde{f}_h = 3.65 \times 10^{-3}$.

C8. Nutritional stress and transmission amplification

C8.1 Malnutrition-dependent transmission scaling

We set the malnutrition transmission scaling parameters to $\alpha_h = 1$ for human-to-human transmission and $\alpha_v = 1$ for vector-mediated transmission, with $p = 2$. These values reflect the known effects of malnutrition on host susceptibility and pathogen dynamics: severe nutritional stress impairs immune function, increases pathogen load, and can prolong infectiousness, thereby amplifying both human-to-human and vector-to-human transmission. With a peak malnutrition index of $\mathcal{M} \approx 0.7$ assumed during the AD 540 famine, the human-to-human transmission factor $\tilde{c}_h = (1 + \mathcal{M})^2$ is more than doubled compared to the pre-famine baseline ($\mathcal{M} = 0.25$, with $\tilde{c}_h = 1.56$), and similarly for the vector transmission factor $\tilde{c}_v = (1 + \mathcal{M})^2$. These multipliers are qualitatively consistent with historical accounts of accelerated spread of the Justinianic Plague under famine and climate stress, and provide a formulation for simulations in the absence of direct historical measurements.

C8.2 Empirical constraint from Black Death comparisons

An empirical constraint on the magnitude of malnutrition-related transmission amplification resulting from the above values of α_h, α_v and p is obtained from our inspection of the epidemiological model fits by Dean *et al.* (2018) to observed sequences of death rates in two southern European towns, specifically Givry in 1348 during the first wave of the Black Death shortly after the volcanic eruption of 1345, and Florence in 1400. For Givry in 1348, our simulations of the volcanic climate shock and its impact on harvests during the Black Death suggest $\mathcal{M}_{Givry} \approx 0.55$ (Section 3). The ratio of the fitted transmission coefficients between the two towns reported by Dean *et al.* (2018, their Supplementary Table S4) for the vector-driven model ("EP," their best model) is 0.39 [Givry] / 0.32 [Florence] = 1.22. Comparing cases from the 14th and 15th centuries in the study by Dean *et al.* (2018), there is little correlation between population size and the fitted EP coefficients. If this ratio in transmission coefficients is assumed to arise chiefly from a contrast in volcanic-cooling-induced malnutrition (with no comparable volcanic eruption around 1400), then interpreting the ratio as a difference in transmission amplification in our model gives

$$\left(1 + \mathcal{M}_{Givry}\right)^2 / \left(1 + \mathcal{M}_{Florence}\right)^2 = 1.22$$

which, using the above parameter values, yields $\mathcal{M}_{Florence} = 0.4$. This value, higher than our standard background value ($M = 0.25$), is plausible for late fourteenth-century Florence, where nutritional access was likely already compromised: wheat prices approximately doubled from 1354–1367 to 1368–1378, while wages declined by up to 20% due to heavy indirect taxation in the city and rural hinterland, despite continued urban population growth (Roncière, 1968). Since our

https://doi.org/10.5194/egusphere-2026-5195
Preprint. Discussion started: 8 September 2026
© Author(s) 2026. CC BY 4.0 License.

alternative observational malnutrition proxy (Section 3) is based on the reciprocal of food availability and purchasing power, incorporating per capita agricultural output, real wages and grain prices, it represents food accessibility rather than agricultural production alone and such changes would be expected to increase nutritional stress even without a major reduction in agricultural output. The above estimate of $M_{\mathrm{Florence}} \approx 0.4$ is therefore consistent with independent historical evidence for elevated background nutritional stress. This comparison does not uniquely determine the exponent p, but provides an independent plausibility check supporting the nonlinear transmission amplification assumed here.

C9. Infection duration, recovery, and fatality ratios

Regarding the infection period, we neglect migration of sick people. We propose that the timescale for deaths from vector-transmitted plague is governed by malnutrition, such that that $\tau_{I,\mathrm{mort,v}} = a_I + b_I(1 - \mathcal{M})$. First, we note that $\tau_{I,\mathrm{mort,v}} = 7$ days for $\mathcal{M} \approx 0.5$. This baseline timescale of 7 days was chosen from historical descriptions of untreated bubonic plague and is assumed to correspond to moderate nutritional stress. Assuming extremes of $\mathcal{M}$ cause $\tau_{I,\mathrm{mort,v}}$ to vary between 3.5 and 10 days, being about 7 days mid-way in between, we assign $a_I = 3.5$ and $b_I = 6.5$ days. Also, the recovery period in pre-industrial times without medical treatment for bubonic plague (pneumonic plague victims almost all die) is 10-14 days, so $\tau_{I,\mathrm{rec}} = 12$ days. So $\frac{1}{\tau_{\mathrm{I,ave}}} = \frac{1}{\tau_{I,\mathrm{mort,v}}} + \frac{1}{\tau_{I,\mathrm{rec}}}$ so $\tau_{\mathrm{I,ave}} = 4.4$ days and $\tilde{f}_h \approx 4/4.4 = 0.9$ when $\mathcal{M} = 0.5$. Then, the theoretical infection fatality ratio for vector-borne disease is $IFR_v = \tau_{I,\mathrm{mort,v}}^{-1}/(\tau_{I,\mathrm{mort,v}}^{-1} + \tau_{I,\mathrm{rec}}^{-1}) \approx 0.63$, which is the upper bound on the fraction of the population that dies, while that for human-to-human transmission is $IFR_h = 1$. The overall IFR is $(1 - \tilde{\phi}) \times IFR_v + \tilde{\phi} \times IFR_h$. Assuming $\tilde{\phi} = 0.5$ yields an IFR of 0.82, while more realistically (Sec. 5), $\tilde{\phi} = 0.66$ yields an IFR or 0.87. These high ratios are plausible for plague without medical treatment.

The ectoparasite ('EP') model of Dean *et al.* (2018) predicts eventual mortality ratios of 0.565 for Givry and 0.473 for Florence. These values are lower than the intrinsic IFR expected in the absence of behavioural limitation of transmission because they are based on reconstructed population-at-risk denominators rather than directly observed numbers of infections. Applying a modest factor of 1.25 gives theoretical IFR estimates of 0.70 and 0.59, respectively. Since the EP model describes vector-driven transmission, these values are used to constrain the vector-borne fatality component ($f = 0$). With $\tau_{I,\mathrm{rec}} = 12$ days, they imply mortality timescales of 5.0 days (Givry) and 8.3 days (Florence), compared with 6.4 and 7.4 days from the adopted malnutrition-dependent parameterization. Given uncertainties in historical attack rates, behavioural responses, and model structure, this agreement is considered satisfactory.

C10. Summary

Finally, the chosen values of many of these parameters, such as $\tilde{I}_{\mathrm{panic}}$, $\tilde{I}_{\mathrm{return}}$, $\tilde{\tau}_{\mathrm{out}}$, and $\tilde{\tau}_{\mathrm{in}}$, should be regarded as phenomenological constitutive parameters constrained by historical plausibility and epidemic timescales rather than directly observed historical quantities. Appendix D lists the values of parameters derived for the standard case ('[…]').

https://doi.org/10.5194/egusphere-2026-5195
Preprint. Discussion started: 8 September 2026
© Author(s) 2026. CC BY 4.0 License.

https://doi.org/10.5194/egusphere-2026-5195
Preprint. Discussion started: 8 September 2026
© Author(s) 2026. CC BY 4.0 License.

Appendix D

Table of Symbols

Symbol	Meaning	Value [standard case] & units
$\tilde{\mathbf{A}}$	Matrix for the evolution equation of $\tilde{\mathbf{X}}$	
a_I, b_I	Coefficients in expression for $\tau_{I,\mathrm{mort,v}}$	[3.5, 6.5] days
A_f	Harvest source coefficient	[1 yr^{-1}] s^{-1}
c_d	Heat capacity of column of unit area of climate system for mixed- layer (55 m)	$\rho_L d_d c_L$ [2.3×10^8] J $\mathrm{m}^{-2}\mathrm{K}^{-1}$
$\tilde{c}_h$	Dimensionless transmission factor for malnutrition (human-to-human)	[1.75]
c_L	Specific heat capacity of water	4200 J/kg/K
c_s	Heat capacity of column of unit area of climate system for surface layer (18 m)	$\rho_L d_s c_L$ [0.76×10^8] J $\mathrm{m}^{-2}\mathrm{K}^{-1}$
$\tilde{c}_v$	Dimensionless transmission factor for malnutrition (vector-to-human)	[1.5]
C_m	Constant for change of malnutrition due to lack of food stock	[5 yr^{-1}] s^{-1}
d_s, d_d	Depth of surface and mixed layer of ocean	[18, 55] m
d_h	Transmission coefficient: vector → human	[0.0066] km2 per (lice · day)
$\tilde{d}_h$	Dimensionless vector → human transmission	$d_h\ \tau_v\ \tilde{c}_v\ U_{v,0}$ [2]
D_h	Density of humans killed by the plague	people per km² [0 initially]
$\tilde{D}_h$	Dimensionless dead human density	$D_h/U_{h,0}$ [0 initially]
D_m	Density of humans killed by malnutrition	people per km² [0 initially]
$\tilde{D}_m$	Dimensionless density of humans killed by malnutrition	$D_m/U_{h,0}$ [0 initially]
e_r	Source rate of infected lice (births + other vector infection)	[2.5×10^{-5}] per km² day^{-1}
$\tilde{e}_r$	Dimensionless source rate	$e_r\ \tau_v/U_{r,0}$ [10^{-6} maximum]
$\tilde{f}_h$	Dimensionless rate for waning immunity	τ_v/τ_{wane} [3.65×10^{-3}]
$\tilde{f}_p$	Dimensionless rate for conversion of bubonic cases from vector-mediated infection to become secondary pneumonic	$\tau_v/\tau_{I,p}$ [0.8]

https://doi.org/10.5194/egusphere-2026-5195
Preprint. Discussion started: 8 September 2026
© Author(s) 2026. CC BY 4.0 License.

Symbol	Meaning	Value [standard case] & units
$\tilde{f_r}$	Dimensionless rate for depletion of reservoir hosts (rodents/mammals)	τ_v/τ_r [0.011]
f_s	Food stock index (0 for no storage, unity for total storage, more than unity for surplus)	[1 initially]
f_w	External source of seeds for crops	[0.1]
F	Radiative forcing from volcanic eruption	W/m²
F_0	Peak value of F	W/m²
F_{peak}	Minimum value of $F < 0$	W/m²
g_v	Transmission coefficient: human → vector	[0.008] km² per (infected human · day)
$\tilde{g}_v$	Dimensionless human → vector transmission	$g_v\, U_{h,0}\, \tau_v$ [0.32]
g_{rv}	Transmission coefficient: reservoir host (e.g. rodent) → vector (e.g. lice)	[2.5×10^{-4}] km² per (infected human · day)
$\tilde{g}_{rv}$	Dimensionless reservoir host (e.g. rodent) → vector (e.g. lice) transmission	$g_{rv}\, U_{r,0}\, \tau_v$ [0.1]
h_h	Transmission coefficient: human → human (pneumonic)	[0.011] per (human · human · day)
$\tilde{h}_h$	Dimensionless human → human transmission coefficient	$h_h\, U_{h,0}\, \tau_v\, \tilde{c}_h$ [1.1]
I_h	Density of infected humans	people per km² [0.02 pre-epidemic background]
$\tilde{I}_h$	Dimensionless infected human density	$I_h/U_{h,0}$ [~0.002 pre-epidemic]
I_{hv}	Density of vector-mediated (bubonic) infected humans	people per km² [0.02 pre-epidemic background]
$\tilde{I}_{hv}$	Dimensionless vector-mediated (bubonic) infected human density	$I_{hv}/U_{h,0}$ [~0.002 pre-epidemic]
I_{hvp}	Density of secondary pneumonic cases from vector-mediated (bubonic) infected humans	people per km² [0.02 pre-epidemic background]
$\tilde{I}_{hvp}$	Dimensionless density of secondary pneumonic infected humans	$I_{hvp}/U_{h,0}$ [~0.002 pre-epidemic]
I_{panic}	Threshold on I_h for infection-driven migration	people per km² [0.05]
$\tilde{I}_{panic}$	Dimensionless version of threshold I_{panic}	$I_{panic}/U_{h,0}$ [0.005]
I_r	Number density of plague-infected reservoir host animals (e.g.	per km²

https://doi.org/10.5194/egusphere-2026-5195
Preprint. Discussion started: 8 September 2026
© Author(s) 2026. CC BY 4.0 License.

Symbol	Meaning	Value [standard case] & units
	rodents/mammals)	
$\tilde{I}_r$	Dimensionless density of infected body lice	$I_r/U_{r,0}$
I_{return}	Threshold on I_h for return from migration	people per km² [0.05]
$\tilde{I}_{return}$	Dimensionless version of threshold I_{return}	$I_{return}/U_{h,0}$ [0.005]
I_v	Number density of plague-infected body lice	per km² (9×10^{-2} pre-epidemic)
$\tilde{I}_v$	Dimensionless density of infected body lice	$I_v/U_{v,0}$ (9×10^{-4} pre-epidemic)
IFR_v, IFR_h	Infection fatality ratio	$IFR_v = \tau_{I,\mathrm{mort,v}}^{-1}/(\tau_{I,\mathrm{mort,v}}^{-1} + \tau_{I,\mathrm{rec}}^{-1})$, $IFR_h = 1$
$\widetilde{j_h}$	Dimensionless loss rate for infected humans (vector transmission)	$\tau_v/\tau_{\mathrm{I,ave}}$ [0.90]
$\tilde{j}_h^*$	Dimensionless loss rate for all infected humans	$\tilde{\phi}\widetilde{k_h} + (1-\tilde{\phi})\widetilde{j_h}$ [1.25]
$\widetilde{k_h}$	Dimensionless loss rate for infected humans (human-to-human transmission)	$\frac{\tau_v}{\tau_{I,\mathrm{mort},h}}$ [1.6]
m, m_{eq}, m_{peak}	Sigmoid-malnutrition index corresponding to $\mathcal{M}, \mathcal{M}_{eq}, \mathcal{M}_{peak}$	$m_{peak} \approx m_{eq} + C_m\tau_{recover}(1 - f_w)$
$\mathcal{M}$	Health-related malnutrition index (1 = starvation, 0 = modern health)	[0.5 during epidemic]
$\mathcal{M}_{eq}$	Value of $\mathcal{M}$ initially before climate shock	[0.25]
$\mathcal{M}_{peak}$	Peak value of $\mathcal{M}$	[0.7]
M_h	Density of uninfected humans who migrated	people per km² [0 initially]
$\widetilde{M}_h$	Dimensionless migrated human density	$M_h/U_{h,0}$ [0 initially]
p	Exponent for malnutrition index factor	[2]
$R_{eff,h}$	Instantaneous reproduction number of plague for human-to-human transmission	$\frac{\tilde{\phi}\widetilde{h_h}\,\widetilde{U}_h}{\tilde{j}_h^*}$
$R_{eff,v}$	Same as $R_{eff,h}$ but for vector-borne transmission	$\frac{\widetilde{d_h}\,\widetilde{U}_h\,\tilde{I}_v}{\tilde{j}_h^*\,\tilde{I}_h}$
$R_{0,h}$	Reproduction number of plague for human-to-human transmission (number of secondary infections per primary infection) for a hypothetically disease-free population	[0.7] $\frac{\widetilde{h_h}}{\widetilde{k_h}}$

https://doi.org/10.5194/egusphere-2026-5195
Preprint. Discussion started: 8 September 2026
© Author(s) 2026. CC BY 4.0 License.

Symbol	Meaning	Value [standard case] & units
$R_{0,v}$	Same as for $R_{0,h}$ except for vector-borne transmission	[0.7] $\frac{\tilde{g}_v \tilde{d}_h}{j_h}$
R_h	Density of humans who recovered from infection	people per km² [0 initially]
$\tilde{R}_h$	Dimensionless recovered human density	$R_h/U_{h,0}$ [0 initially]
S, S_0	regional food stock in storage, pre-disturbance reference value	kg
t	Time since start of epidemic or since eruption	s
$\tilde{t}$	Dimensionless time since epidemic start	t/τ_v
t_{lag}	Lagged time for onset of decay of aerosol, for delay of onset of washout	[1 yr] s
$T_c{}'$	Threshold of T_s' for non-zero influence on seeding of epidemic.	[0.5] °C
T_d'	Anomaly of global mean, annually averaged, ocean mixed-layer temperature	°C
T_s'	Anomaly of global mean, annually averaged, near surface temperature	°C
U_h	Density of uninfected susceptible humans	per km²
$\tilde{U}_h$	Dimensionless uninfected susceptible human density	$\frac{U_h}{U_{h,0}}$ [1 pre-epidemic]
$U_{h,0}$	Number density of all humans (initially before any infection)	[10] per km²
$\tilde{U}_{h,crit}$	Critical value of $\tilde{U}_h$ above which there is unstable growth of the epidemic	$\frac{\tilde{J}_h^*(\tilde{\phi})}{\tilde{\phi}\widetilde{h_h} + \widetilde{g_v}\,\widetilde{d_h}}$
$U_{r,0}$	Number density of all reservoir hosts (initially before any infection)	[100] per km²
$U_{v,0}$	Number density of all body lice (initially before any infection)	[100] per km²
$\tilde{\mathbf{X}}$	Vector for perturbations of infected and uninfected humans along trajectory in the 2D phase-space	$\tilde{\mathbf{X}} = (\delta\tilde{I}_h, \delta\tilde{U}_h)$
Y	Climate feedback parameter	[1.7] W m^{-2}K^{-1}
$\tilde{\alpha}_h$	Enhancement by malnutrition of human-to-human transmission	[1.0]
$\tilde{\alpha}_v$	Enhancement by malnutrition of vector-to-human transmission	[1.0]
$\gamma_{s,d}$	Surface-deep ocean coupling coefficient	[3.8]
κ	Coefficient for response of crop growth to cooling anomaly	[0.75] K^{-1}
$\tilde{\lambda}_h$	Dimensionless growth rate of perturbations $\tilde{\mathbf{X}} = (\delta\tilde{U}_h, \delta\tilde{I}_h)$ during the	

https://doi.org/10.5194/egusphere-2026-5195
Preprint. Discussion started: 8 September 2026
© Author(s) 2026. CC BY 4.0 License.

Symbol	Meaning	Value [standard case] & units
	epidemic	
λ_m	Coefficient for impaired agricultural productivity from malnutrition	[0.5]
μ	Fractional rate of deaths per year from malnutrition	per day
$\tilde{\mu}$	Dimensionless form of μ	- $\mu\tau_v$
$\mu_{m,max}$	Maximum of μ when $\mathcal{M} = 1$	[0.1 per year] per day
$\tilde{\eta}_h$	Dimensionless growth rate of infected human density ($\tilde{I}_h$) from a disease-free equilibrium	$\tilde{\phi}\widetilde{h_h} + \widetilde{g_v}\,\widetilde{d_h} - \widetilde{j_h}$ initially [0.7 pre-epidemic]
ρ_L	Density of water	1000 kg m^{-3}
$\tau_{\mathrm{a,r}}$	Growth time-scale for volcanic aerosol forcing	[0.1 yr] sec
$\tau_{\mathrm{a,d}}$	Decay time-scale for volcanic aerosol forcing	[10 months] sec
$\tau_{I,\mathrm{mort}}$	Infected human mortality timescale	[7] days
$\tau_{I,\mathrm{mort,h}}$	Infected mortality timescale from human-to-human transmission	[2] days
$\tau_{I,\mathrm{mort,v}}$	Infected mortality timescale from vector-borne transmission	$a_I + b_I(1 - \mathcal{M})$ [7] days
$\tau_{\mathrm{I,ave}}$	Combined infected human timescale	$\frac{1}{\tau_{I,\mathrm{mort}}} + \frac{1}{\tau_{I,\mathrm{rec}}}$ [4.4] days
$\tau_{I,p}$	Time-scale for bubonic cases from vector-mediated infection to become secondary pneumonic and infectious to humans	[5] days
$\tau_{I,\mathrm{rec}}$	Recovery time-scale from infection	[12] days
τ_r	Time-scale for infected reservoir depletion	[3 years] days
$\tau_{recover}$	Time-scale for recovery from malnutrition	[0.5 years] sec
τ_{storage}	Time-scale for turnover of food (e.g. grain) in storage due to consumption and spoilage (e.g. from pests)	[1 year] sec
$\tau_{U,\mathrm{pop}}$	Time-scale for demographic recovery of population after shock	[36500] days
$\tilde{\tau}_{U,\mathrm{pop}}$	Dimensionless form of $\tau_{U,\mathrm{pop}}$	$\frac{\tau_{U,pop}}{\tau_v}$ [9.1×10^3]
$\tau_{U,\mathrm{ave}}$	Combined uninfected human timescale	[10] days
τ_v	Lifetime of plague-infected lice	[4] days
τ_{wane}	Time-scale for waning immunity of recovered humans	[3 years] days

https://doi.org/10.5194/egusphere-2026-5195
Preprint. Discussion started: 8 September 2026
© Author(s) 2026. CC BY 4.0 License.

Symbol	Meaning	Value [standard case] & units
$\tilde{\phi}$	Fraction of infections from human-to-human transmission	[0.5]
$\tilde{\phi}_v$	Ratio of infected vectors to infected humans	$\tilde{I}_v/\tilde{I}_h$ [relaxes to 0.32]
Φ_{in}, Φ_{out}	Tendencies for uninfected susceptible humans from migration into and out of the target region.	Humans per km² per day
$\tilde{\Phi}_{in}, \tilde{\Phi}_{out}$	Dimensionless versions of F_{in}, F_{out}	$\Phi_{in}/U_{h,0}$, $\Phi_{out}/U_{h,0}$

Appendix E

Results for Validation in Alternative Case

Climate-Harvest/Food-Malnutrition Linkage:

As an independent validation of the climate–harvest–malnutrition component of the model, an alternative case was simulated for the volcanic eruption of 1345 CE and the subsequent Black Death in England. This case was selected because historical estimates of crop yields and agricultural output are available (Campbell 2010; Broadberry *et al*. 2015), allowing evaluation of the environmental and nutritional components of the model. It is not used elsewhere in the present study.

Following the procedure used for the standard case (Sec. 5.1), Eqs (1)–(6) were integrated numerically with $F_0 = -3.5$ W m^{-2}, corresponding to an integrated forcing of -6.9 W yr m^{-2} (Sigl *et al.* 2015). The eruption was at least 50% stronger in radiative forcing than Pinatubo (1991) (Sec. 1; Fig. 1). The model predicts a peak global cooling of about -0.65 °C (Fig. E1a), which would correspond to about -1.3 °C peak average cooling over NH land areas, if an enhancement by a factor of about 2 is assumed (Sec. 5.1.1). This is larger than the observed summertime NH land anomaly of approximately 0.5 °C reported by Büntgen *et al.* (2026), consistent with known low biases in some tree-ring temperature reconstructions following volcanic eruptions (Stoffel *et al*. 2015).

The predicted food storage and malnutrition indices are shown in Fig. E1b. Food storage for the majority-population scenario (defined in Sec. 5.1.2) decreases to approximately 47% of its initial level, while the malnutrition index reaches values (0.55) approaching acute famine. No substantial non-plague mortality from malnutrition is predicted, consistent with historical accounts indicating that deaths in England after 1348 were dominated by plague rather than starvation.

https://doi.org/10.5194/egusphere-2026-5195
Preprint. Discussion started: 8 September 2026
© Author(s) 2026. CC BY 4.0 License.

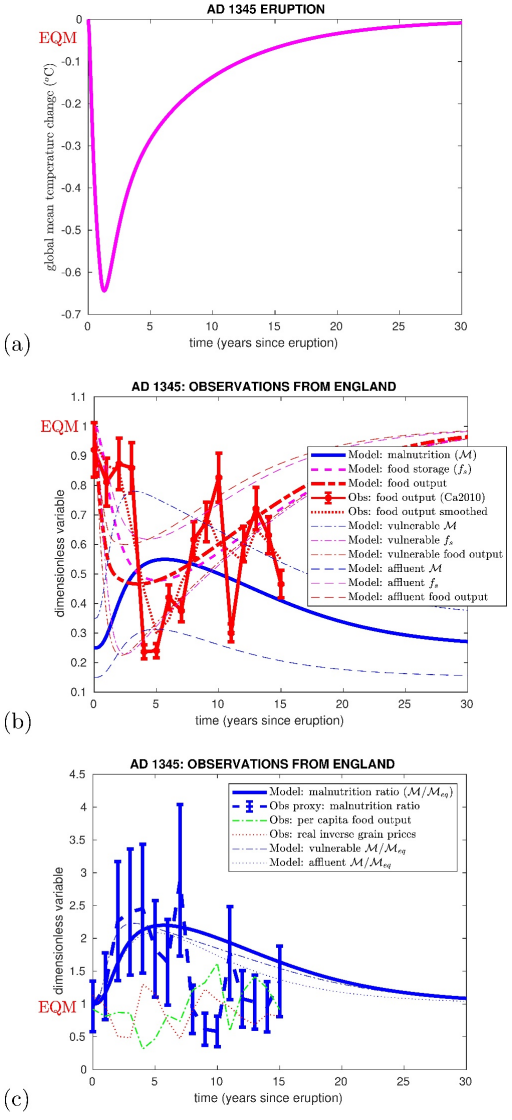

Figure E1: (a) Global mean cooling predicted by the model (Eqs (1)-(3)) following the 1345 CE eruption. (b) Predicted ratio of annual agricultural output of all crops on selected English manors relative to 1345 (Eqs (4)–(6)), compared with observations from Campbell (2010) and Broadberry *et al.* (2015), using 1335–1344 as the baseline. Also shown are the predicted food storage and malnutrition index. (c) Predicted ratio of malnutrition index relative to 1345 compared with an observational proxy, which is the reciprocal of the product of per capita agricultural output and the ratio of real wages to grain prices (Campbell 2010; Campbell and Ó Gráda 2011). Observational uncertainties are shown as error bars (see text for estimation of uncertainties and proxy construction).

https://doi.org/10.5194/egusphere-2026-5195
Preprint. Discussion started: 8 September 2026
© Author(s) 2026. CC BY 4.0 License.

The predicted total agricultural output is compared with historical estimates from England using the harvest-yield proxy of Campbell (2010), adjusted for cultivated area changes following the approach of Broadberry *et al*. (2015). The comparison (Fig. E1b) shows adequate agreement between model (majority-population scenario) and observations of agricultural output (various thick red lines), with both indicating a reduction in output of approximately 60% during the decade following the eruption and a minimum occurring within 3–4 years. The predicted mean output ratio for the 1350s relative to 1300–1309 is 0.60, compared with the observed value of 0.59 ± 0.08 (Broadberry *et al*. 2015). Moreover, the corresponding predictions of output (thin red lines) for the vulnerable- and affluent-population scenarios (Sec. 5.1.2) span most of the spread of interannual variability of the observed proxy, reflecting plausibility in the choice of parameter values defining both scenarios given below.

Figure E1c compares the predicted malnutrition index with an observational proxy that we derived from English economic records (Campbell 2010; Campbell and O'Gráda 2011). Our proxy combines real wages, grain prices, and per capita agricultural output, reflecting the expectation that nutrition improves with higher food availability and purchasing power. A sudden halving of the population during the intense phase of the Black Death (1348–1350) was assumed based on long-term demographic estimates (Broadberry *et al*. 2015). Both model and proxy indicate a broad increase (by a factor of two at least) in malnutrition following the eruption in all three scenarios, with persistence into the following decade. This prolonged recovery is consistent with the long-lasting demographic and agricultural effects observed after other major crises, such as the Great Famine of 1315–1317 (DeWitte and Slavin 2013).

However, the observational proxy returns to the pre-1345 normality at the end of the first decade (1354) while the prediction relaxes back to it more gradually during the second decade (Fig. E1c). Arguably, in this second decade, our observational proxy reflects instantaneous food availability and does not capture the isotopic observations of the recent history (last 5 years) of malnutrition of plague victims from London in 1361 (Godde et al. 2025), which agree well with the model prediction (see below).

Overall, the model reproduces the magnitude and timing of the observed decline in agricultural output and captures the subsequent nutritional stress. This provides independent support for the climate–harvest–malnutrition linkage used in the model.

Malnutrition-Disease linkage:

Godde *et al.* (2025) combined dietary-isotope, pathological and demographic evidence from medieval London cemeteries to investigate factors associated with mortality during the second plague epidemic in England. In particular, skeletons attributed

https://doi.org/10.5194/egusphere-2026-5195
Preprint. Discussion started: 8 September 2026
© Author(s) 2026. CC BY 4.0 License.

to plague deaths in 1361 were compared with skeletons attributed to famine and to other causes of death. Rib-bone collagen was analysed for its ^{15}N isotope composition (δ^{15}N), which provides an indicator of nutritional status. Previous work, including Walter *et al.* (2020), has shown that nutritional stress and famine can be associated with elevated δ^{15}N.

Godde *et al.* reported mean δ^{15}N values of approximately 12.1‰ for plague deaths, 12.5‰ for famine deaths, and 12.7‰ for deaths classified as attritional. Their multinomial logistic regression found a statistically significant negative association between and the relative probability of plague mortality. For the comparison between plague deaths in 1361 and deaths from other causes over the wider period represented by the archaeological sample, the fitted relationship included the term

$$\ln\left(\frac{P_{plague}}{P_{other}}\right) = A + B\,\log_2(\delta^{15}\mathrm{N}) + \ldots \qquad \text{(C1)}$$

where the ellipsis denotes additional covariates included in the multinomial regression. The estimated coefficient of $\log_2(\delta^{15}\mathrm{N})$ was $B = -32$, with standard error 11. The regression also included an intercept and coefficients for age, sex, skeletal characteristics, δ^{13}C date and their interactions. Since these individual-level covariates are not represented explicitly in the present epidemiological model, we compare the slope B of the relationship rather than its absolute intercept or predicted probabilities.

In order to simulate the dynamics of the plague during the alternative case of the Black Death and its aftermath in England, we used the climate–harvest–malnutrition model described above to provide the nutritional boundary condition for the epidemiological model. Three demographic/resilience scenarios (Table 2) were simulated from 1345 CE until dimensionless time 2000, corresponding approximately to 1367 CE. In the calibrated simulations, malnutrition-related mortality was allowed to increase from $\mathcal{M} = 0.25$, 0.35 and 0.15 in the three population-resilience scenarios, with a maximum malnutrition mortality rate of $\mu_{m,max} = 0.1$. The eventual plague mortality in the majority-population scenario was predicted to be about 46%, while malnutrition-related non-plague mortality was predicted as 5%.

We assumed a linear relationship between the malnutrition index $\mathcal{M}$ and δ^{15}N, with $\mathcal{M}$ = 0 corresponding to 10.8‰, representative of the mean measured in a modern English human bone-collagen sample (Chidimuro 2020), and $\mathcal{M}$ = 1 corresponding to 14.0‰, approximately representing the upper range of values associated with severe nutritional stress in the available archaeological literature. For each mortality category, the resulting δ^{15}N values were weighted by the number of deaths in that category. The three demographic scenarios were then combined using their initial population fractions (60% majority, 20% vulnerable/poor and 20% affluent/elite).

https://doi.org/10.5194/egusphere-2026-5195
Preprint. Discussion started: 8 September 2026
© Author(s) 2026. CC BY 4.0 License.

Curiously, the "attritional" non-plague deaths reported by Godde *et al.* had a higher mean δ^{15}N than their deaths classified as famine. We therefore interpret the nutritional signal represented by the combined famine and attritional categories as more comparable to the malnutrition-related non-plague mortality represented explicitly in our model than to a nutritionally independent background mortality process. Accordingly, P_{other} in this validation refers solely to malnutrition-related non-plague mortality.

Figure E2a compares the mortality-weighted mean δ^{15}N values predicted by the model with the archaeological observations. For plague deaths, the population-weighted model prediction is 12.07‰ across all three scenarios, compared with approximately 12.1‰ in Godde *et al.* For malnutrition-related mortality, the corresponding model prediction is 12.36‰, compared with 12.6‰ for the mean of the famine (12.5‰) and attritional (12.7‰) categories. Thus, the model reproduces the observed nutritional-isotope values associated with both mortality categories reasonably closely.

Each epidemiological simulation represents individuals as homogeneous within a given demographic scenario and therefore produces a single mortality-weighted mean δ^{15}N value together with the corresponding relative probability of plague mortality. The model does not explicitly represent the distribution of skeletal characteristics, age, sex or other individual-level covariates available in the archaeological sample. The three scenarios nevertheless provide three distinct pairs of values of $\log_2(\delta^{15}\mathrm{N})$ and $\ln\left(P_{plague}/P_{other}\right)$, spanning the scenarios of the simulated population.

To reproduce the scale of the empirical relationship, we calculated $x = \log_2(\delta^{15}\mathrm{N})$ and $y = \ln\left(P_{plague}/P_{other}\right)$. A weighted least-squares regression through the three modelled points was then fitted, with each point weighted according to the number of deaths represented by its demographic scenario. Specifically, the weight was proportional to the initial population fraction multiplied by the cumulative number of deaths contributing to the comparison.

The resulting slope was

$$B_{model} = -42.6\,.$$

This has the same negative sign as the empirical estimate of $B = -32 \pm 11$ from Godde *et al.* and differs from the empirical estimate by less than one standard error. Thus, despite the very different levels of aggregation and the absence from the model of several individual-level covariates included in the archaeological regression, the model reproduces both the direction and approximate magnitude of the observed association between nutritional status and relative plague mortality.

Figure E2b compares this modelled relationship with the fitted relationship reported by Godde *et al.* Because the intercept of the published regression depends on covariates that are not represented explicitly in the present model, the comparison is

https://doi.org/10.5194/egusphere-2026-5195
Preprint. Discussion started: 8 September 2026
© Author(s) 2026. CC BY 4.0 License.

made using the slope rather than the absolute intercept. The published regression line was therefore translated vertically, without altering its slope, to pass through the mortality-weighted centroid of the three modelled points. The thin dashed lines indicate the corresponding uncertainty in the empirical slope. This procedure permits comparison of the shape and magnitude of the association without assigning unsupported values to the unmodelled covariates.

Given the simplifying assumptions of the three-scenario representation, the limited number of modelled points and the absence of several covariates represented in the archaeological analysis, we regard this agreement as supportive validation of the model's malnutrition–plague mortality mechanism, rather than as a test of the full multinomial regression. The close agreement in mortality-associated $\delta^{15}\mathrm{N}$ values, and the reproduction of an empirical slope to within about one standard error, provide independent evidence that the model represents adequately the linkage between nutritional stress and mortality during plague epidemics.

https://doi.org/10.5194/egusphere-2026-5195
Preprint. Discussion started: 8 September 2026
© Author(s) 2026. CC BY 4.0 License.

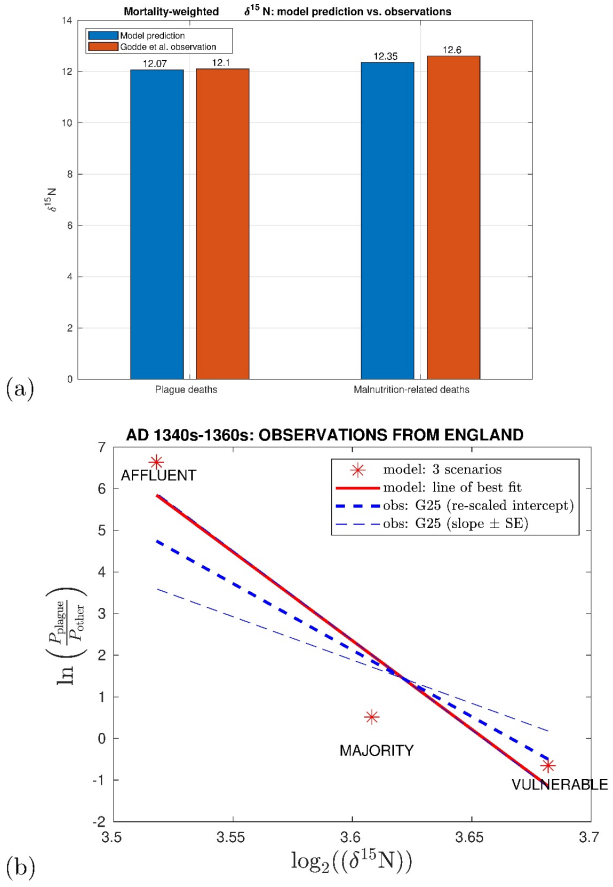

Figure E2: ***(a)*** **Comparison of mortality-weighted mean δ^{15}N values between the model predictions and observations reported by Godde *et al.* (2025) for plague deaths and for deaths attributed to famine and attritional causes. Model predictions combine the majority, vulnerable/poor and affluent/elite scenarios using their initial population fractions and mortality weighting.** ***(b)*** **Comparison of the modelled relationship between $\log_2(\delta^{15}\mathrm{N})$ and $\ln(P_{plague}/P_{other})$ with the corresponding fitted relationship reported by Godde *et al.* (2025). The three modelled points represent the majority, vulnerable/poor and affluent/elite scenarios. The solid red line is the mortality-weighted least-squares regression through the model predictions ($B = -42.6$). The dashed blue line represents the published empirical slope ($B = -32$), translated vertically to pass through the weighted centroid of the modelled relationship. Thin blue dashed lines indicate the published uncertainty in the empirical slope. Because the archaeological regression includes covariates not represented explicitly in the present model, the comparison is intended to test the direction and approximate magnitude of the association rather than the absolute intercept or predicted probabilities.**

https://doi.org/10.5194/egusphere-2026-5195
Preprint. Discussion started: 8 September 2026
© Author(s) 2026. CC BY 4.0 License.

Code and data availability

Data and codes used in the present study will be placed on the Zenodo website in accordance with FAIR principles, at the time of final publication.

Author contributions

VTJP directed the study, constructed the model, developed all code and performed all simulations. TA, HC, RG, SJ, MS, MT, JR, MP, FCL, and JIY improved the manuscript by reviewing it or contributing text. Clinicians CJF and AL researched the literature for specific issues about choice of epidemiological parameters. JS and MT provided palaeoclimate data. Most co-authors participated in discussions of the paper at a meeting in early 2026 in Stockholm University.

Competing interests

The authors declare that they have no conflict of interest.

Acknowledgements and financial support

The work was funded by an award to Vaughan Phillips from the Swedish Research Council (Vetenskapsrådet), grant no. 2024-00413. Fredrik Charpentier Ljungqvist and Martin K. Skoglund were additionally supported by the Marianne and Marcus Wallenberg Foundation (grant no. MMW 2022-0114), and Ljungqvist also by the Swedish Research Council (Vetenskapsrådet, grant no. 2023-00605).

References

Adapa, S.R., Hendrix, K., Upadhyay, A., Dutta, S., Vianello, A., O'Corry-Crowe, G., Monroy, J., Ferrer, T., Remily-Wood, E., and G. C. Ferreira, 2025: Genetic Evidence of *Yersinia pestis* from the First Pandemic. *Genes*, **16,** 926

Arjava, A. 2005. The mystery cloud of 536 CE in the Mediterranean sources. *Dumbart. Oaks Pap.* **59**:73-94

Arthur, F., Hatlestad, K., Lindholm, K.-J., Loftsgarden, K., Löwenborg, D., Solheim, S., Roche, D. M., and H. Renssen, 2024: The impact of volcanism on Scandinavian climate and human societies during the Holocene: Insights into the Fimbulwinter eruptions (536/540 AD). *The Holocene*, **34**(5), 619–633.

https://doi.org/10.5194/egusphere-2026-5195
Preprint. Discussion started: 8 September 2026
© Author(s) 2026. CC BY 4.0 License.

Ayyadurai, S., Sebbane, F., Raoult, D., and M. Drancourt, 2010: Body lice, Yersinia pestis orientalis, and Black Death. *Emerg. Infect. Dis.,* **16**, 892–893

Baillie, M. G. L., 1991: Marking in marker dates: Towards an archaeology with historical precision. *World Archaeol.*, **23**(2), 233–243

Baillie, M. G. L., 1994: Dendrochronology raises questions about the nature of the CE 536 dust-veil event. *The Holocene*, **4**(2), 212–217

Baten, J., 2001: Climate, grain production and nutritional status in southern Germany during the XVIIIth century. *Journal of European Economic History*, **30**, 9–47

Bauch, M., and U. Büntgen, 2025: Climate-driven changes in Mediterranean grain trade mitigated famine but introduced the Black Death to medieval Europe. *Commun. Earth Environ.*, **6,** Article 986

Beillouin, D., Schauberger, B., Bastos, A., Ciais, P., and D. Makowski, 2020: Impact of extreme weather conditions on European crop production. *Philos. Trans. Roy. Soc. B*, **375**(1810), 20190510

Belich, J., 2022: *The World the Plague Made: The Black Death and the Rise of Europe*. Princeton: Princeton University Press

Biraben, J.-N., 1975–1976: *Les hommes et la peste en France et dans les pays européens et méditerranéens*. 2 vols. Paris & The Hague: Mouton. (Civilisations et Sociétés, nos. 35–36)

Blanc, G., and M. Baltazard 1942: Rôle des ectoparasites humains dans la transmission de la peste. *Bull Acad Natl Med* **126**:446

Bos, K. I., Schuenemann, V. J., Golding, G. B., Burbano, H. A., Waglechner, N., Coombes, B. K., McPhee, J. B., DeWitte, S. N., Meyer, M., Schmedes, S., Wood, J., Earn, D. J. D., Herring, D. A., Bauer, P., Poinar, H. N., and J Krause, 2011: A draft genome of *Yersinia pestis* from victims of the Black Death**.** *Nature,* **478**(7370): 506–510

Broadberry, S., Campbell, B. M. S., Klein, A., Overton, M., and Leeuwen, B. V., 2015: *British economic growth 1270–1870*. Cambridge University Press

Burke, A., Philip, S. Y., Anchukaitis, K. J., D'Arrigo, R., Stoffel, M., Wilson, R., Büntgen, U., Hegerl, G. C., and Oppenheimer, C., 2023: High sensitivity of summer temperatures to stratospheric sulfur loading from volcanoes in the Northern Hemisphere. *Proc. Natl. Acad. Sci. U.S.A.*, **120**(47), e2221810120

Büntgen, U., Myglan, V. S., Ljungqvist, F. C., McCormick, M., Di Cosmo, N., Sigl, M., Jungclaus, J., Wagner, S., Krusic, P. J., Esper, J., Kaplan, J. O., de Vaan, M. A. C., Luterbacher, J., Wacker, L., Tegel, W., and A. V. Kirdyanov, 2016: Cooling and societal change during the Late Antique Little Ice Age from 536 to around 660 AD. *Nat. Geosci.*, **9**, 231–236.

Büntgen, U., Myglan, V. S., Ljungqvist, F. C., McCormick, M., Di Cosmo, N., Sigl, M., Jungclaus, J., Wagner, S., Krusic, P. J., Esper, J., Kaplan, J. O., de Vaan, M. A. C., Luterbacher, J., Wacker, L., Tegel, W., and A. V. Kirdyanov, 2017: Reply to "Limited Late Antique Cooling". *Nat. Geosci.*, **10**, 243

Büntgen, U., Allen, K., Anchukaitis, K. J., Arseneault, D., Boucher, É., Bräuning, A., Chatterjee, S., Cherubini, P., Churakova (Sidorova), O. V., Corona, C., Gennaretti, F., Grießinger, J., Guillet, S., Guiot, J., Gunnarson, B., Helama, S.,

https://doi.org/10.5194/egusphere-2026-5195
Preprint. Discussion started: 8 September 2026
© Author(s) 2026. CC BY 4.0 License.

Hochreuther, P., Hughes, M. K., Huybers, P., Kirdyanov, A. V., Krusic, P. J., Ludescher, J., Meier, W. J.-H., Myglan, V. S., Nicolussi, K., Oppenheimer, C., Reinig, F., Salzer, M. W., Seftigen, K., Stine, A. R., Stoffel, M., St. George, S., Tejedor, E., Trevino, A., Trouet, V., Wang, J., Wilson, R., Yang, B., Xu, G., and J. Esper, 2021: The influence of decision-making in tree ring-based climate reconstructions. *Nature Communications*, **12,** 341

Büntgen, U., Crivellaro, A., Arseneault, D., Baillie, M., Barclay, D., Bernabei, M., Bontadi, J., Boswijk, G., Brown, D., Christie, D. A., Churakova, O. V., Cook, E. R., D'Arrigo, R., Davi, N., Esper, J., Fonti, P., Greaves, C., Hantemirov, R. M., Hughes, M. K., Kirdyanov, A. V., Krusic, P. J., Le Quesne, C., Ljungqvist, F. C., McCormick, M., Myglan, V. S., Nicolussi, K., Oppenheimer, C., Palmer, J., Qin, C., Reinig, F., Salzer, M., Stoffel, M., Torbenson, M., Trnka, M., Villalba, R., Wiesenberg, N., Wiles, G., Yang, B., and A. Piermattei, 2022: Global wood anatomical perspective on the onset of the Late Antique Little Ice Age (LALIA) in the mid-6th century CE. *Sci. Bull.*, **67**, 2336–2344

Büntgen, U., Di Cosmo, N., Esper, J., Frachetti, M., Khalidi, L., Mauelshagen, F., Rohland, E., and C. Oppenheimer, 2026: Volcanoes, climate, and society. *Annu. Rev. Earth Planet. Sci.*, **54**, 23–53

Campbell, B. M. S., 2010: Nature as historical protagonist: environment and society in pre-industrial England. *Econ. Hist. Rev.*, **63**, 2, 281–314

Campbell, B. M. S., 2017: Global climates, the 1257 mega-eruption of Samalas volcano, Indonesia, and the English food crisis of 1258. *Trans. Royal Hist. Soc.,* **27**, 87–121

Campbell, B. M. S., and C. Ó Gráda, 2011: Harvest shortfalls, grain prices, and famines in preindustrial England. *J. Econ. Hist.,* **71**(4), 859–886

Campbell, G. L. and Hughes, J. M., 1995: Plague in India: a new warning from an old nemesis. *Ann. Intern. Med*. **122**, 151–153

Cassiodorus, 1992: *The Variae of Magnus Aurelius Cassiodorus Senator*. Translated by S. J. B. Barnish. Liverpool: Liverpool University Press

Chidimuro, B., 2020: *A multi-isotope, multi-tissue study of diets in industrialised societies of 17th to 19th century England*. PhD thesis, University of York

Comeau, R., Seaman, A., and A. Bloxam, 2023: Plague, climate and faith in Early Medieval Western Britain: Investigating narratives of change. *Medieval Archaeology,* **67**(1), 1–28

Creighton, C., 1891: *A History of Epidemics in Britain from A.D. 664 to the Extinction of Plague*. Vol. 1. Cambridge: Cambridge University Press.

Cui, Y., Yu, C., Yan, Y., Li, D., Li, Y., Jombart, T., Weinert, L. A., Wang, Z., Guo, Z., Xu, L., Zhang, Y., Zheng, H., Qin, N., Xiao, X., Wu, M., Wang, X., Zhou, D., Qi, Z., Du, Z., Wu, H., Yang, X., Cao, H., Wang, H., Wang, J., Yao, S., Rakin, A., Li, Y., Falush, D., Balloux, F., Achtman, M., Song, Y., Wang, J., and R. Yang, 2013: Historical variations in mutation rate in an epidemic pathogen, *Yersinia pestis*. *Proc. Natl. Acad. Sci. U.S.A.*, **110**(2), 577–582

https://doi.org/10.5194/egusphere-2026-5195
Preprint. Discussion started: 8 September 2026
© Author(s) 2026. CC BY 4.0 License.

Dean, K. R., Krauer, F., Walløe, L., Lingjærde, O. C., Bramanti, B., Stenseth, N. C., and B. V. Schmid, 2018: Human ectoparasites and the spread of plague in Europe during the Second Pandemic. *Proc. Natl. Acad. Sci. USA*, **115**(6), 1304–1309

Curtis, D. R., 2022: Reduction in grain pollen indicates population decline, but not necessarily Black Death mortality. *Nature Ecology & Evolution* **6**: 1626–1627

de Jong, S. M. H., 2026: Ash clouds, Famine, and Epidemics: Societal Responses to Volcanic-Induced Climate Shocks in mid-sixth Century Ostrogothic Italy and Eastern Roman Anatolia. *Geografiska Annaler: Series A, Physical Geography*, in press.

Del Valle, S., Hethcote, H., Hyman, J., and Castillo-Chavez, C. 2005: Effects of behavioral changes in a smallpox attack model. *Math. Biosci*. **195**, 228–251

Demeure, C. E., Dussurget, O., Fiol, G. M., Le Guern, A.-S., Savin, C., and J. Pizarro-Cerdá, 2019: Yersinia pestis and plague: an updated view on evolution, virulence determinants, immune subversion, vaccination, and diagnostics. *Genes Immun.,* **20**:357–370

Dennis, D. T., Gage, K. L., Gratz, N. G., Poland, J. D., and E. Tikhomirov (eds.), 1999: *Plague Manual: Epidemiology, Distribution, Surveillance and Control*. Geneva: World Health Organization

DeWitte, S. and Slavin, P., 2013: Between famine and death: England on the eve of the Black Death—evidence from paleoepidemiology and manorial accounts. *J. Interdiscip. Hist.*, **44**(1), 37–60

Drancourt M., Houhamdi L., and Raoult D., 2006: Yersinia pestis as a telluric, human ectoparasite-borne organism. *Lancet Infect. Dis.,* **6**:234–241

Dull, R. A., Southon, J. R., Kutterolf, S., Anchukaitis, K. J., Freundt, A., Wahl, D. B., Sheets, P., Amaroli, P., Hernandez, W., Wiemann, M. C., and Oppenheimer, C., 2019: Radiocarbon and geologic evidence reveal Ilopango volcano as source of the colossal 'mystery' eruption of 539/40 CE. *Quat. Sci. Rev.*, **222**, 105855

Epstein, J. M., Parker, J., Cummings, D. & Hammond, R. A., 2008: Coupled contagion dynamics of fear and disease: mathematical and computational explorations. *PLoS ONE,* **3,** e3955

Feldman, M., Harbeck, M., Keller, M., Spyrou, M. A., Rott, A., Trautmann, B., Scholz, H. C., Päffgen, B., Peters, J., McCormick, M., Bos, K. I., Herbig, A., and Krause, J., 2016: A high-coverage Yersinia Pestis genome from a sixth-century Justinianic Plague victim. *Mol. Biol. Evol.*, **33**(11), 2911–2923

Fell, H. G., Baldini, J. U. L., Dodds, B., and Sharples, G. J., 2020: Volcanism and global plague pandemics: Towards an interdisciplinary synthesis. *J. Hist. Geogr.*, **70,** 36–46

Fuks, D., Ackermann, O., Ayalon, A., Bar-Matthews, M., Bar-Oz, G., Levi, Y., Maeir, A. M., Weiss, E., Zilberman, T., and Safrai, Z., 2017: Dust clouds, climate change and coins: consiliences of palaeoclimate and economy in the Late Antique southern Levant. *Levant*, **49**(2), 205–223

https://doi.org/10.5194/egusphere-2026-5195
Preprint. Discussion started: 8 September 2026
© Author(s) 2026. CC BY 4.0 License.

Geoffroy, O., Saint-Martin, D., Olivié, D. J. L., Voldoire, A., Bellon, G., & Tytéca, S., 2013: Transient climate response in a two-layer EBM. Part I: Analytical solution and parameter calibration using CMIP5 AOGCM experiments. *J. Clim.,* **26**, 1841–1857

Gildas, 1978: *The Ruin of Britain and Other Works*. Edited and translated by Michael Winterbottom. Chichester: Phillimore

Goold, C., S. Pfuderer, W. H. James, N. Lomax, F. Smith, and L. M. Collins, 2020: A Mathematical Model of National-Level Food System Sustainability. arXiv preprint https://arxiv.org/abs/2012.08355

Godde, K., DeWitte, S. N., Beaumont, J., Walter, B. S., Redfern, R. and J. J. Bekvalac, 2025: Selective mortality during famine and plague events in medieval London. *Scientific Reports*, **15**, 27133

Gregory of Tours, 1974: *The History of the Franks (Historia Francorum).* Translated by Lewis Thorpe. Harmondsworth: Penguin Classics

Guzowski, P., 2022: Did the Black Death Reach the Kingdom of Poland in the Mid-Fourteenth Century? *J Interdisc. Hist.*, **53**(2), 193–215.

John of Ephesus, 1935–1936: *The Third Part of the Ecclesiastical History*. Translated by R. Payne Smith. Oxford: Oxford University Press

Guillet, S., Corona, C., Stoffel, M., Khodri, M., Lavigne, F., Ortega, P., Eckert, N., Dkengne Sielenou, P., Daux, V., Churakova (Sidorova), O. V., Davi, N., Edouard, J.-L., Zhang, Y., Luckman, B. H., Myglan, V. S., Guiot, J., Beniston, M., Masson-Delmotte, V., and Oppenheimer, C., 2017: Climate response to the Samalas volcanic eruption in 1257 revealed by proxy records. *Nat. Geosci.*, **10,** 123–128

Haldon, J., Elton, H., and Izdebski, A., 2022: *Managing the Roman Empire for the Long Term: Risk Assessment and Management Policy in the Fifth to Seventh Centuries.* In: Izdebski, A., Haldon, J., and Filipkowski, P. (eds.), Perspectives on Public Policy in Societal-Environmental Crises: What the Future Needs from History. Risk, Systems and Decisions. Cham: Springer, pp. 237–246

Hamerow, H., Bogaard, A., Charles, M., Forster, E., Holmes, M., McKerracher, M., Ramsey, C. B., Stroud, E. & Thomas, R., 2025: *Agricultural Land Use, c. AD 300–1500*. In 'Feeding Medieval England: A Long 'Agricultural Revolution', 700–1300', pp. 177–202

Hansen, J., Nazarenko, L., Ruedy, R., Sato, M., Willis, J., Del Genio, A., Koch, D., Lacis, A., Lo, K., Menon, S., Novakov, T., Perlwitz, J., Russell, G., Schmidt, G. A., and N. Tausnev, 2005: Earth's energy imbalance: Confirmation and implications. *Science*, **308**, 1431–1435.

Harbeck, M., Seifert, L., Hänsch, S., Wagner, D.M., Birdsell, D., Parise, K.L., Wiechmann, I., Grupe, G., Thomas, A., Keim, P., Zöller, L., Bramanti, B., Riehm, J.M. and H. C. Scholz, 2013: Yersinia pestis DNA from skeletal remains from the 6th century AD reveals insights into Justinianic Plague. *PLoS Pathog.,* **9**(5): e1003349

Harper K. 2017. *The fate of Rome: climate, disease, and the end of an empire*. Princeton University Press, Princeton, NJ.

Harper, K. 2023. The First Plague Pandemic in Italy: The Written Evidence. *Speculum* **98**(2).

Harrak, A. (ed. and trans.), 2017: *The Chronicle of Zuqnīn, Parts III and IV: A.D. 488–775*. Piscataway, NJ: Gorgias Press.

https://doi.org/10.5194/egusphere-2026-5195
Preprint. Discussion started: 8 September 2026
© Author(s) 2026. CC BY 4.0 License.

Helama, S., Arppe, L., Uusitalo, J., Holopainen, J., Mäkelä, H. M., Mäkinen, H., Mielikäinen, K., Nöjd, P., Sutinen, R., Taavitsainen, J.-P., Timonen, M., and M. Oinonen, 2018: Volcanic dust veils from sixth century tree-ring isotopes linked to reduced irradiance, primary production and human health. *Sci. Rep.*, **8,** 1339

Huebner, S. R., and B. MacDonald, 2023: Egypt as a gateway for the passage of pathogens into the ancient Mediterranean. *J. Interdiscip. Hist.*, **54**(2), 163–204

Izdebski, A., 2019: Catastrophes aside: environment and the end of Antiquity. In: A. Izdebski and M. Mulryan (eds.), *Environment and Society in the Long Late Antiquity*. Brill, Leiden, pp. 367–370

Izdebski, A., Guzowski, P., Poniat, R., Masci, L., Palli, J., Vignola, C., Bauch, M., Cocozza, C., Fernandes, R., Ljungqvist, F.C., Newfield, T., Seim, A., Abel-Schaad, D., Alba-Sánchez, F., Björkman, L., Brauer, A., Brown, A., Czerwiński, S., Ejarque, A., Fiłoc, M., Florenzano, A., Fredh, E.D., Fyfe, R., Jasiunas, N., Kołaczek, P., Kouli, K., Kozáková, R., Kupryjanowicz, M., Lagerås, P., Lamentowicz, M., Lindbladh, M., López-Sáez, J.A., Luelmo-Lautenschlaeger, R., Marcisz, K., Mazier, F., Mensing, S., Mercuri, A.M., Milecka, K., Miras, Y., Noryśkiewicz, A.M., Novenko, E., Obremska, M., Panajiotidis, S., Papadopoulou, M.L., Pędziszewska, A., Pérez-Díaz, S., Piovesan, G., Pluskowski, A., Pokorny, P., Poska, A., Reitalu, T., Rösch, M., Sadori, L., Sá Ferreira, C., Sebag, D., Słowiński, M., Stančikaitė, M., Stivrins, N., Tunno, I., Veski, S., Wacnik, A., and Masi, A., 2022. Palaeoecological data indicates land-use changes across Europe linked to spatial heterogeneity in mortality during the Black Death pandemic. *Nat. Ecol. Evol*. **6**, 297–306.

John of Ephesus, 1860: *The Third Part of the Ecclesiastical History*. Translated by R. Payne Smith. Oxford: Oxford University Press

Katona, P. and J. Katona-Apte, 2008: The interaction between nutrition and infection. *Clinical Infectious Diseases*, **46**(10), 1582–1588

Keeling, M. J., and C. A. Gilligan, 2000: Metapopulation dynamics of bubonic plague. *Nature*, **407**, 903-905

Keller, M., Spyrou, M. A., Scheib, C. L., Neumann, G. U., Kröpelin, A., Haas-Gebhard, B., Päffgen, B., Haberstroh, J., Ribera i Lacomba, A., Raynaud, C., Cessford, C., Durand, R., Stadler, P., Nägele, K., Bates, J. S., Trautmann, B., Inskip, S. A., Peters, J., Robb, J. E., Kivisild, T., Castex, D., McCormick, M., Bos, K. I., Harbeck, M., Herbig, A., and J. Krause, 2019: Ancient *Yersinia pestis* genomes from across Western Europe reveal early diversification during the First Pandemic (541–750). *Proc. Natl. Acad. Sci. USA*, **116,** 12363–12372

Larsen, L. B., Vinther, B. M., Briffa, K. R., Melvin, T. M., Clausen, H. B., Jones, P. D., Siggaard-Andersen, M.-L., Hammer, C. U., Eronen, M., Grudd, H., Gunnarson, B. E., Hantemirov, R. M., Naurzbaev, M. M., and K. Nicolussi, 2008: New ice core evidence for a volcanic cause of the A.D. 536 dust veil. *Geophys. Res. Lett.*, **35**(4), L04708

Lee, H.-F., Fei, J., Chan, C. Y. S., Pei, Q., Jia, X., and Yue, R. P. H., 2017: Climate change and epidemics in Chinese history: A multi-scalar analysis. *Soc. Sci. Med.*, **174**, 53–63

Little, L. K. (Ed.), 2007: *Plague and the End of Antiquity: The Pandemic of 541–750*. Cambridge University Press, Cambridge

Livi-Bacci, M., 2012: *A Short History of Migration.* Polity Press, Cambridge

https://doi.org/10.5194/egusphere-2026-5195
Preprint. Discussion started: 8 September 2026
© Author(s) 2026. CC BY 4.0 License.

Livi-Bacci, M., 2021: Nature, politics, and the traumas of Europe. *Population and Development Review*, 47, 579–609

Ljungqvist, F. C., Thejll, P., Christiansen, B., Seim, A., Hartl, C., and J. Esper, 2022: The significance of climate variability on early modern European grain prices. *Cliometrica*. **16**:29–27

Ljungqvist, F. C., Seim, A., and D. Collet, 2024: Famines in medieval and early modern Europe—Connecting climate and society. *WIREs Clim Change*. **15**:e859

Loveluck, C. P., Millett, M. J., Chenery, S., Chenery, C., Ferraby, R., French, C., Langdon, C., Moore, F. E., Pears, B., Scaife, R., and Toms, P., 2025: Aldborough and the metals economy of northern England, c. AD 345–1700: a new post-Roman narrative. *Antiquity*, **99**(407), 1320–1340

Franklin-Lyons, A., 2022: *Shortage and Famine in the Late Medieval Crown of Aragon: Vulnerability and Resilience in the Late-Medieval Crown of Aragon*, Penn State University Press, University Park, 266 pp.

Mac Airt, S., and G. Mac Niocaill (eds.), 1983: *The Annals of Ulster (to A.D. 1131)*. Dublin: Dublin Institute for Advanced Studies

Maddicott, J. R., 2007: *Plague in Seventh-Century England*. In L. K. Little (Ed.), *Plague and the End of Antiquity: The Pandemic of 541–750*. Cambridge University Press, Cambridge, pp. 171–214

Malalas, John. 1986. *The Chronicle of John Malalas: A Translation*. Translated by Elizabeth Jeffreys, Michael Jeffreys, and Roger Scott, with Brian Croke et al. *Byzantina Australiensia*, 4. Melbourne: Australian Association for Byzantine Studies

McMichael, A. J., 2012: Insights from past millennia into climatic impacts on human health and survival. *Proc. Natl. Acad. Sci. USA*, **109**(13), 4730–4737

McCormick, M., 2001: *Origins of the European Economy: Communications and Commerce, A.D. 300–900*. Cambridge: Cambridge University Press

McCormick, M., 2007: Toward a Molecular History of the Justinianic Pandemic. In *Plague and the End of Antiquity: The Pandemic of 541–750*, edited by Lester K. Little, 290–312. Cambridge: Cambridge University Press

McCormick, M., 2021: Gregory of Tours on Sixth-Century Plague and Other Epidemics. *Speculum* **96** (1): 38–96

Meier, M., 2016. The 'Justinianic Plague': the economic consequences of the pandemic in the eastern Roman empire and its cultural and religious effects. *Early Mediev. Europe,* **24**:267–292

Miller, D. J. D., and P. Sarris, trans. 2018. *The Novels of Justinian: A Complete Annotated English Translation*. 2 vols. Cambridge: Cambridge University Press

Mordechai, L., Eisenberg, M., Newfield, T. P., Izdebski, A., Kay, J. E., and H. Poinar, 2019: The Justinianic Plague: an inconsequential pandemic? *Proc. Natl. Acad. Sci. USA*, **116**: 25546–54

Morice, C. P., Kennedy, J. J., Rayner, N. A., Winn, J. P., Hogan, E., Killick, R. E., Dunn, R. J. H., Osborn, T. J., Jones, P. D., and Simpson, I. R., 2021: An Updated Assessment of Near-Surface Temperature Change From 1850: The HadCRUT5 Data Set. *J. Geophys. Res.-Atmos.*, **126**, e2019JD032361

Newfield, T., 2022: One plague for another? Interdisciplinary shortcomings in plague studies and the place of the Black Death in histories of the Justinianic Plague. *Stud. Late. Antiq.,* **6**:4, 575–626

https://doi.org/10.5194/egusphere-2026-5195
Preprint. Discussion started: 8 September 2026
© Author(s) 2026. CC BY 4.0 License.

1985 Oppenheimer, C., 2003: Volcanic hazards in the Mediterranean: implications for risk assessment and emergency management. *Progr. Phys. Geogr.*, **27**(2), 230–264

Oppenheimer, C., 2011: *Eruptions that Shook the World*. Cambridge University Press

Paul the Deacon, 1974: *History of the Lombards (Historia Langobardorum).* Translated by William Dudley Foulke. Edited by Edward Peters. University of Pennsylvania Press, Philadelphia

1990 Perry, R. D., and J. D. Fetherston, 1997: *Yersinia pestis* – etiologic agent of plague. *Clin. Microbiol. Rev*., **10**, 35-66

Preiser-Kapeller, J., McGrath, W. A., Pfister, R., Gong, S., Keller, M., Newfield, T. P., Schamiloglu, U., Büntgen, U., Spyrou, M. A., Averbuch, B., Chen, F., Schindel, N., Xie, H., and Xoplaki, E., 2025: The circulation of *Yersinia pestis* in Central Eurasia before and during the First Plague Pandemic (Second to Eighth Century CE): Palaeogenetic and historical evidence and sociopolitical, ecological, and climatic factors. *Hum. Ecol.*, **53,** 703–721

1995 Procopius, 1914-1928: *History of the Wars*, 7 vols. Translated by H. B. Dewing. *Loeb Classical Library*, 217. Cambridge, MA: Harvard University Press

Procopius, 1966: *The Secret History*. Translated by G. A. Williamson. Harmondsworth: Penguin Books

Pseudo-Dionysius of Tel-Mahre, 1996: *The Chronicle of Pseudo-Dionysius of Tel-Mahre*. Translated by Witold Witakowski. Liverpool: Liverpool University Press

2000 Rampino, M. R., Self, S., and Stothers, R. B., 1988: Volcanic winters. *Annu. Rev. Earth Planet. Sci.*, **16,** 73–99

Ren, X., Wu, W., Ge, Q., Cui, J., Zhang, X., Seim, A., Skoglund, M. K., Wang, K., Liu, M., Cheng, J., Zeng, Z., and F. C. Ljungqvist, 2025: Climate and Society in Chinese History. *WIREs Clim. Change,* **16**(6), e70032

Ripoll, S., Niederberger, E., and L. Jones, 2022: *Key Considerations: Behavioural, Social and Community Dynamics related to Plague Outbreaks in Madagascar*. Social Science in Humanitarian Action Platform (SSHAP)

2005 Robock, A., 2000: Volcanic eruptions and climate. *Reviews of Geophysics*, **38**, 191–219

de la Roncière, C.-M., 1968: *Indirect Taxes or 'Gabelles' at Florence in the Fourteenth Century: The Evolution of Tariffs and Problems of Collection*. In *Florentine Studies: Politics and Society in Renaissance Florence*, edited by Nicolai Rubinstein, London: Faber and Faber, 140–182

Russell, J. C., 1965: Recent Advances in Mediaeval Demography. *Speculum,* **40**(1): 84–101.

2010 Russell, J. C., 1968: That earlier plague. *Demography,* **5:**174–184

Samia, N. I., Kausrud, K. L., Heesterbeek, H., Ageyev, V. S., Begon, M., Chan, K.-S., and N. C. Stenseth, 2011: Dynamics of the plague–wildlife–human system in Central Asia are controlled by two epidemiological thresholds.. *Proc. Natl. Acad. Sci. USA,* **108**(36): 14527–14532

Sarris, P., 2022: Viewpoint: New Approaches to the 'Justinianic Plague'**.** *Past Present*, **254**(1), 315–346

2015 Scott, S. and C. J. Duncan, 2001: *Biology of plagues: evidence from historical populations.* Cambridge, UK: Cambridge University Press

https://doi.org/10.5194/egusphere-2026-5195
Preprint. Discussion started: 8 September 2026
© Author(s) 2026. CC BY 4.0 License.

Schmid, B. V., Büntgen, U., Easterday, W. R., Ginzler, C., Walløe, L., Bramanti, B., and N. Chr. Stenseth, 2015: Climate-driven introduction of the Black Death and successive plague reintroductions into Europe. *Proc. Natl. Acad. Sci. USA*, **112**(10), 3020–3025

Schoeberl, M. R., Toohey, M., Wang, Y., and R. Ueyama, 2025: Stratospheric injection lifetimes. *J. Geophys. Res.: Atmos.*, **130,** e2025JD043928

Scrimshaw, N. S., Taylor, C. E. and Gordon, J. E., 1968: *Interactions of Nutrition and Infection*. Geneva: World Health Organization, WHO Monograph Series No. 57

Seaman, A., 2023: Hillforts in Southern Britain: Power and Place in the Late Antique Landscape. In *Imperial Archaeologies*. Leiden: Brill, pp. 420–432

Self, S., 2006: The effects and consequences of very large explosive volcanic eruptions. *Philos. Trans. A. Math. Phys. Eng. Sci*., **364**, 2073–97

Shrewsbury, J. F. D., 1970: *A History of Bubonic Plague in the British Isles*. Cambridge University Press

Sigl, M., Winstrup, M., McConnell, J. R., Welten, K. C., Plunkett, G., Ludlow, F., Büntgen, U., Caffee, M., Chellman, N., Dahl-Jensen, D., Fischer, H., Kipfstuhl, S., Kostick, C., Maselli, O. J., Mekhaldi, F., Mulvaney, R., Muscheler, R., Pasteris, D. R., Pilcher, J. R., Salzer, M., Schüpbach, S., Steffensen, J. P., Vinther, B. M., and Woodruff, T. E., 2015: Timing and climate forcing of volcanic eruptions for the past 2,500 years. *Nature*, **523**, 543–549

Smerlak, M. and B. Vaitla, 2016: A non-equilibrium formulation of food security resilience. *Environmental Research Letters,* **11**, 125010

Spyrou, M.A., Musralina, L., Gnecchi Ruscone, G.A., Kocher, A., Borbone, P.-G., Khartanovich, V.I., Buzhilova, A., Djansugurova, L., Bos, K.I., Kühnert, D., Haak, W., Slavin, P. & Krause, J., 2022: The source of the Black Death in fourteenth-century central Eurasia. *Nature*, **606**, 718–724.

Stathakopoulos, D. C., 2004: *Famine and Pestilence in the Late Roman and Early Byzantine Empire: A Systematic Survey of Subsistence Crises and Epidemics*. Aldershot: Ashgate

Stathakopoulos, D. C., 2007: *Crime and Punishment: The Plague in the Byzantine Empire, 541–749*. In *Plague and the End of Antiquity: The Pandemic of 541–750*, edited by Lester K. Little, 99–118. Cambridge: Cambridge University Press

Stathakopoulos, D. C., Newfield, T. P., Xoplaki, E., Haldon, J., Keller, M., Roberts, N., Bourbou, C., Mordechai, L., Paulus, C., Grimm-Stadelmann, I., Hartmann, E., Luterbacher, J., Luther, N., Sessa, K., Slootjes, D., & Zhang, M., 2025: The First Plague Pandemic in the Byzantine Empire – Toward a New Dynamic Consensus. *Hum. Ecol.,* **53**(4), 681–701

Stenchikov, G. L., Kirchner, I., Robock, A., Graf, H.-F., Antuña, J. C., Grainger, R. G., Lambert, A., and Thomason, L., 1998: Radiative forcing from the 1991 Mount Pinatubo volcanic eruption. *J. Geophys. Res.*, **103**, 13837–13857

Stoffel, M., Khodri, M., Corona, C., Guillet, S., Poulain, V., Bekki, S., Guiot, J., Luckman, B. H., Oppenheimer, C., Lebas, N., Beniston, M., and V. Masson-Delmotte, 2015: Estimates of volcanic-induced cooling in the Northern Hemisphere over the past 1,500 years. *Nat. Geosci.,* **8,** 784–788

Stokes, W. (ed. and trans.), 1895–1897: *The Annals of Tigernach*. *Revue Celtique*, vols. 16–18, Paris

https://doi.org/10.5194/egusphere-2026-5195
Preprint. Discussion started: 8 September 2026
© Author(s) 2026. CC BY 4.0 License.

Stothers, R. B., 1984: The great Tambora eruption in 1815 and its aftermath. *Science*, **224**, 1191–1198

Stothers, R. B., 1999: Volcanic dry fogs, climate cooling, and plague pandemics in Europe. *Clim. Change,* **42**, 713–723

Stothers, R. B., 2000: Climatic and demographic consequences of the massive volcanic eruption of 1258. *Clim. Change,* **45**, 361–375

Tardif, R., Hakim, G. J., Perkins, W. A., Horlick, K. A., Erb, M. P., Emile-Geay, J., Anderson, D. M., Steig, E. J., and D. Noone, 2019: Last Millennium Reanalysis with an expanded proxy database and seasonal proxy modeling. *Clim. Past,* **15**(4), 1251–1273

Thompson, D. W. J., Wallace, J. M., Jones, P. D., and Kennedy, J. J., 2009: Identifying signatures of natural climate variability in time series of global-mean surface temperature: methodology and insights. *J. Clim*., **22**, 6120–6141

Timmreck, C., Lorenz, S. J., Crowley, T. J., Kinne, S., Raddatz, T. J., and M. A. Thomas, 2010: Limited temperature response to the very large Toba eruption 74,000 years ago. *Geophys. Res. Lett.*, **37,** L18705

Toohey, M., Krüger, K., Sigl, M., Stordal, F., and H. Svensen, 2016: Climatic and societal impacts of a volcanic double event at the dawn of the Middle Ages. *Clim. Change*, **136**:401–412

Toohey, M., Jia, Y., Khanal, S., and Tegtmeier, S., 2025: Stratospheric residence time and the lifetime of volcanic stratospheric aerosols. *Atmos. Chem. Phys., 25*, 3821–3839

Toohey, M. and Morovati, M., 2026: *Using simple models to understand the global mean temperature response to volcanic aerosol forcing.* EGU General Assembly 2026, Vienna, Austria, 3–8 May 2026, EGU26-14229

van Dijk, E., Jungclaus, J., Lorenz, S., Timmreck, C. and K Krüger, 2022: Was there a volcanic-induced long-lasting cooling over the Northern Hemisphere in the mid-6th-7th century? *Clim. Past.* **18**:1601-1623

van Dijk, E., Gundersen, I. M., de Bode, A., Høeg, H., Loftsgarden, K., Iversen, F., Timmreck, C., Jungclaus, J., and Krüger, K., 2023: Climatic and societal impacts in Scandinavia following the 536 and 540 CE volcanic double event. *Clim. Past*, **19,** 357–398

Wagner, D. M., Klunk, J., Harbeck, M., Devault, A., Waglechner, N., Sahl, J. W., Enk, J., Birdsell, D. N., Kuch, M., Lumibao, C., Poinar, D., Pearson, T., Fourment, M., Golding, B., Riehm, J. M., Earn, D. J. D., DeWitte, S., Rouillard, J. M., Grupe, G., Wiechmann, I., Bliska, J. B., Keim, P. S., Scholz, H. C., Holmes, E. C., and Poinar, H., 2014: Yersinia pestis and the Justinianic Plague 541–543 AD: a genomic analysis. *Lancet Infect. Dis.*, **14,** 319–326

Walter, B.S., DeWitte, S.N., Dupras, T.L. & Beaumont, J. (2020). Assessment of nutritional stress in famine burials using stable isotope analysis. *Am. J. Phys. Anthropol.*, **172**(2), 214–226

Whitby, M., 2000.: The Ecclesiastical History of Evagrius Scholasticus. *Translated Texts for Historians* 33. Liverpool.

Williams ab Ithel, J. (ed.), 1860: *Annales Cambriae*. London: Longman, Green, Longman, and Roberts. Rerum Britannicarum Medii Aevi Scriptores, no. 20

Zanchettin, D., Timmreck, C., Khodri, M., Schmidt, A., Toohey, M., Abe, M., Bekki, S., Cole, J., Fang, S.-W., Feng, W., Hegerl, G., Johnson, B., Lebas, N., LeGrande, A. N., Mann, G. W., Marshall, L., Rieger, L., Robock, A., Rubinetti, S.,

https://doi.org/10.5194/egusphere-2026-5195
Preprint. Discussion started: 8 September 2026
© Author(s) 2026. CC BY 4.0 License.

Tsigaridis, K., and H. Weierbach, 2022: Effects of forcing differences and initial conditions on inter-model agreement in the VolMIP volc-pinatubo-full experiment. *Geosci. Mod. Dev.,* **15**(5), 2265–2292

Zanette, D., and S. Risau-Gusman, 2008: Infection spreading in a population with evolving contacts. *J. Biol. Phys*. **34**, 135–148

Zonneveld, K. A. F., Harper, K., Klügel, A., Chen, L., de Lange, G., and G. J. M. Versteegh, 2024: Climate change, society, and pandemic disease in Roman Italy between 200 BCE and 600 CE. *Sci. Adv.*, **10**(4), eadk1033